Isolation of electrode performance issues for lithium ion batteries during calendar and cycle life

A Dissertation

Presented in Partial Fulfillment of the Requirements

for the Degree of Doctor of Philosophy

with a

Major in Chemical Engineering

in the

College of Graduate Studies

of the

University of Idaho

by

Jeffrey R. Belt

May 2014

Major Professor: Vivek P. Utgikar, Ph.D.

Authorization to Submit Dissertation

This dissertation of Jeffrey R. Belt, submitted for the degree of Doctor of Philosophy with a major in Chemical Engineering and titled "**Isolation of electrode performance issues for lithium ion batteries during calendar and cycle life**," has been reviewed in final form. Permission, as indicated by the signatures and dates given below, is now granted to submit final copies to the College of Graduate Studies for approval.

Major Professor: _____Date_____
Vivek Utgikar

Committee Members: _____Date_____
I. Francis Cheng

_____Date_____
Dean Edwards

_____Date_____
Supathorn Phongikaroon

Department Administrator: _____Date_____
Wudneh Admassu

Dean of Engineering: _____Date_____
Larry Stauffer

Final Approval and Acceptance

Dean of the College of Graduate Studies: _____Date_____
Jie Chen

Abstract

In an effort to reduce fuel consumption by improving vehicle efficiency, several automakers have offered electrified vehicles options to consumers. Development, testing, in-depth failure analysis and modeling of lithium ion battery technology are critical for the continued development and growth of the electrified vehicle market. In this work, lithium ion cells were cycle and calendar aged under various conditions, such as temperature and state of charge, to identify capacity fade, resistance rise and power fade associated with the Plug-In Hybrid Vehicle (PHEV) usage scenarios. A reference electrode was inserted to several cells to separate the electrode performance from the cell performance. The testing results were modeled to estimate life for the cells at common operating temperatures.

Focused destructive analyses were performed with half-cell testing utilizing a lithium reference electrode to understand the mechanisms that affect power, energy, resistance and capacity fade in the path dependence studies of commercial Lithium Ion cell testing. The reference electrode is used to investigate voltage characteristics of the individual electrodes throughout calendar (i.e., zero current) and current cycle-ageing regimes. The response of the electrode voltages (vs. reference) to a given current pulse prior to and during interruptions of the aging regime indicates that the resistance of the positive-electrode is much larger than that of the negative electrode.

Modeling of the calendar and cycle life testing results using an Arrhenius based semi-empirical model was demonstrated for temperature and state of charge accelerated calendar and cycle life testing. Calendar life estimation has become critical for the continued development of electrified vehicles and the warranties associated with them. A methodology

is presented that can be used to characterize the performance degradation of cells for use in automotive applications.

Battery manufacturers, by understanding the factors that limit life and which electrode limits cell performance over life can improve cell technology: life, performance, and cost. Battery advancements will be accompanied by reduced petroleum consumption, which will facilitate the acceptance of electrified vehicles that will be competitive at the same cost and performance level in a market dominated by gasoline engines.

Acknowledgements

I am grateful for the support that I have received from many people during my graduate studies at the University of Idaho. I appreciate the support from my wife, Autumn and our girls, Jazlynn, Audriana, and Rebecca and my son, Joshua for the many hours that were spent away from them studying and attending class. They bring great joy and fulfillment to my life. I appreciate the support of my parents and in-laws. I wish to thank my advisor, Professor Vivek Utgikar for the instruction I received from him and the guidance he has provided during this process. I would like to thank Professors I. Francis Cheng, Supathorn Phongikaroon, and Dean Edwards for serving on my doctoral thesis committee and reviewing this work.

The U.S. Department of Energy, FreedomCAR and Vehicle Technologies Program funded this work. Additionally, the United States Advance Battery Consortium, the Electrochemical Energy Storage Technical Team and Quallion supported this work.

Dedication

To Autumn

The LOVE of MY LIFE

Table of Contents

List of Figures

List of Tables

List of Acronyms

AFM	Atomic Force Microscopy
BOL	Beginning of Life
$C_1/1$	The current corresponding to the manufacturer's rated capacity for a one-hour discharge.
CD	Charge Depleting
CS	Charge Sustaining
DOD	Depth of Discharge
DOE	Department of Energy
DST	Dynamic Stress Test
EOL	End of Life
EV	Electric Vehicle
FTIR	Fourier Transform Infrared
GEO	Geosynchronous Earth Orbit
HEV	Hybrid Electric Vehicle
HPPC	Hybrid Pulse Power Characterization
I_{max}	Maximum Current (A)
INL	Idaho National Laboratory
NiMH	Nickel Metal Hydride
NMP	N-Methyl Pirolidone
NMR	Nuclear Magnetic Resonance
PHEV	Plug-In Hybrid Electric Vehicle
PNGV	Partnership for a New Generation of Vehicles
PVDF	Polyvinylidene Flouride
OCV	Open Circuit Voltage (V)
RPT	Reference Performance Test
SEI	Solid Electrolyte Interphase
SEM	Scanning Electron Microscope
SOC	State of Charge
SNL	Sandia National Laboratories

TEM	Transmission Electron Microscope
USABC	United States Advanced Battery Consortium
V_{MAX}	Maximum Voltage
V_{MIN}	Minimum Voltage
XRD	X-Ray Diffraction

Chapter One: Introduction

1.1 Background

Liquid fuels derived from petroleum have long been the primary source for transportation due to their high energy density and low cost. However, as the U.S. transportation market has become dependent on petroleum, the costs for fuel have continued to rise. In 2011, the United States used 21.6% of the 87.3 million barrels of petroleum per day consumed worldwide, yet only accounted for 9.5% of the 82.6 million barrels per day that were produced. The production shortfall versus consumption required the importation of 11.4 million barrels of petroleum each day to meet the demands of consumption, equal to 60.2% of U.S. consumption, 18.84 million barrels per day. Although the importation of petroleum has been dropping since 2006, when it reached a high of 13.7 million barrels of petroleum each day due to higher domestic production, the U.S. still imports a large portion of petroleum. The U.S. transportation sector used 12.7 million barrels per day, or two-thirds of these petroleum resources. This dependence on imported oil is estimated to cost $300 billion to the U.S. economy in 2011 [1, 2]. Unless the efficiency of the transportation sector can be dramatically increased or substantial domestic alternative energy sources are developed, the United States will be increasingly dependent upon the rest of the world for petroleum, making the U.S. economy vulnerable to external disturbances.

Although fossil fuel vehicles have become the norm over the last 100 years, electric vehicles were very prominent during a period of time. However, they were limited in their range due to the batteries that were available at that time, just as they are today. Nevertheless, in an effort to improve efficiency and reduce oil consumption, the U.S.

automotive companies have been involved in research and development for advanced battery systems that can be used in a variety of vehicles ranging from Hybrid Electric Vehicle (HEV), to Plug-In Hybrid Electric Vehicle (PHEV), with the final goal being an Electric Vehicle (EV).

An HEV is a vehicle that mainly is propelled by gasoline and has a small battery system to assist in propulsion and collect excess energy through regenerative braking. It has no capability; normally for 100% electric propulsion, it is only a propulsion assist. A PHEV is similar to an HEV except that it has a limited range of electric propulsion, normally 10 to 40 miles in addition to the propulsion assist. Additionally, it has the capability of directly recharging the on-board energy storage system, a battery, from the electrical grid while it is plugged into an outlet and not in use. This design allows for improved efficiency and lower cost operation since the cost of gasoline tends to be higher than the cost of electricity, especially if the battery is charged at night using lower cost electricity. An electric vehicle (EV) has no gasoline propulsion and is entirely run by electricity. It is fueled from the electricity from an outlet when it is not being used and can achieve ~100 mile/gal (gasoline equivalent). However, the range is limited compared to a gasoline fueled vehicle. The cost for these vehicles also tends to be higher than a comparable gasoline vehicle.

The overall objective of this work is to aid the efforts by the Department of Energy (DOE) to advance the development of batteries to enable a large market penetration of hybrid and electric vehicles to achieve large national benefits. As the development since 1990 has evolved, the work is currently focused on two DOE targets:

- By *2014,* develop a PHEV battery that can deliver a 40-mile all-electric range and costs $3,400

- By *2020,* develop an EV battery that can store 40 kWh of electricity and costs $5,000 [1]

Cost, life, performance, and safety are the main impediments for the application of batteries for vehicular use. Overcoming these hurdles so that batteries can be used for automotive transportation has been a major driving force behind many of the programs in vehicle technologies instituted by the DOE.

1.2 FreedomCAR Partnership

FreedomCAR, a partnership between the U.S. DOE, Chrysler, Ford, and General Motors, was formed in January 2002. The partnership focuses "collaborative, pre-competitive, high-risk research to develop the component technologies necessary to provide a full range of affordable cars and light trucks that will free the nation's personal transportation system from petroleum dependence and from harmful vehicle emissions, without sacrificing freedom of mobility and freedom of vehicle choice [3]." The CAR in FreedomCAR stands for Cooperative Automotive Research. The Freedom principle is based on the following: freedom from petroleum dependence; from pollutant emissions; for Americans to choose the kind of vehicle they want to drive; to drive where and when they want; and to obtain fuel affordably and conveniently. This Partnership aims at developing hybrid electric vehicles with gasoline engines that can be replaced in the future with a fuel cell engine, powered by hydrogen. This will allow the continued use of a range of vehicle sizes by the American driver while also providing greater fuel efficiency and reducing our dependence on oil imports.

FreedomCAR visualizes the reality of vehicles and fuels that will lead to a clean and sustainable energy future. The Partnership offers the United States a historic opportunity to embrace an environmentally sustainable future. The main challenge is to make this future economically viable through technological advances, which would also establish the United States as a global leader for environmental and energy technologies that will help maintain competitiveness in the global economy. This is the underlying goal for the FreedomCAR Partnership.

A major focus of the FreedomCAR Partnership is to support research and development for hydrogen-powered fuel cell vehicles. Fuel cell vehicles can have much higher efficiencies, 40% to 60%, compared to internal combustion engine vehicles that are around 20% [4]. One of the enabling technologies for hydrogen-powered fuel cell vehicles is battery development, which facilitates high-power with moderate energy, since the same components used for a hybrid vehicle would also be used for a hydrogen-powered fuel cell vehicle. The FreedomCAR battery goals for hypothetical minimum and maximum plug-in hybrid electric vehicle applications are shown in Table 1.1 [5].

1.3 Lithium Ion Batteries

The two most prominent cell chemistries for use in hybrid electric vehicles include Li-Ion and Nickel Metal Hydride (NiMH). Although NiMH batteries were being used in hybrid electric vehicles, such as the Prius, Li-Ion batteries have the capability to offer longer life and higher power. The focus of this work is the Li-Ion chemistry batteries. To understand the effects of a calendar life test on lithium ion batteries, it is necessary to review some basic concepts of electrochemistry and the chemistry of a lithium ion battery.

Table 1.1: Energy storage system performance targets for plug-in hybrid electric vehicles

Characteristics at End-of-Life (EOL)	**Unit**	**Minimum PHEV Battery**	**Maximum PHEV Battery**
Reference Equivalent Electric	miles	10	40
Peak Discharge Pulse Power (2 sec /10 sec)	kW	50/45	46/38
Peak Regen Pulse Power (10	kW	30	25
Max. Current (10 sec pulse)	A	300	300
Available Energy for Charge-Depleting (CD) Mode, 10-kW Rate	kWh	3.4	11.6
Available Energy for Charge-Sustaining (CS) Mode, 10-kW Rate	kWh	0.5	0.3
Minimum Round-trip Energy Efficiency (CS 50 Wh profile)	%	90	90
Cold cranking power at -30°C, 2 sec, 3 Pulses	kW	7	7
CD Life / Discharge Throughput	Cycles/MW	5,000 / 17	5,000 / 58
CS HEV Cycle Life, 50 Wh	Cycles	300,000	300,000
Calendar Life, 35°C	year	15	15
Maximum System Weight	kg	60	120
Maximum System Volume	Liter	40	80
Maximum Operating Voltage	Vdc	400	400
Minimum Operating Voltage	Vdc	>0.55 x Vmax	>0.55 x Vmax
Maximum Self-discharge	Wh/day	50	50
Maximum System Recharge Rate at 30°C	kW	1.4 (120V/15A)	1.4 (120V/15A)
Unassisted Operating & Charging Temperature Range 52°C > 100% Available Power 0°C > 50% Available Power -10°C > 30% Available Power -30°C > 10% Available Power	°C	-30 to +52	-30 to +52
Survival Temperature Range	°C	-46 to +66	-46 to +66
Maximum System Production Price @ 100k units/yr	$	$1,700	$3,400

Cost, abuse tolerance, cold temperature performance, and calendar life limit the usefulness of advanced lithium ion batteries. The developers mitigate the cost issues as they

seek lower cost materials that will still meet all the other technical goals. Further development sponsored by the United States Advanced Battery Consortium (USABC), whose members consist of Chrysler, Ford, and General Motors concentrates on cost reduction as the price of materials is reduced through economies of scale and the search for lower cost substitutes. Among others, Sandia National Laboratories (SNL) is addressing the abuse tolerance issue and Idaho National Laboratory (INL) is engaged in research and development that focus on the cold-temperature performance issues, battery life, and performance. The issue of calendar life is a particularly difficult problem to solve because of the ostensibly fifteen-year test period for each new battery design, which is unacceptable to both the battery suppliers and vehicle manufacturers. Real vehicle usage is marked by intermittent use followed by extended idle periods with the vehicle turned off. Furthermore, during usage the battery must provide the required power and energy over a wide range of operating temperatures. The cumulative idle periods, when the vehicle is turned off, are defined as the calendar life of the device, which over time it must continue to meet all the performance requirements including the fifteen-year life. In addition, any degradation that occurs during the idle periods coupled with the degradation during usage must be small enough to allow the battery to perform 5,000 deep cycle discharges and 300,000 specific discharge and charge cycles, which approximate 100,000 miles of driving.

1.4 Objectives

The objective of this work was to determine the performance degradation characteristics of lithium-ion batteries under calendar life and cycle life conditions representing the operation of vehicles. Commercially available 18650, (18 mm in diameter

and 650 mm long) lithium ion batteries were subjected to testing under various conditions to identify the magnitude of resistance rise or capacity fade during calendar and cycle life using the United States Advanced Battery Consortium (USABC) PHEV testing protocols [5]. The tasks conducted to achieve this objective were as follows:

Task A. The batteries were tested under various conditions, such as temperature and state of charge (SOC), to identify resistance rise or capacity fade associated with the positive electrode or negative electrode during calendar and cycle life testing. The static capacity and Hybrid Pulse Power Characterization (HPPC) tests were used to evaluate the performance. New cells, with little to no degradation were compared to cells with various levels of degradation.

Task B. The in situ reference electrode measurement was used to evaluate the capacity of each electrode as well as the resistance contribution from each electrode. These measurements were compared to cells in a new condition to identify the performance limitations. Data from calendar life, cycle life, temperature, and SOC tests were compared to identify differences in the electrode performances.

Task C. Modeling of the calendar and cycle life testing results using an Arrhenius based model was demonstrated. Activation energies were determined from the modeling for comparison purposes. Activation energies from calendar life, cycling, temperature and SOC dependence were compared with each other to identify whether or not the degradation mechanisms were the same or different. Additionally, they were compared with other types of chemical reactions. To break down the performance limitations of a lithium ion battery, electrode performance was separated from the overall cell performance in an environment that can evaluate both resistance rise and capacity fade. The models developed from the

testing work enable the prediction of capacity fade or resistance rise under various conditions for calendar and cycle life conditions.

1.5 Importance and Relevance

Lithium-ion batteries continue to attract much interest in applications where high specific or volumetric power and/or energy is required. High-energy lithium-ion batteries are also being considered for automotive applications by the U.S. DOE-supported USABC [5].

The Li-ion batteries usually consist of a metal-oxide positive electrode, a carbon negative electrode, and an organic electrolyte containing dissolved lithium salts. Layered-oxide positive electrodes, such as $Li(Ni_{1/3}Mn_{1/3}Co_{1/3})O_2$, represent good candidates for automotive applications because of their high specific capacity [6]. However, the cycle life of this oxide was not as high as desired [7]. On the other hand, spinel oxides, such as $LiMn_2O_4$, are also viable candidates. These oxides are low-cost and have fast kinetics, which makes the oxide suitable for high-power applications [6]. The spinels were reported to have lower specific capacity than the layered oxides [6] and would degrade rapidly due to manganese dissolution [7-10]. Reports in the literature have shown that blending these two materials produced a composite with the benefits of both [11-15].

Past tests at the INL and Argonne National Laboratory have concentrated on three positive electrode materials coupled with graphite as the negative material— $LiNi_{0.8}Co_{0.2}O_2$, $LiNi_{0.8}Co_{0.1}Al_{0.1}O_2$, and $Li_{1.05}(Mn_{1/3}Co_{1/3}Ni_{1/3})_{0.95}O_2$ —[16 to 24]. The procedures outlined in the USABC test manuals [1] intend to show the promise of a technology versus a set of performance and cost targets. No knowledge of the actual battery chemistry is needed. Thus, the evaluation of cells concentrates on their performance and life and how their life is

affected by SOC, time, temperature and type of test. Calendar and cycle life tests were performed to determine the aging characteristics of the blended positive electrode material under plug-in hybrid electric vehicle (PHEV) testing conditions [1]. The cycle life test is more complex, depending on what is to be learned.

Vehicle Technologies Program Energy Storage Targets are the primary driving force for the test procedures and methods defined in the PHEV manual. These targets are outlined in Table 1 for a Minimum PHEV Battery and a Maximum PHEV Battery performance specified for the Vehicle Technologies Program. Minimum PHEV Battery target is a sport utility vehicle with a vehicular mass of 2000 kg with an equivalent electric range of 10 miles; the Medium PHEV Battery target is a car with a vehicular mass of 1600 kg with an equivalent electric range of 20 miles; and the Maximum PHEV Battery target is a car with a vehicular mass of 1500 kg with an equivalent electric range of 40 miles. Unless otherwise stated, these targets all pertain to devices operating at 30°C. Establishing or verifying battery performance in comparison to these targets is a major goal in any battery testing studies.

The work described herein quantified the contributions to performance degradation from the positive and negative electrodes. The positive electrode was identified as the electrode limiting the performance of the cell. This information can be used by manufacturers of future battery designs to focus improvement efforts on the positive electrode. The model developed can be used to predict the calendar and cycle life of the batteries. This information will be useful in determining further research needs and directions for advancing the FreedomCAR agenda.

1.6 Organization of the Dissertation

Chapter Two provides a literature review as well as the basics of lithium ion batteries and the roadblocks that impede implementation. Chapter Three details the materials and methods used for this research. Chapter Four summarizes the testing results from the calendar and cycle life testing. Reference electrode testing results to identify the electrode that is limiting overall performance are discussed in Chapter Five. Chapter Six presents the mathematical models that have been developed to understand the effects of temperature and state of charge on lithium ion battery performance. The overall conclusions of the work are presented in Chapter Seven.

Chapter Two: Literature Review

Electrochemical power sources or batteries have experienced a large growth in usage in the last few years as mobile electronics such as cell phones; laptops, iPods, etc. have become widespread. Batteries fill a unique niche in the supply of energy in mobile applications because they can store reasonable quantities of energy for long periods and can be sized for the specific application. For example, batteries are uniquely suited for use in watches because they are long lasting and do not require daily winding. Batteries have become indispensably standard in automotive applications ever since Charles Kettering replaced the old hand crank system for starting combustion engines in vehicles in 1910 with an electrical ignition using lead-acid battery [25]. However, for energy and power intensive applications, such as propulsion motive power in transportation, batteries have not been able to compete successfully with the high-energy and power characteristics of the gasoline internal combustion engine, except in limited circumstances. This chapter briefly summarizes development of batteries up to the advent of the lithium ion concept as well as an understanding of the causes of power and capacity fade in the lithium ion batteries.

2.1 Historical Development of Batteries

Benjamin Franklin first coined the term electrical "battery" in reference to a number of Leyden jars that had been electrically charged, as shown in Figure 2.1. The term "battery," as he used it, refers to a 'battery' of guns in comparison to a single cannon. In this case, it was a 'battery' or group of jars that held an electrical charge [25].

Figure 2.1: Benjamin Franklin's "battery" of Leyden Jars [25]

Alessandro Volta, a Professor of Natural Philosophy designed the first electrochemical battery at the University of Pavia in Italy in 1800 [26]. The Volta pile, shown in Figure 2.2, became a staple for all researchers working on electricity. Batteries capable of substantial current flow without undue voltage loss were first incorporated into the telegraph system in the 1830. The Daniel cells, invented in 1836 by John F. Daniel, somewhat safer and less corrosive than the Volta cell, used copper sulfate and zinc sulfate as the electrolyte between zinc and copper electrodes. In 1840, the electroplating and electroforming industries began to use high current batteries. Gaston Plante, a French inventor, developed in 1859 the first secondary lead acid battery that could be recharged multiple times. Seven years later in 1866, Georges Leclanche created a carbon-zinc wet cell battery called the Leclanche cell. The general consumer market for batteries began in 1870's for electric bell circuits for homes, offices, and hotels. In 1881 Carl Gassner successfully commercialized a zinc-carbon dry battery. Waldmar Jungner invented the nickel-cadmium rechargeable battery in 1899. Twenty years after Edison invented the incandescent lamp in

1879, the flashlight was introduced and the annual production of batteries in the USA exceeded two million units. A couple of years later, Thomas Edison invented the alkaline storage battery that has become so widely available for a multitude of applications [27].

Figure 2.2: Volta Piles, 19th century [28]

A battery is an electrochemical device that converts chemical energy stored in the active material in each electrode half-cell into electrical energy. Non-rechargeable batteries are referred to as primary batteries, while rechargeable batteries such as lithium ion and lead acid are referred to as secondary batteries. Batteries are capable of 90-95% chemical to electrical energy conversion efficiencies because they do not involve combustion nor are they limited by the Carnot cycle for energy conversion. Short-term efficiency losses are mainly

attributed to Joule heating, while long-term losses result from degradation due to aging and other chemical or structural instabilities.

Lithium has long been sought for use in a battery because of its high specific energy, 150 Wh/kg in comparison to lead acid and NiCd batteries at 50 Wh/kg, and nickel metal hydride batteries at 70 Wh/kg [29]. The first paper ever presented on a lithium battery titled, "Lithium Nonaqueous Secondary Batteries" was presented in 1962 in Boston at the Electrochemical Society fall meeting by Chilton Jr. and Cook [30]. Chilton originally was seeking a battery with high specific energy and a long cycle life for use in a satellite. The main obstacles were the high reactivity of lithium with the electrolyte and difficulty of finding a good reversible positive electrode, cathode. A rechargeable lithium battery was developed in the mid-eighties, but it suffered from cycle life problems. It had a capability of less than 200 cycles, compared to 800 deep discharge cycles for a lead acid battery. In 1980, Lazzari and Scrosati [30] proposed using insertion compounds based on metallic oxides or sulfides to overcome the problems associated with the pure metal anode. However, the 'lithium battery' did not measure up to the expected high specific energy of 150 Wh/kg as compared to 520 Wh/kg for a Li/TiS_2 cell. Researchers investigated many different cathode materials were until Mizushima and Goodenough [30] proposed the use of Li_xCoO_2 and Li_xNiO_2 as possible cathode materials in 1980. In 1987 a patent was filed showing that disordered carbon had a capability of accepting lithium into the structure with a stable protective passivating layer. Sony, the first company to introduce the lithium ion cell in 1990, used the Li_xCoO_2 as the cathode and their previous work on disordered carbons as the anode. At 4.2 V versus Li/Li+, this system was capable of 145 Ah/kg (500 Wh/kg at a nominal voltage of 3.5V) with good electrochemical performance [30].

2.2 Lithium Ion Batteries

Five key components, a cathode, an anode, a separator, a current collector and an electrolyte enclosed within a sealed case, constitute a battery. Some battery chemistries such as Li-Ion, sensitive to contamination from moisture and air, must be hermetically sealed for protection. By definition, the cathode is the reducing electrode where lithium ions get reduced to lithium metal, which is intercalated into the electrode structure, while the anode is the oxidizing electrode where lithium metal is oxidized and de-intercalated from the electrode as lithium ion. During discharge, the positive electrode of the cell is the cathode, but during charge, the electrochemical processes reverse and the negative electrode is the cathode. However, the convention most common for lithium ion batteries is to refer to the positive electrode as the cathode and the negative electrode as the anode as they are defined in the discharge process. The literature commonly uses cathode and positive interchangeably as well as anode and negative when discussing lithium ion batteries.

The separator, a porous membrane such as polyethylene or polypropylene, isolates the two electrodes from each other, allowing the transfer of ions. The electrolyte is an ionic conductor while not permitting electron conduction between the two electrodes. For lithium ion batteries, it is comprised of a solvent with a dissolved salt that increases the ionic conductivity.

A schematic of a Lithium Ion battery is shown in Figure 2.3. Both the positive and negative electrodes consist of lithium intercalation materials.

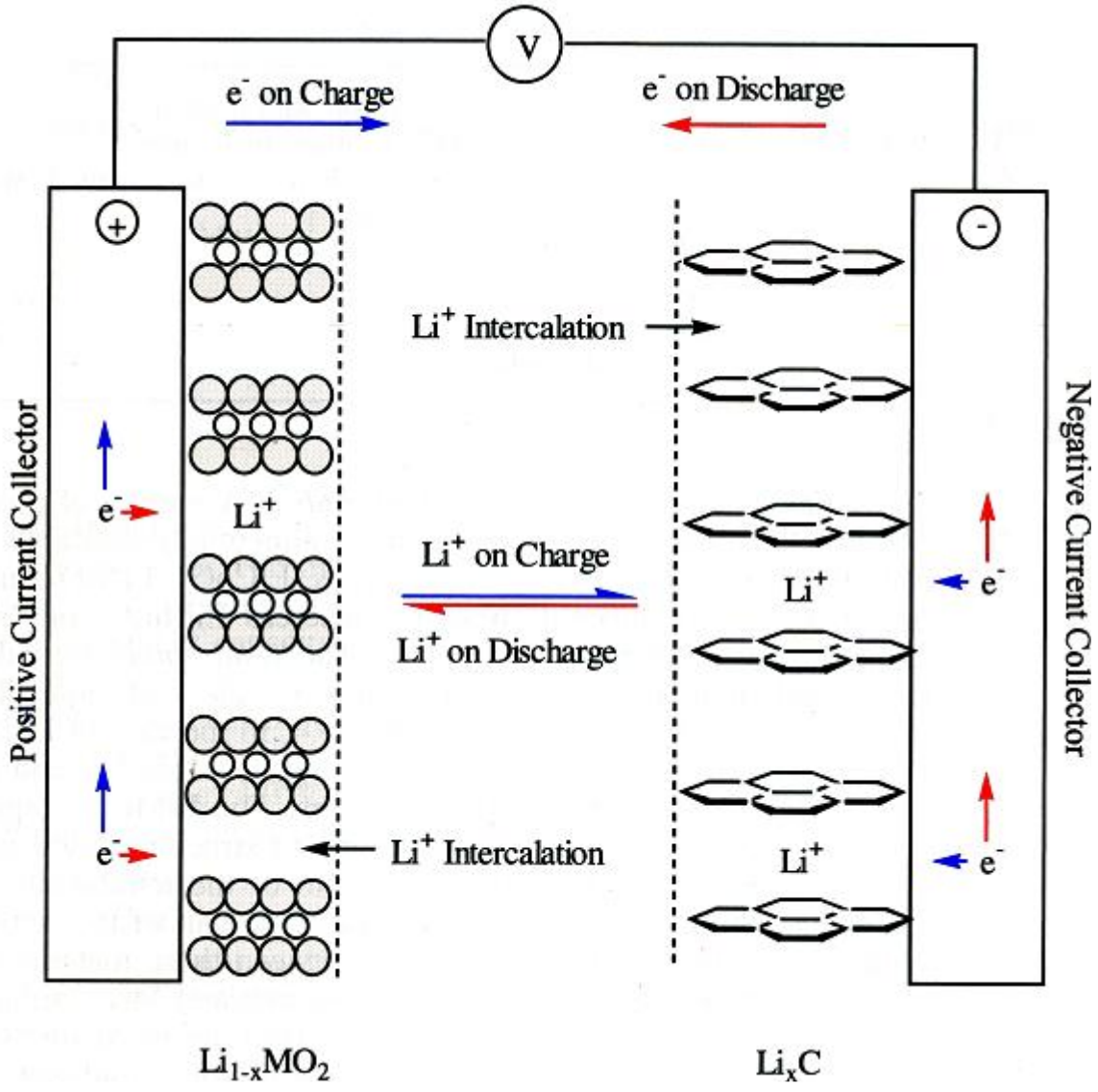

Figure 2.3: Lithium Ion cell concept in charge and discharge mode [29]

As the battery is charged and discharged, lithium ions (Li^+) exchange between the cathode and anode. The cathode, or positive electrode, is comprised of a metal oxide with a layered structure such as Li_xNiO_2.

The metal oxide is mixed with an inert binder such as Polyvinylidene Fluoride (PVDF) and a conductive carbon, a high surface area carbon or graphite in small quantities using N-

Methyl Pirolidone (NMP) to dissolve the PVDF. This mixture is laminated to aluminum foil which serves as the current collector.

The anode, or negative electrode, is comprised of a graphitic carbon which is a layered material. The carbon is mixed with a non-fluorinated polymer binder and laminated to copper foil which serves as the current collector. Although copper is heavier, it is used in this case, because lithium will alloy with the aluminum on the anode and be removed from the system causing a loss of energy and capacity. The chemical reactions for the positive electrode, negative electrode, and overall are shown in Equations 2.1, 2.2, and 2.3.

The chemistry of the cells being tested for this study is as follows:

Positive: Lithiated Nickel Manganese Cobalt oxide blended with Lithiated Manganese (M) oxide based with conductors and binders on an Al substrate

Negative: Graphite based with binder on Cu substrate

Electrolytes: $LiPF_6$ salt with a blend of organic solvent and additives.

Separator: Microporous Polyolephene material

$$\text{Positive} \qquad LiMO_2 \underset{\text{discharge}}{\overset{\text{charge}}{\rightleftharpoons}} Li_{1-x}MO_2 + xLi^+ + xe^-$$

Equation 2.1

This is the reaction at the positive electrode

$$\text{Negative} \qquad C + xLi^+ + xe^- \underset{\text{discharge}}{\overset{\text{charge}}{\rightleftharpoons}} Li_xC$$

Equation 2.2

This is the reaction at the negative electrode

$$\text{Overall} \qquad LiMO_2 + C \underset{\text{discharge}}{\overset{\text{charge}}{\rightleftharpoons}} Li_xC + Li_{1-x}MO_2$$

Equation 2.3

This is the overall chemical reactions

One of the greatest advantages of the Lithium Ion chemistry is its high energy and high power density, which makes it well suited for use in hybrid electric vehicle batteries. A significant disadvantage of the chemistry relates to safety. Some of the components which comprise current lithium ion batteries e.g., electrolyte, carbon, and intercalated lithium are reactive, which tends to make the automotive companies cautious. Table 2.1 lists specific advantages and disadvantages.

Table 2.1: Advantages and disadvantages of lithium ion batteries. [29]

Advantages	**Disadvantages**
Sealed cells; no maintenance required	Moderate initial cost
Long cycle life	Degrade at high temperature
Broad temperature range of operation (-30 to 60°C)	Need for protective balancing circuitry
Long shelf life	Capacity loss or thermal runaway when over-charged.
Low self-discharge rate	
Rapid charge capability	Venting and possible thermal runaway when crushed or short-circuited
High rate and high power discharge capability	
High coulombic and energy efficiency	Cylindrical designs typically result in lower power density than NiCd or NiMH
High specific energy (Wh/kg) and energy density (Wh/L)	
No memory effect	

Many design options exist for the lithium ion chemistry. They can be either prismatic or spiral wound design. Figure 2.4 shows the prismatic design and Figure 2.5 shows the spiral wound design. Both the prismatic and spiral wound designs can be used for either a high-energy or a high-power cell, depending of the thickness of the electrode.

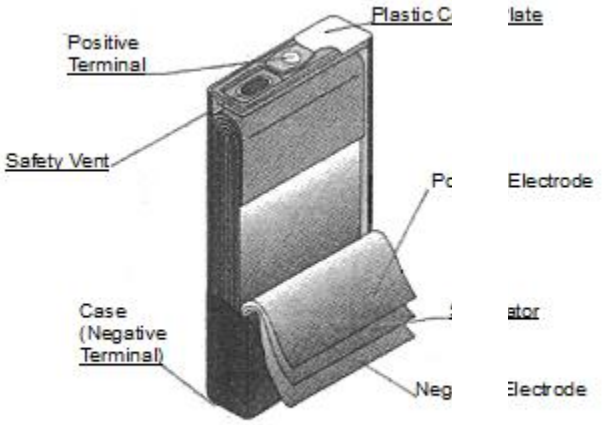

Figure 2.4: Prismatic design [29]

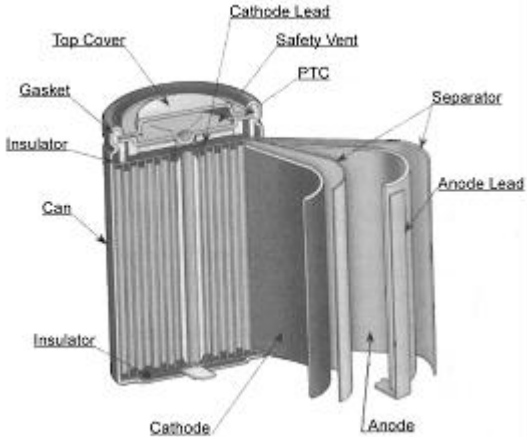

Figure 2.5: Spiral wound design [29]

Lithium ion cells have been made using button cell hardware, pouches, and stainless steel cans. The container must be well sealed and can only be vented to mitigate an explosion through a pressure relief device since the material is extremely sensitive to air and water, which can rapidly cause substantial degradation of performance.

2.3 Roadblocks to Battery Use in Vehicles

Calendar life, cost, abuse tolerance and cold-temperature performance comprise the unmet goals in the FreedomCAR Partnership for Li-Ion batteries. Abuse tolerance issues may be mitigated with engineered safety features such as vents and additives while cold temperature issues can be ameliorated by actively heating the cells or using special low-temperature electrolytes. Battery calendar life must be designed into the cell. Thus, a need exists to develop an accelerated calendar life test which can be performed in a small fraction of the 15 year time, (calendar life goal) and yet give realistic results and provide a predictive capability for similar battery chemistries. Additionally, the calendar life of the lithium ion batteries, although projected to be able to meet the goals, had never been tested for verification of that fact. The goal of this work was to quantify performance degradation of the battery. Capacity fade, power fade, and resistance rise can be extrapolated to estimate the calendar life of a cell over the temperature range of interest.

Power fade is the most limiting and thus the primary indicator for end of life determination. By FreedomCAR definition, once the full-scale battery pack power drops below 45,000 watts, the battery has reached end of life conditions for either the cycle life test or the calendar life test. The HPPC test [5], a procedure used by battery testers to determine the battery's power capability with its accompanying energy capability, measures power

fade. Power fade can be determined after multiple repetitions of the HPPC test as a function of time. Power fade is often attributed to a buildup of the solid electrolyte interphase (SEI) through lithium corrosion, which is also related to capacity fade and contributes to power fade. However, initial buildup of SEI is imperative to the life of a lithium ion cell. It serves as a protective layer preventing further chemical interaction of the electrode with the electrolyte. However, the continuing growth of the SEI layer with time leads to increasing cell impedance and a reduction in power and energy performance. The SEI is insoluble in the solvent, electrically insulating, but is still permeable to Li+ ions. The protective layer on the surface of the carbon serves as an electrolyte, which has a transference number of one, i.e. passes 100% of ions but 0% of electrons [31]. Power fade can also be attributed to the decrepitation of the cathode material and a buildup of solid materials on the surface of the cathode that leads to an increase in impedance. The known acceleration factors include SOC (battery state of charge), cycling, charge rate, discharge rate, rest period frequency, voltage limitations and temperature. No simple deterministic relations exist for SOC or cycling, but some can be applied for temperature. Previous cycling tests performed at the Idaho National Laboratory have indicated that temperature shows the greatest effect on power fade. Temperature comprises a fundamental acceleration factor because of the kinetics associated with chemical-based batteries, and even though temperature-dependent testing requires more equipment, results can easily be applied to an Arrhenius based rate expression. The Arrhenius equation, first suggested by the great Swedish chemist Svante Arrhenius in 1889, constituted a part of his work on activation energy[*]. Thermodynamics, collision theory and transition-state theory support this temperature dependence of the reaction rate. Although the

[*] Arrhenius suggested that the specific reaction rate, kA(T), could be correlated using an equation.

reactions that cause power fade are difficult to quantify, it is known that most chemical reactions exhibit a dependence on temperature. Therefore, as the temperature increases, the reaction rate increases or reactions that cause power fade occur faster. If temperature directly affects calendar life, then the Arrhenius expression can be used to model the calendar life of a battery at various temperatures. Therefore, temperature can be used to accelerate a calendar life test for a given battery chemistry. The results can be used to construct a mathematical relation of power fade as a function of temperature and time. This model can be used to extrapolate calendar-life at normal operating conditions. The main caveat, the elevated temperatures must not introduce any new degradation mechanisms that do not otherwise occur at normal operating conditions, remains.

Power fade can be extrapolated to estimate the calendar life of a cell over the temperature range of interest. Calendar life can be estimated at 30°C not only for comparison with the FreedomCAR goals, but also to determine the calendar life of a battery at various temperatures.

2.4 Cycle Life

Cycle and Calendar life continue to be foci of improvement for lithium ion batteries as they were when Chilton and Cook imagined the first lithium cells [30]. Cycle life is defined as the number of 25 Wh cycles available from a battery before it fails to meet the 25 kW and 300 Wh FreedomCAR power and energy goals. Calendar Life is the amount of time with limited use available from a battery before it fails to meet the 25 kW and 300 Wh FreedomCAR power and energy goals. Since it doesn't have to be replaced as often, the longer the battery lasts, the lower the life cycle cost. Considerable effort has been expended

researching and quantifying cycle life in lithium ion batteries to correlate the amount of degradation caused by cycling and to investigate the origins of this degradation. Takei and coworkers investigated the cycle life capability of Sony cells using five different acceleration or stress factors for home-use electric load leveling systems [32]. These systems were required to complete 3500 cycles while retaining at least 70% of the initial cell capacity (0.875 Ah). The stress factors were charge rate (the rate or current used to charge the cell), discharge rate, a combined charge and discharge rate, depth of discharge, and temperature. Takei determined that temperature, which ranged from 10ºC to 50ºC, caused the highest acceleration while the charge rate, which ranged from 0.2C to 1C (the 1C-rate is the rate required to completely discharge a fully-charged cell in one hour with the 2C-rate being two times the 1C-rate), showed the second highest acceleration factor in deterioration of performance, half of the acceleration rate for temperature. However, if the charging rate were higher, the acceleration factor could be the equal to or higher than the temperature acceleration factor. Takei noted that the degradation reaction might be different at higher temperatures from those of the standard operation cycle life test conditions. However, analyzing any change in cell component materials at the end of testing verified any secondary reaction mechanisms [32].

Bogel et al. similarly identified the acceleration parameters such as ambient temperature, depth of discharge, and peak power demand [33]. Additionally, he points out that rest periods also play an important role in accelerated testing by adding a new dimension to the testing and that can either improve life or accelerate degradation. Laboratory results for lead acid batteries showed a cycle life of more than 700 cycles, but in actual vehicle testing, researchers obtained only 300 cycles. Consequently, Bogel and his team conclude

that a balance must be made between performing the tests quickly and developing an accelerated life test with a proven correlation to forecast expected life [33].

Takeno et al. performed an in-depth study on the cycle life of cell phone batteries by looking at capacity fade and impedance rise for various test patterns for mobile phones and states of charge at 50°C. They determined that the capacity fade increases in proportion to the number of cycles and the average charge [34].

Popov et al. also studied the capacity fade and resistance rise in cycled Sony Li-ion cells using different discharge rates at ambient temperature [35]. The results showed a definitive dependence of capacity fade on the discharge rate. The higher the discharge rate, whether it is the 1C, 2C, or 3C-rates, the higher the capacity fade after 300 cycles. Their initial results showed that the discharge rate had very little effect on the capacity fade until 50 cycles, but began to play a greater role as cycling continued. In addition, by taking reference capacity measurements after every cycle, the 1C-rate degraded linearly. The capacities of the 2C-rate and 3C-rate cells drop quickly in the first few cycles followed by a linear degradation mechanism like the 1C-rate cell. Further investigation with half-cells, which allows the capacity fade at each electrode to be quantified indicated that the anode (the negative electrode) is responsible for more of the capacity fade of the whole cell as the discharge rate is increased, up to twice that of the cathode for the 3C-rate. In addition to the capacity fade that was measured, resistance rise was also quantified, that was intrinsically coupled with the capacity fade. Similar to the capacity fade results, the resistance increases with discharge rate. The resistance rise appears to be related to a buildup of an insulating, protective layer, the SEI, solid electrolyte interphase, that builds up on the surface of the carbon particles. Scanning Electron Microscopy revealed that the higher the discharge rate, the more the

cracks developed on the surface film protecting the lithiated carbon. These cracks caused of increased capacity loss as the electrolyte continued to react with the lithium in the carbon as each crack exposed new LiC_6. Equations 2.4 shows the proposed solid electrolyte interphase reaction sequence of the intercalated lithium as it reacts with the electrolyte. Figure 2.6 shows a graphical representation of the SEI buildup on the anode [35].

$$2Li^+ + 2e^- + 2(CH_2O)CO[EC] \Rightarrow$$
$$CH_2(OCO_2Li)CH_2OCO_2Li + CH_2CH_2 + 2Li^+ + 2e^- + (CH_2O)CO[EC] \Rightarrow$$
$$Li_2CO_3 + C_2H_4 + Li^+ + e^- + CH_3OCH_2CH_3[DMC] \Rightarrow$$
$$CH_3OCO_2Li + CH_3$$

Equation 2.4 Solid electrolyte reaction EC is Ethylene Carbonate and DMC is Dimethyl Carbonate

Striebel and co-workers took an in-depth look at the changes to the cathode and anode in the lithium battery as a result of cycling at temperatures of 60ºC and 25ºC as well as at Depth of Discharge (DOD) ranges of 70% and 100% [36]. They found that the higher the temperature and the higher the DOD, the greater the degradation. Furthermore, using extensive analytical techniques such as X-Ray Diffraction (XRD), Fourier Transform Infrared (FTIR), Transmission Electron Microscope (TEM), Nuclear Magnetic Resonance (NMR), Current sensing Atomic Force Microscopy (AFM), and Micro Raman analysis of the cathode and anode, they developed an understanding of the cause of the capacity fade and rise in impedance. Solvent reduction on the anode most likely caused the loss of capacity, which was determined to be a linear reaction with cell test time. The room temperature cells at ~25°C showed that the composition of the SEI, and the disorder in the graphite on the

surface of the anode roughly correlated with the extent of the lithium consumption or the capacity loss. On the cathode, TEM and NMR results showed evidence of crystalline defects and degradation of the Li-Ni environment, which was proposed to be the cause of the capacity fade overall and the impedance rise of the cell. Current sensing AFM also showed that the electronic conductance of the surface of the cathode diminished significantly and the loss of conductance increased for the 60ºC cell [36].

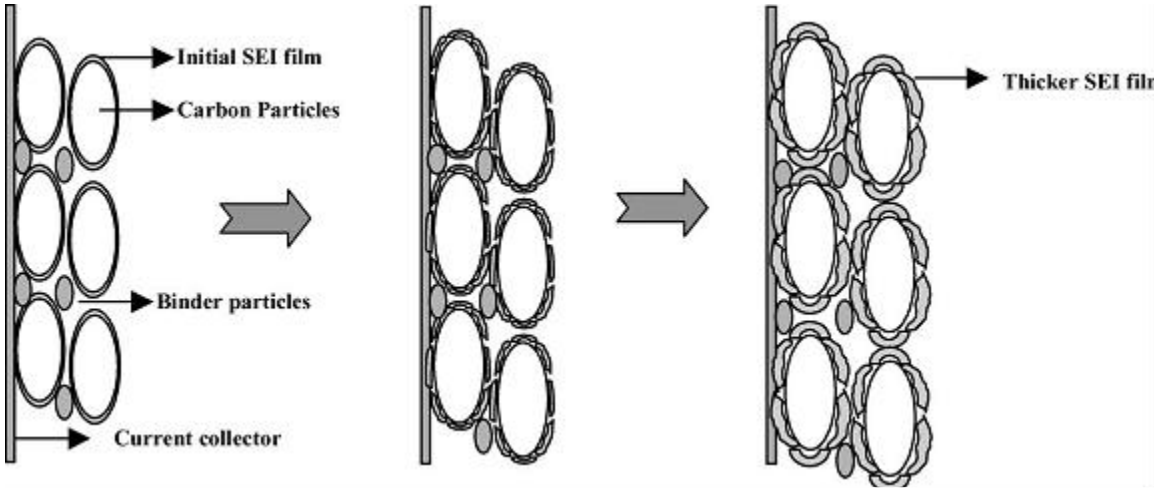

Figure 2.6: SEI buildup mechanism [35]

2.5 Calendar Life

In addition to the cycle life studies researchers have performed, they have investigated calendar life and the degradation mechanisms associated with lithium ion batteries. However, most of the researched technologies did not show very long life capabilities. Asakura and colleagues found that temperature and charge voltage had a significant effect on calendar life. Their results determined that a 15ºC temperature increase

cut the cell life in half and a 0.1 V increase in charging voltage also cut the cell life in half [37].

Takeno et al. studied the calendar life of cell phone batteries by looking at the impedance rise and capacity fade at various states of charge [34]. In terms of impedance rise, storage deterioration affects the lifetime of the battery the same as cycle deterioration. However, if capacity fade is combined with impedance rise, they found that storage deterioration affects the lifetime of the mobile phone more than cycle deterioration for their storage and cycling parameters [34].

2.6 Aging Mechanisms

Some researchers have concentrated more on understanding the different mechanisms behind cell degradation than on the testing that results in degradation. The Vetter et al. summary covers the aging mechanisms not only for the anode, but for the cathode as well [38]. Impedance growth has been directly linked to the power fade and is caused by the growth in the SEI as well as the overall composition of the SEI. It was noted that when the SEI initially forms and throughout life, gaseous electrolyte decomposition products, such as CO_2, CO, hydrogen, methane, ethylene, and propylene are released. Studies indicate the breakdown or cracking of this layer and the subsequent buildup of the new SEI to cover the newly exposed lithiated carbon causes the growth of the SEI at elevated temperatures as has been previously discussed. Researchers note that this SEI changes morphology and composition at elevated temperatures. Cycle life creates more dramatic changes than calendar life at elevated temperatures. The elevated temperature is proposed to change the organic SEI, which supposedly has lower ionic conductivity to an inorganic SEI that is more

stable and less easily penetrated by solvent molecules and thus has a higher ionic conductivity. The volume changes during intercalation and deintercalation are considered to be on the order of 10%, and thus have a minor impact. However, exfoliation, the process of breaking of pieces of the electrode layer by layer and particle cracking due to solvent co-intercalation, causes degradation and will contribute to aging. The growth of a surface layer causes for capacity fade and some power fade in lithium ion batteries. Figure 2.7 shows a graphical representation of some of the aforementioned degradation mechanisms. Additional mechanical or electronic mechanisms, such a contact loss between the carbon particles and collector or other carbons as well as changes in the electrode porosity, can affect aging. Table 2.2 is a summary of the causes, effects, and influences on aging for the anode. As seen in the table, many interactions can lead to capacity or power fade which can either be accelerated by usage or mitigated during the manufacturing process and thus affect the life of the anode.

Just as there are many different mechanisms that cause aging in the anode, the cathode also suffers capacity and power fade as a result of specific aging mechanisms, such as aging of the active material; degradation or changes of electrode components like conducting agents, binder, and corrosion of the current collector; oxidation of electrolyte components and surface film formation; and interaction of aging products with the negative electrode. Figure 2.8 shows an overview of the basic failure modes in the cathode. These basic mechanisms can then cause power or capacity loss in the cathode as shown in the flowchart in Figure 2.9. Additionally, the cathode can also suffer

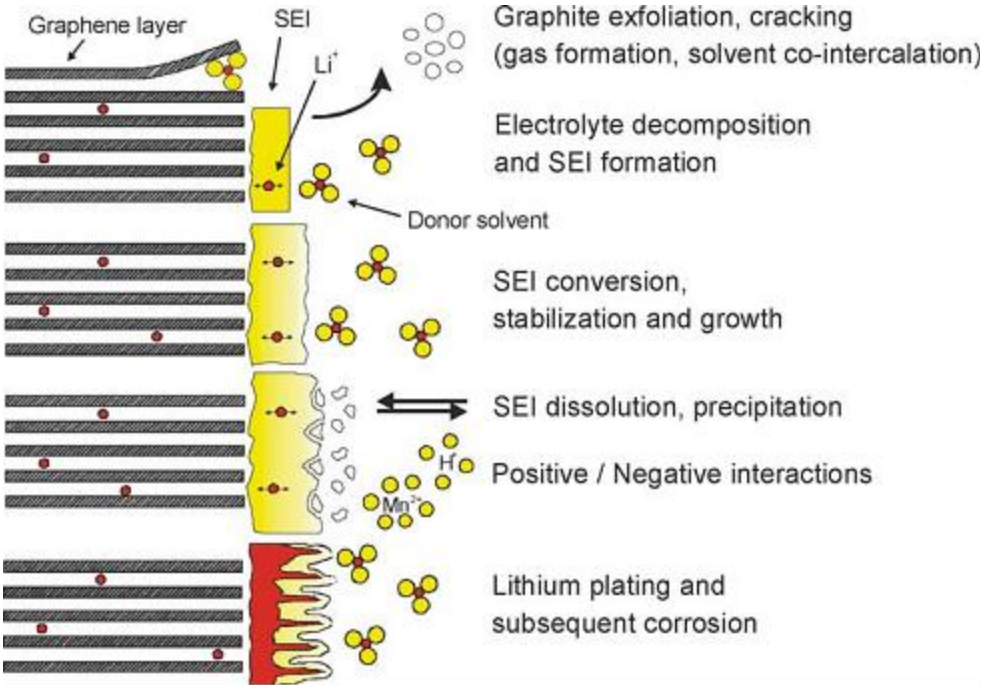

Figure 2.7: Changes at the anode/electrolyte interface [38]

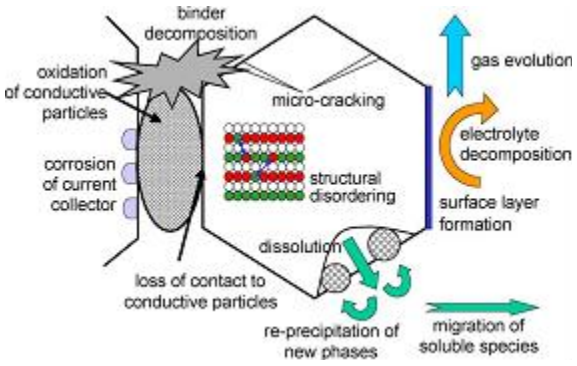

Figure 2.8: Overview on basic aging mechanisms of cathode materials [38].

degradation due to surface alteration as shown in Figure 2.10. A considerable increase in interfacial impedance, which results in power loss, comprises the most prominent failure mode in cathodes of high power batteries. In addition, the decomposition of electrolyte,

evolution of gas and the formation of a rock salt type of structure can lead to an increase in surface impedance and more power loss. [38]

Table 2.2: Lithium-ion anode aging [38].

Cause	**Effect**	**Leads to**	**Reduced by**	**Enhanced by**
Electrolyte decomposition	Loss of lithium	Capacity	Stable SEI	High temperatures
(→SEI) (Continuous side	Impedance rise	fade	(additives)	
reaction at low rate)				
Solvent co-intercalation,	Loss of active	Capacity	Stable SEI	Overcharge
gas evolution and	material	fade	(additives)	
subsequent cracking	(graphite exfoliation)		Carbon pre-	
formation in particles	Loss of lithium		treatment	
Decrease of accessible	Impedance rise	Power fade	Stable SEI	High temperatures
surface area due to			(additives)	High SOC (low
continuous SEI growth				potential)
Changes in porosity	Impedance rise	Power fade	External pressure	High cycling rate
due to volume	Overpotentials		Stable SEI	High SOC (low
changes, SEI			(additives)	potential)
formation and growth				
Contact loss of active	Loss of active	Capacity	External pressure	High cycling rate
material particles due to	material	fade		High DOD
volume changes during				
cycling				
Decomposition of binder	Loss of lithium	Capacity	Proper binder	High SOC (low
	Loss of mechanical	fade	choice	potential)
	stability			High temperatures

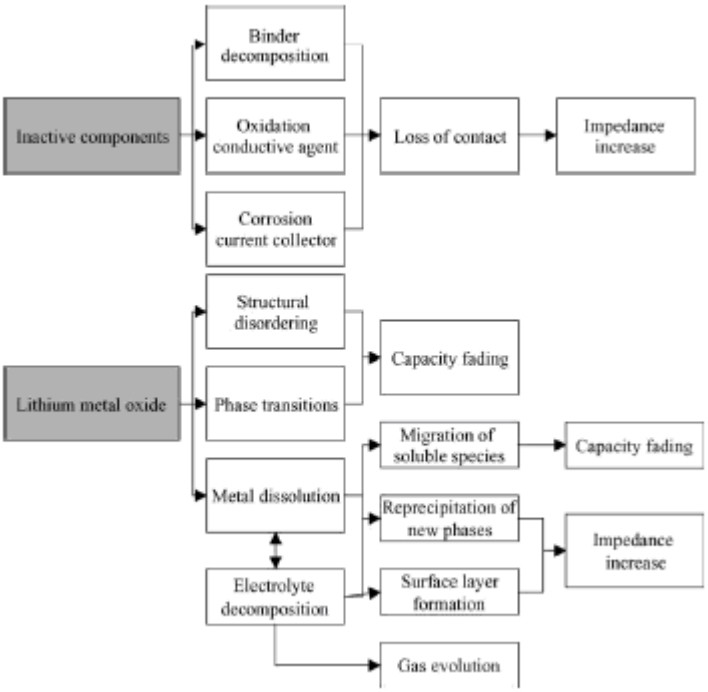

Figure 2.9: Cause and effect of aging mechanisms of cathode materials [38].

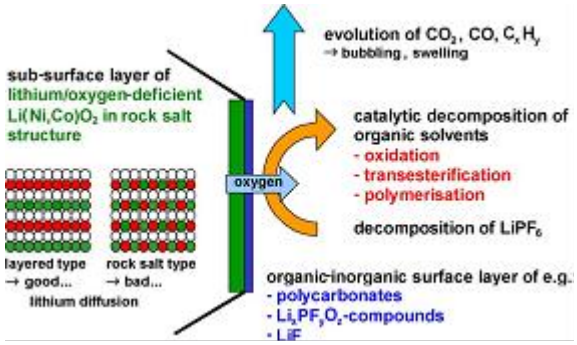

Figure 2.10: Mechanisms of surface alterations of lithium nickel cobalt oxide electrodes in $LiPF_6$ based electrolytes [38].

2.7 Aging Studies

In addition to all the research being performed on lithium ion batteries by scientists and engineers in national laboratories and universities, lithium ion battery manufacturers like Saft, in Bordeaux, France, have begun to publish their in-house research to elucidate the life

issues associated with their batteries. The testing by Broussely et al. focused on capacity fade as a function of temperature at 15, 30, 40 and 60°C. The fade mechanism is modeled by an Arrhenius expression [39]. The primary stress factor is temperature with state of charge showing a lesser secondary influence. Results at 40°C after 1 year showed no measurable loss. The most widely accepted concepts for irreversible capacity loss point to side reactions between the active materials and the electrolyte. The positive active materials will be oxidized while the negative active materials will be reduced. It was concluded that all Li-ion systems suffer reversible capacity losses in the range of a few percent per month over temperature ranges of 15°C to 60°C over the lifetime of the battery, but the effect is not observed until the excess capacity in the positive electrode is used up at 15°C, 25°C and 40°C. A significant difference in the initial capacity fade rates at 25 and 60°C exist when compared with the fade at 60°C being the larger of the two[39].

Both cells tested at 25°C and 60°C were designed to be positive limited at 25°C, which means that the positive electrode cannot accept all the lithium that is available for intercalation from the negative electrode. Thus, the capacity at 25°C, the bottom curve (with the square symbols), does not show any fade until the excess lithium in the system is consumed after four months. However, at 60°C, the top curve (with the diamond symbols), the cell exhibits a higher and negative limited capacity. Consequently, the capacity, limited by the negative electrode at 60°C, shows no initial stability and decreases continuously. In fact, after the excess lithium is consumed at 25°C, the fade rates are similar, as shown in Figure 2.11. This shows that the negative electrode is primarily responsible for capacity fade.

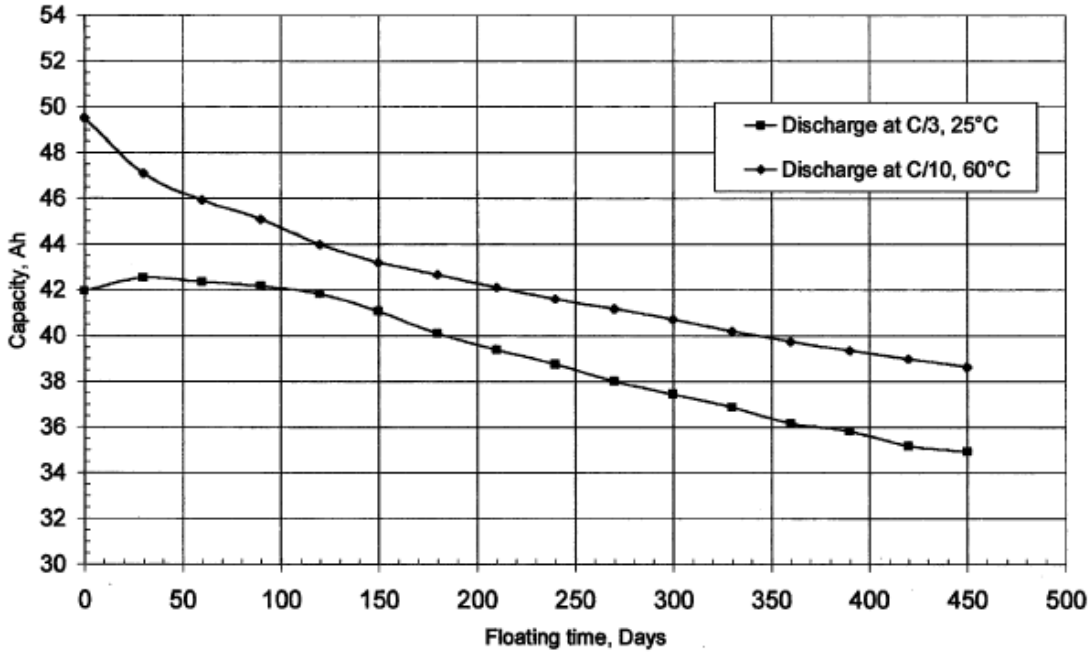

Figure 2.11: Anode limited versus cathode limited capacity loss [39].

After a year of storage testing at 60°C the negative electrodes were removed from the cell, washed in water, vacuum dried, and reassembled versus a lithium metal electrode. The negative electrodes were able to cycle versus a lithium reference electrode at the same initial, beginning of life specific capacity and polarization. This same procedure was performed with the positive electrode. The results showed an increase in polarization, or the change in potential from the equilibrium state as a result of current flow, which would tend to affect the power characteristics but not the measured effect of the capacity. Although the positive material had the same crystalline structure that they started with, the polarization observed seemed to indicate that some reactions occurred on the surface to increase the electrical resistance of the material. The author states that the Saft high-energy Li-ion design produced

in 2001 show an outstanding calendar life capability, which is enhanced by the unique property of the nickel-based oxides to provide a lithium reserve [39].

Another paper from Saft by Sarre et al. shows Partnership for a New Generation of Vehicles (PNGV), cycling results at 20 and 40°C for a lithiated nickel oxide positive electrode, Li $Ni_xCo_yAl_zO_2$ with vinylene carbonate as the electrolyte additive, which is one of the additives used to extend life [40]. The results of the work are shown in Table 2.3, which gives life predictions for various applications. As seen in the table, the calendar life prediction for the hybrid application at 30°C is 15 years, which happens to coincide with the previous PNGV and the new FreedomCAR calendar life goals [40].

Table 2.3: Life prediction for various Saft lithium-ion designs [40]

Application	**Average conditions**				**Life**
	SOC (%)	DOD (%)	Temp (°C)	Cycle Numbers	(years)
Automotive					
Hybrid	50	5	30	500000	15
Electric	100	80	30	1500	5
Stand-by Telecom or UPS	90	Variable	30	5000	15
Space					
GEO	90	60	20	2500	20
LEO	80	20	25	50000	8

Sarre et al. reveal some of their cycling and storage testing data as the properties of the nickel mixed oxides are presented. Power fade for testing at 20°C is negligible while the fade at 40°C is around 7% after 700 days. Peak power retentions for 12 months at 25, 40, and 60°C show an increase for the two lower temperatures and a decrease of ~7% at 60°C.

In addition to the cycling results, their calendar life results show that the goal of 30 seasons, which they equate to 15 years is exceeded for GEO (Geosynchronous Earth Orbit) satellite cycling for their VES 120 space cell, a Saft cell designation [40].

In another article, Broussely et al. [41] discuss a long cycle-life test that was performed using C size cells. The test only measured the capacity for the Dynamic Stress Test (DST) style cycles (an Electric Vehicle type of cycle) and shows the capacity loss of 40% after 1000 cycles at 100% depth of discharge. After the 1000 cycles, a cell postmortem analysis was performed on these cells. The results showed that 91% of the initial capacity was recovered after a low rate charge and that the capacity loss shown after 1000 cycles was of a 'kinetic' nature, or transport limited. It was determined that no significant lithium corrosion was occurring at room temperature, which shows the excellent stability of the SEI for the carbon for this application. They also looked at the positive electrode to investigate changes in the structure and texture of the material. XRD and SEM studies were performed, but they were unable to come to a conclusion of the structural refinement, or change in the structure of the positive from the XRD studies. It was noticed that there was some increase in polarization of the positive on the "high voltage part" from the SEM studies [42].

Broussely et al. performed a Saft Lithium-ion chemistry specific-summary of the main aging mechanisms that affect their chemistry during cycle life and calendar life testing. The basic concept behind energy degradation is a transformation of the active materials into inactive phases that reduce the cell capacity, and/or increase cell impedance or lower the operating voltage. The power loss experienced during life is directly related to impedance growth. It is proposed that aging during storage is primarily due to side reactions that result from thermodynamic instability, while cycling degrades the performance through kinetically

induced effects such as volume variations, concentration gradients, or the rate of electron transport. Although the aging during storage and cycling are often considered additive, secondary effects or interactions cannot be ruled out. Cycle life degradation is caused by a degradation of the active materials reversibility that occurs during phase transformations as a result of lithium insertion. This degradation can be accelerated by improper electrolyte composition, discharge rates, temperature, and voltage limits. The degradation is caused by a buildup of a passivation growth layer on the anode, which must be stabilized in order to obtain good life characteristics. This buildup reduces the electrode porosity and is proposed as one of the first-order parameters controlling capacity fade on cycling. Volume changes of the negative electrode during cycling also result in a degradation of the SEI layer, which cause an immediate repairing of this layer, thereby requiring the use of more of the available lithium, in what has been referred to by the Saft investigators as lithium corrosion. One method used to reduce the volume variation in the anode is to have excess lithium available in the cell to prevent complete delithiation of the anode. It has been determined that the 10% volume variation of the anode occurs during the first 20% of lithium insertion. Their calendar life studies have shown that the thermodynamic stability of the materials in the cell will govern the aging. This relates directly to the buildup of the SEI layer. Although this phenomenon, once formed allows the use of the negative electrode in the presence of the organic electrolyte, this layer is not totally impervious to additional cracking, which results in additional formation of SEI. As a consequence, lithium corrosion is a function of time during storage or calendar life testing. An SEI model has been proposed that had been derived from their experimental data of the following form that allows the estimation of time for a specified layer thickness.

This model shows a very good correlation with actual lithium loss data. The initial extrapolation of one year of data still continues to follow the same trend after four years of testing. However, this model requires knowledge of the amount of lithium in the cell at the beginning of life.

A similar analysis has been performed for the cathode. Spectroscopic analysis at Lawrence Berkley National Laboratory showed a loss of electronic conductivity and solid deposits on the surface of the positive electrode as previously discussed. In addition to this increase in impedance, high temperature and high voltage have a tendency to induce CO_2 gas evolution as well as increase the oxidizing properties of the positive electrode against the electrolyte. It is proposed that organic species that have been reduced at the negative electrode migrate to the positive electrode where they are oxidized to produce protons and organic radicals that may polymerize. This reaction leads to reaction products such as insoluble salts and polycarbonates, which deposit on the surface and pore structure of the positive electrode, causing an increase in polarization and impedance of the electrode. These deposits do not protect the cathode from continued reactions like the SEI does on the anode. Additionally, it has been determined that high temperature limits life because of the evolution of CO_2 gas. Figure 2.12 shows that although the Cobalt based cathodes started out at a low initial pressure, their pressure continued to rise as time progressed, whereas the pressure for the Nickel based cathodes rose quickly initially, but then quickly leveled off as time progressed [43].

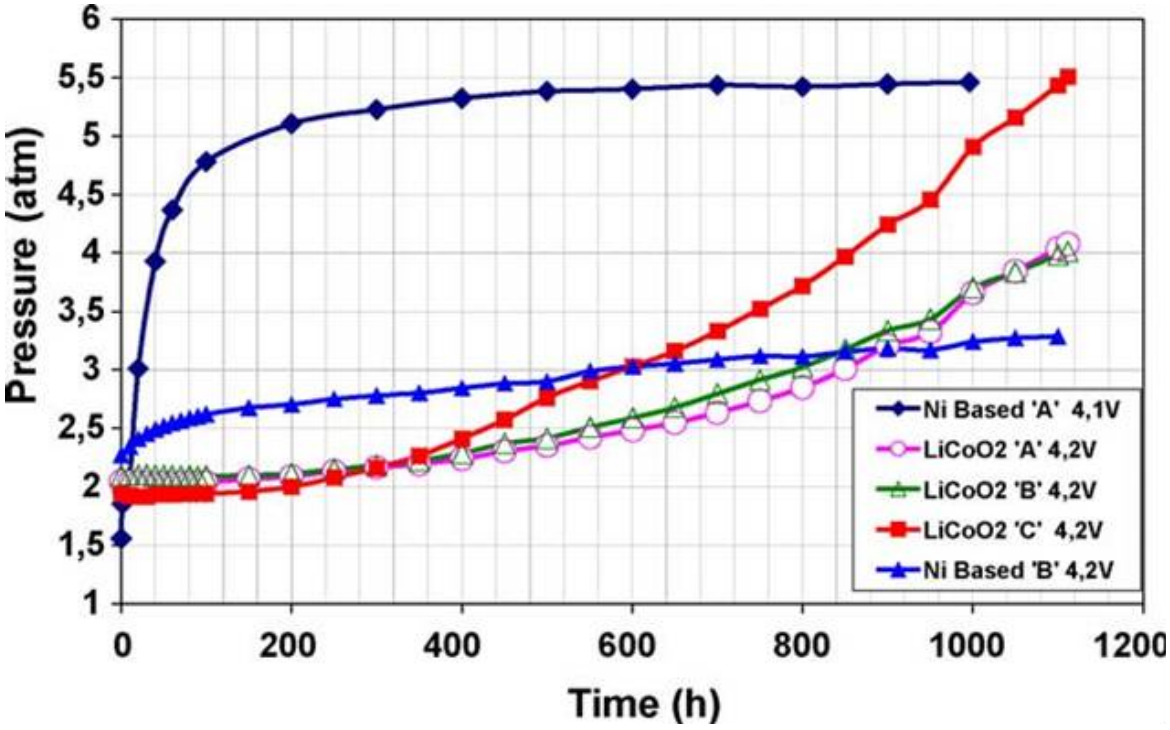

Figure 2.12: Pressure evolution in laboratory cells stored at 60°C, 100% SOC, for several positive materials [43]

The optimization of both calendar and cycle life has been a concern of researchers since Chilton Jr. and Cook et al. [30] first discussed "Lithium Nonaqueous Secondary batteries," in their quest for a long life satellite battery. While some parameters such as high temperature, high voltage, and high usage rates accelerate the degradation reactions that occur in lithium ion batteries, extra care during the manufacturing and formation process, optimization of cathode and anode capacity, and the usage of Vinylidene Carbonate can extend the life of current lithium ion technologies. The in-depth diagnostics of failure mechanisms is invaluable to help focus future research and development efforts to continue to extend life.

Although there is a good understanding of failure mechanisms, there has been little effort to isolate the degradation to one or both electrodes. The use of reference electrodes is crucial to isolate performance issues between the positive and negative electrode.

2.8 Reference Electrodes

Wu et al. embedded a reference electrode into an 18650 can cell during the prototype manufacturing [44]. The reference electrode showed the changes in charge-transfer resistance and the film resistance for the cathode and anode. The reference electrode also shows the increase in the cathode voltage versus reference during cycling, indicating that the cathode is limiting the performance of the whole cell. Other researchers have proposed that the $LiCo_2$ materials begin to structurally degrade, trapping the lithium ions so that can no longer participate in intercalation [45].

Verbrugge et al. use a reference electrode to interpret the electrode behavior in a lithium ion cell. Their analysis indicates that the interfacial resistance plays a dominant role in limiting the available capacity at high current rates. They use the reference electrode voltage to understand the fractional occupancy of the negative electrode, as shown in Figure 2.13. This figure is a representation of the voltage of the negative electrode versus a lithium reference. The jagged line represents experimental data, while the smooth curve represents the potential vs. lithium as predicted by their model. Aside from the noise in the experimental data, the results match up very well.

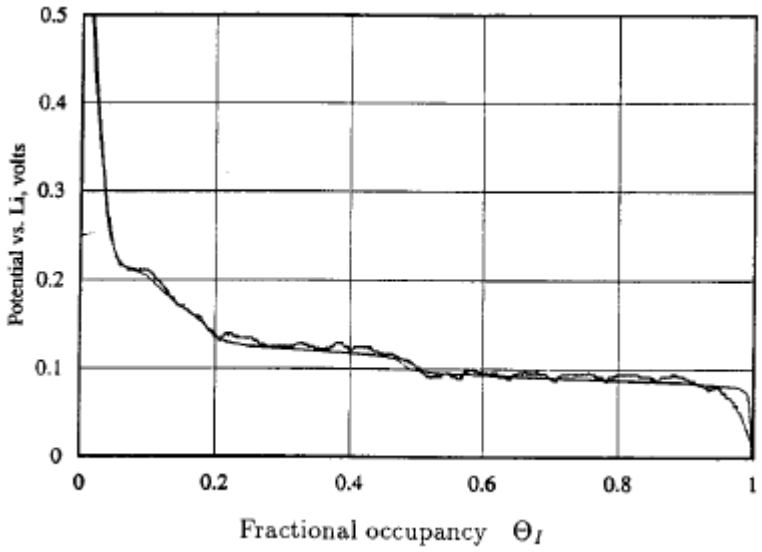

Figure 2.13: Fractional occupancy versus potential for the negative electrode [46]

Wu et al. inserted a reference electrode into the center of a spiral wound cell inside a glove box and cycle life tested the cell. Results showed that the cathode limits the current capability of the cell. Additionally, based on the HPPC tests and discharge tests, the cathode is also responsible for the capacity and resistance degradation that resulted from cycling. However, due to the nature of the reference electrode insertion, the cell was no longer hermetically sealed during cycling and this may have increased the rate of degradation. Figure 2.14 shows the change in resistance from the beginning to the end of cycle life testing, the lack of change in the negative electrode resistance, and the change in the positive electrode resistance. The term "ASI" used in the graph is the area specific impedance, or another way to show the resistance based on the area of the electrode. This methodology is used to compare the resistance of electrodes of different sizes.

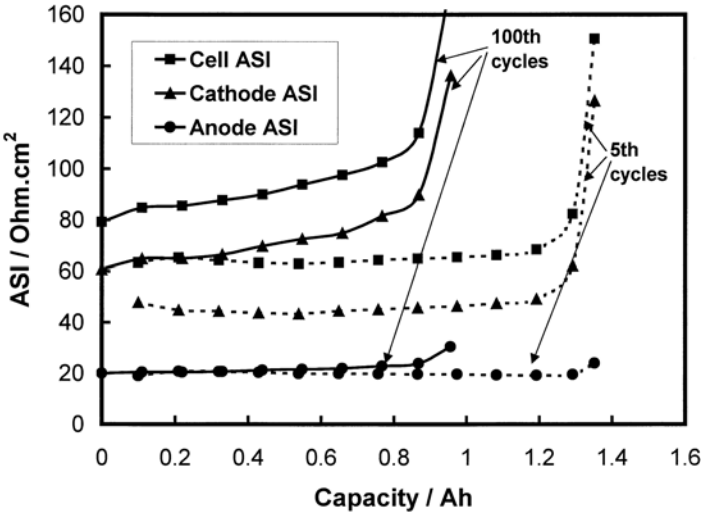

Figure 2.14: Fractional occupancy versus potential for the negative electrode [47]

Liu et al. investigated the performance loss of lithium ion batteries containing lithium iron phosphate as the positive electrode and a carbon negative, made by A123, in Boston Massachusetts systems. A reference electrode setup was designed to allow the cell to be tested in an excess of electrolyte with a lithium metal reference electrode. The bottom of the cell can was removed and dipped into the excess electrolyte in the beaker. Multiple temperatures, states of charge and discharge rates were evaluated during the course of the testing. The results from the electrochemical impedance spectroscopy and HPPC tests indicated no increase in impedance. However, a reduction in the capacity was observed from analyzing the charge-discharge profiles. Additionally, these results were confirmed by cycling a cell in the reference electrode setup for 700 cycles. Figure 2.15 shows the capacity degradation as seen by the isolation of the negative electrode using a reference electrode.

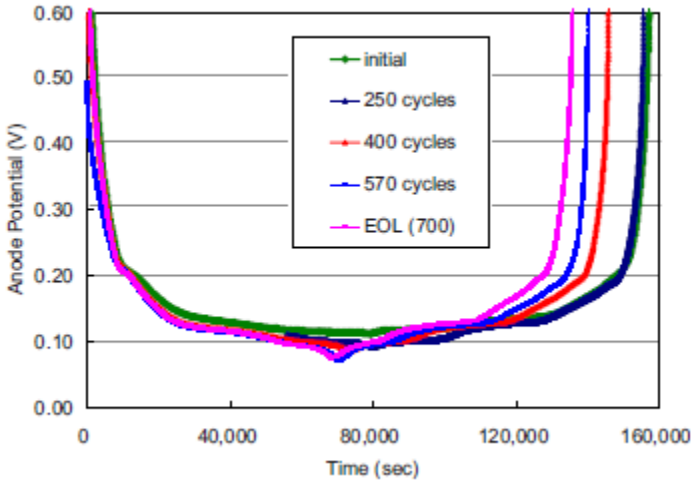

Figure 2.15: Evolution of charge/discharge profiles of the carbon negative during the battery's life measured with a lithium reference electrode. [48]

They determined that since the negative potential never reached 0 Volts, that the negative electrode never became fully intercalated. It was also observed that there is a reduction in the end of charge voltage on the carbon negative. This implies that the lithium concentration in the available interstitial sites increases with cell capacity loss [48].

Abraham et al. also constructed cells with reference electrodes. Electrodes, supplied by Quallion, (Sylmar California) were inserted into a cell fixture with a lithiated tin reference electrode. One drawback to using a cell fixture is the resistance of the cell may not be the consistent with cells that are produced through high volume manufacturing. The lithiated tin reference electrode had a tendency to drift toward the positive electrode voltage during the calendar life testing, indicating an unstable reference electrode. Most of the impedance rise was contributed to the positive electrode. At 3.85 V, there was no impedance rise at the negative electrode, but at 3.72 V, there was a 10% increase. He concluded that capacity fade reflects lithium consumption in the cell, which is a result of reactions that cause a growth of

the solid electrolyte interphase (SEI) film that is formed on the graphite-anode surface. Capacity fade can also be attributed to the inability of the oxide particles to accept and deliver lithium at the required rates [49].

Cycle and calendar life for lithium ion cells have certainly improved from the early days due to use of more robust materials and better manufacturing methods. While many parameters can affect life such as depth of discharge, discharge or charge rate, etc., increased temperature appears to have the greatest effect on life. The degradation methods for capacity loss and resistance rise focus on a buildup of the SEI on the negative electrode and a decrepitation (micro-cracking, structural disordering, and dissolution) of the active material of the positive electrode. However, reference electrode work is crucial to further understand the degradation mechanisms that occur during calendar and cycle life aging. Most of the work done with reference electrodes shows degradation on the positive electrode. Consequently, in order to further improve lithium ion technology, reference electrodes coupled with long term testing must be used to identify which electrodes limit overall cell capacity and resistance performance.

The improvement of calendar life, abuse tolerance and cold-temperature performance of lithium ion technology will enable widespread use in automotive applications. In situ reference electrodes can provide the researcher a window into the battery to greater understand the individual electrodes contribution to life, abuse tolerance and cold-temperature performance. With understanding, new materials or methods can be developed to overcome these limitations without sacrificing the benefits of the high energy and high power capabilities offered by lithium ion chemistries.

Chapter Three: Materials and Methods

3.1 Task A. Cell Testing

A large number of cells were subjected to performance testing at various conditions to evaluate capacity fade, resistance rise, and power fade and performance degradation. The cells and the apparatus used for testing are described below.

3.1.1 Cells

1.2 Ah high power lithium ion cells representing commercially available cell technology at the start of testing in 2009 that could meet the energy and power needs of a PHEV were used in the study. The cycle life and calendar life of these cells was unknown at that time. The commercially available 1.2 Ah, 18650-size[†] cylindrical, high-power lithium-ion cells (see Figure 3.1), -employed a blended positive-electrode active material (i.e., Ni–Mn–Co layered oxide and spinel manganese oxide), dissolved lithium salts in organic solvents, and a carbonaceous negative electrode.

Figure 3.1: Commercially available cells

[†] The designation "18650" refers to the dimensions 18 mm diameter and 65 mm axial length.

3.1.2 Tester

The battery tester was a Maccor model 4000 (Maccor Inc., Tulsa, OK) as shown in Figure 3.2, that is capable of either charging or discharging a battery over a voltage range of 5 V to 0 V at 30 A. A programmable battery tester, capable of not only generating the appropriate procedural algorithm required, also can limit the voltage and currents during the procedure for safety reasons. With the capability of monitoring the temperatures of the cell, it can stop the test if the temperature deviates from the specified range. The tester, a high precision testing station for battery and ultracapacitor testing worldwide, can provide high quality data to characterize the battery and perform the calendar life test. It is a highly accurate battery tester, with the uncertainty of the voltage measurement within $\pm$ 0.081% of full scale, ~ 4.05 mV, and the uncertainty of the current measurements within $\pm$ 0.13% of full scale, 78 mA [50, 51]. Temperature and reference electrode measurements were made via connection to the auxiliary voltage inputs.

Figure 3.2: Maccor 4000 battery tester (www.maccor.com)

3.1.3 Temperature Chambers

Vital to this work, the temperature chambers are maintain the appropriate temperature during testing and minimize daily temperature fluctuations that would otherwise occur in a

laboratory environment. Three Tenney Jr. temperature chambers, identical to the unit shown in Figure 3.3, made by Thermal Product Solutions, (White Deer, Pa) were used in the study. The batteries were placed inside the chambers. The electrical wires were connected to the batteries and then run through a hole in the side of the chamber to the Maccor 4000 battery tester. The temperature chambers also help by exhausting excess heat that is generated by the battery during testing and maintain a constant temperature during the test.

Figure 3.3: Temperature chamber

3.1.4 Testing Methods

The planned test was a long-term validation test to determine the validity and effect of the plug-in hybrid electric battery test procedures. This involves performing tests of a large number of cells at various conditions to evaluate capacity / power fade and performance degradation. Some of these cells were selected for further reference electrode testing later. Each of the baseline conditions involved testing of 10 cells, with 5 cells tested at the other conditions to give good statistical replication. The Maccor 4000 collected and recorded the results of the testing; time, voltage, current, etc., which were processed using HPPCALC, a software package that performs the necessary calculations and plots the results in Excel.

This study investigated the effects of temperature on calendar life, on CS cycle life, and on CD cycle life; the effects of SOC on calendar life and on CS cycle life; and the effects of rest time on CD cycle life. To track the capacity, energy, and power fade every 32 days, this study used RPT. During the RPT, a 7.1 W discharge test as well as a HPPC test was performed.

The following matrix shown in Table 3.1 was used for the cell testing phase.

Table 3.1: Cell testing matrix

Test Number	Cell #'s	Condition	Temperature (°C)	Battery Test Condition	Testing Focus
1	1-10	CD Cycle Life	30		CD Cycle Life Temp.
2	31-35		40		
3	41-45		50		
4	51-55		60		
5	26-30	Calendar Life	30	90% SOC	Calendar Life State of Charge
6	11-20			60% SOC	
7	21-25			30% SOC	
8	11-20		30	60% SOC	Calendar Life Temp.
9	36-40		40		
10	46-50		50		
11	56-60		60		
12	61-70	CS Cycle Life	60		CS Cycle Life Temp.

All testing was performed in accordance with the PHEV battery test manual [5] and the test plan [52]. The test plan included the appropriate ratings, safety precautions, specific procedures to be performed, and final disposition of the batteries upon completion of the test.

3.1.5 Test Procedure

Testing proceeded in two phases. The first phase of testing was characterization testing to establish the baseline performance for the battery. The second phase of testing was

the calendar or cycle life test, which established power and capacity fade behavior over time at various conditions. Measurements were made during the characterization testing and the cycle/calendar life testing. The characterization testing consisted of the following tests: Capacity, C_1/25 Capacity, and HPPC. The calendar and cycle life tests consisted of the pulse per day calendar life test and the RPTs. The RPTs consisted of a single capacity test and the HPPC test. All of these tests are further described below [5].

3.1.6 Capacity

The capacity test measures the capacity of a device in Ampere-hours at a constant discharge current. The C_1/1 rate is the rate which the cell can be discharge in exactly 1 hour. Discharge begins following a one-hour rest from a fully-charged state, either at the 7.1 W, rate or the HPPC current rate (~2.1 C_1/1), which is the equivalent of a 10 kW rate and is terminated on a manufacturer-specified discharge voltage limit, followed by a one-hour rest at open-circuit voltage. The HPPC-Current rate is used as the reference for capacity and energy measurement and as a 'standard' constant current rate for module and system-level testing. The test is repeated at least three times, but not more than ten times to verify the stability of the device's capacity. During most of the RPTs, 7.1 W discharge capacity tests (to a 2.7 V cutoff) as well as pulse power tests were performed. Charging in all RPTs was performed at the C_1/1 rate, except for the C_1/25 capacity tests. In both capacity tests, discharge from a fully-charged state is preceded and followed by a 1 h rest at open circuit and is terminated on the manufacturer's specified cutoff voltage, 2.7 V. The fully charged state is obtained by charging at the C_1/1 rate to 4.2 V, which is maintained until the current drops below 50 mA. The 7.1 W capacity test corresponds to the discharge rate of a single

cell in a 1400 cell pack at the 10 kW[‡] rate for 10 miles of all-electric range. This rate is not changed as capacity changes during aging from the original 1.2 Ah. This constant-power discharge test is used in place of the more common $C_1/1$ constant current discharge test used in HEV testing [53]. Depth-of-discharge (DOD) is taken to be the fraction of the rated capacity (i.e., 1.2 Ah) removed from the cell during a discharge, whereas in this work SOC is defined by the open-circuit voltage (as measured at the beginning-of-life [BOL, i.e., RPT 0] in a HPPC test). This definition of SOC simplifies the programming of the test equipment because the test programs do not have to be changed at each RPT. Therefore, only at Beginning of Life (BOL) is SOC = 1 − DOD. In the majority of published works SOC is based on a $C_1/1$ discharge capacity at each RPT to define 100% SOC, and intermediate values are coulombic fractions thereof.

3.1.7 $C_1/25$ Capacity

The $C_1/25$ (i.e., 50 mA to a 2.7 V cutoff) discharge and charge test also measures the device capacity in ampere-hours at $1/25^{th}$ the rate of the capacity test. The $C_1/25$ rate is the rate which the cell can be discharged in exactly 1 hour divided by 25. Discharge begins following a one-hour rest from a fully-charged state and terminates on a discharge voltage limit, followed by a recharge at the $C_1/25$ rate to the maximum voltage limit. This test normally shows the real capacity, unhindered by the limits of kinetics.

[‡] Approximately 10 kW will sustain an average passenger vehicle at typical freeway velocities. The 1400 cell pack meets the power and energy targets for a 10 mile PHEV in accordance with the Battery Test Manual [5].

3.1.8 Hybrid Pulse Power Characterization

The HPPC Test [5] measures the dynamic power capability over the device's useable voltage range using both discharge and regen (high rate charge) pulses. This test establishes the discharge power capability for a 10-second pulse and the charge power capability for a 10-second pulse as a function of depth of discharge. This test is performed during the characterization as well as during calendar and cycle life testing as part of the RPT. It is the main test by which the power and energy capability of the device are measured throughout life.

The HPPC test is made up of single repetitions at 10% DOD increments of a 5.3 A discharge pulse, 40-s rest, a 4.0 A charge pulse, separated by 2.13 A constant-current discharge segments to the next DOD, and followed by a 1-hour rest to allow the cell to return to an equilibrium state at open circuit. The test is initiated at 0% DOD, or full charge, and ends after completing the final profile at 90% DOD or when the manufacturer's minimum voltage is reached.

Figure 3.4 shows the pulse power characterization profile, which is performed using constant current with a cut-off between the manufacturer's maximum and minimum recommended voltages. The voltage and current measurements used for the discharge resistance are indicated at points t0 and t1, while the data points used for the regen resistance are indicated as points t2 and t3.

The HPPC Test is made up of single repetitions of the Pulse Power Characterization Profile, separated by 10% DOD (depth of discharge) constant current HPPC-current discharge segments, and followed by a 1-hour rest to allow the cell to return to an equilibrium state at open circuit voltage. The test is initiated at 0 % Depth of Discharge, or

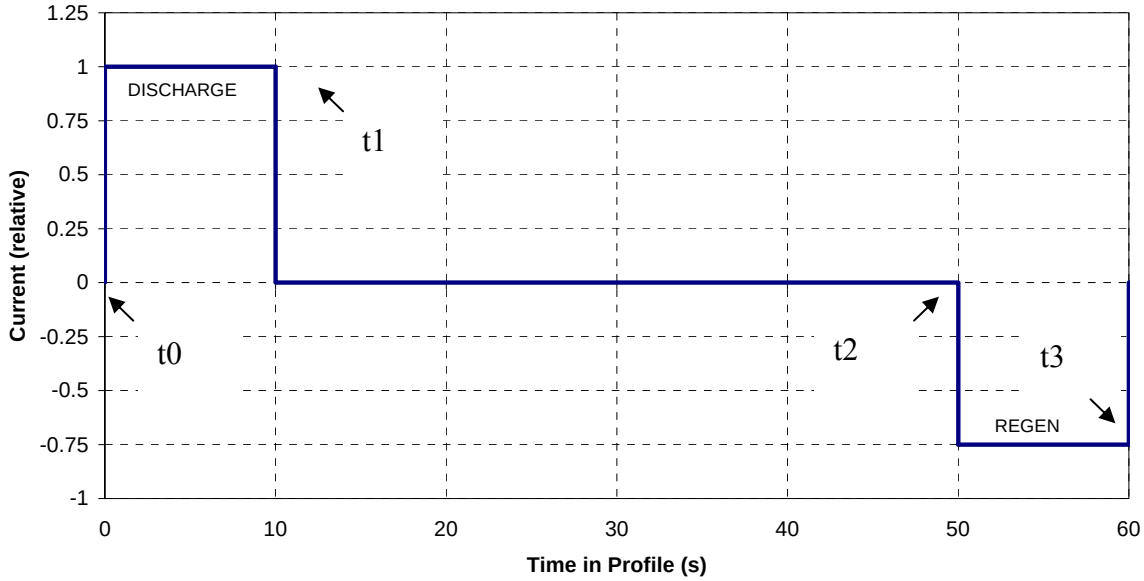

Figure 3.4: Pulse power characterization profile

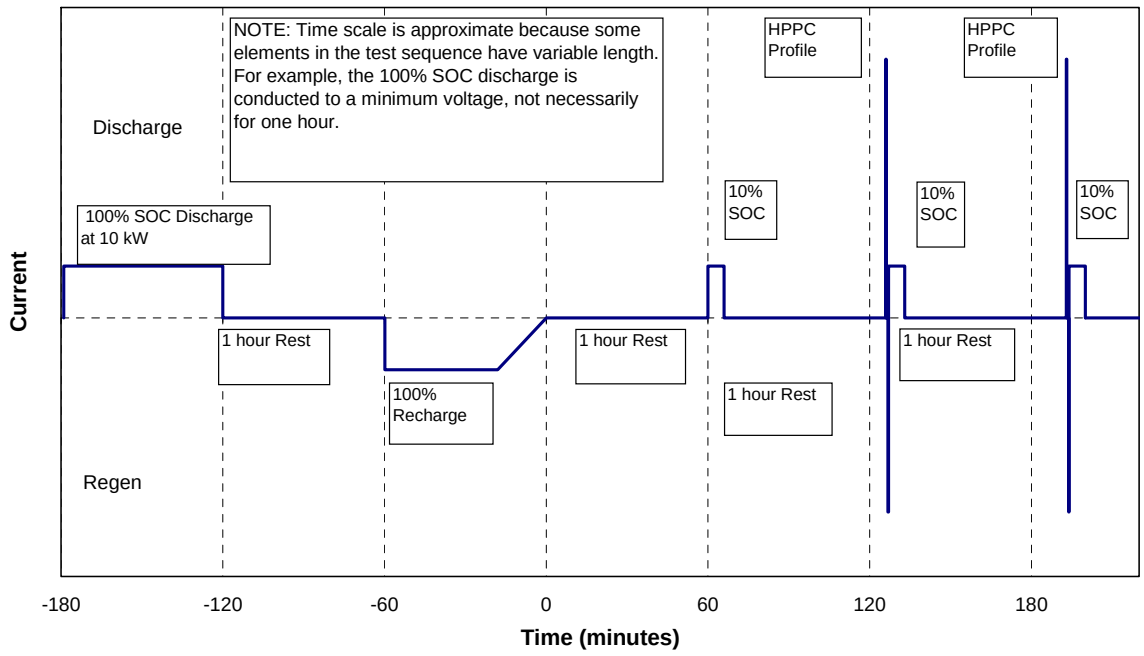

Figure 3.5: Initial hybrid pulse power characterization sequence

full charge and ends after completing the final profile at 90% Depth of Discharge or when the manufacturer's minimum voltage is reached. The initial sequence of profiles is shown in Figure 3.5. The complete HPPC Test is shown in Figure 3.6. The HPPC Test is normally performed at two different current levels, a low and high current level test. The low current test is performed at an HPPC-Current rate. The high current test is performed at 75% of Imax. Imax is the maximum recommended current that can be applied to the device.

The HPPC-Current, 2.1 A is a constant current that will closely resemble the steady state current during a 10-KW constant power discharge test. In order to relate the energy removed at the 10-kW rate and the energy removed during the HPPC Test, the "HPPC current" will be used for the 10% DOD (depth-of-discharge) constant current discharge segments.

The HPPC-Current is calculated using the formula below.

$$IHPPC = PCPDT/(Vavg * BSF) \qquad \text{Equation 3.1}$$

where IHPPC is the HPPC discharge current between pulses, PCPDT is the constant power discharge test power, and Vavg is the average voltage between Vmax, the maximum voltage and Vmin, the minimum voltage recommended by the manufacturer. For example, if Vmax = 4.2V and Vmin = 2.5V, and Vavg = (Vmax-Vmin)/2 + Vmin= 3.35V, and the BSF = 1400, and where PCPDT = 10-kW, then IHPPC = 10,000W/(3.35V * 1400) = 2.13 A. The BSF (battery size factor) is a scaling factor that allows cell results to be compared to pack results. This value is used extensively once the BSF is determined for the Capacity and HPPC tests.

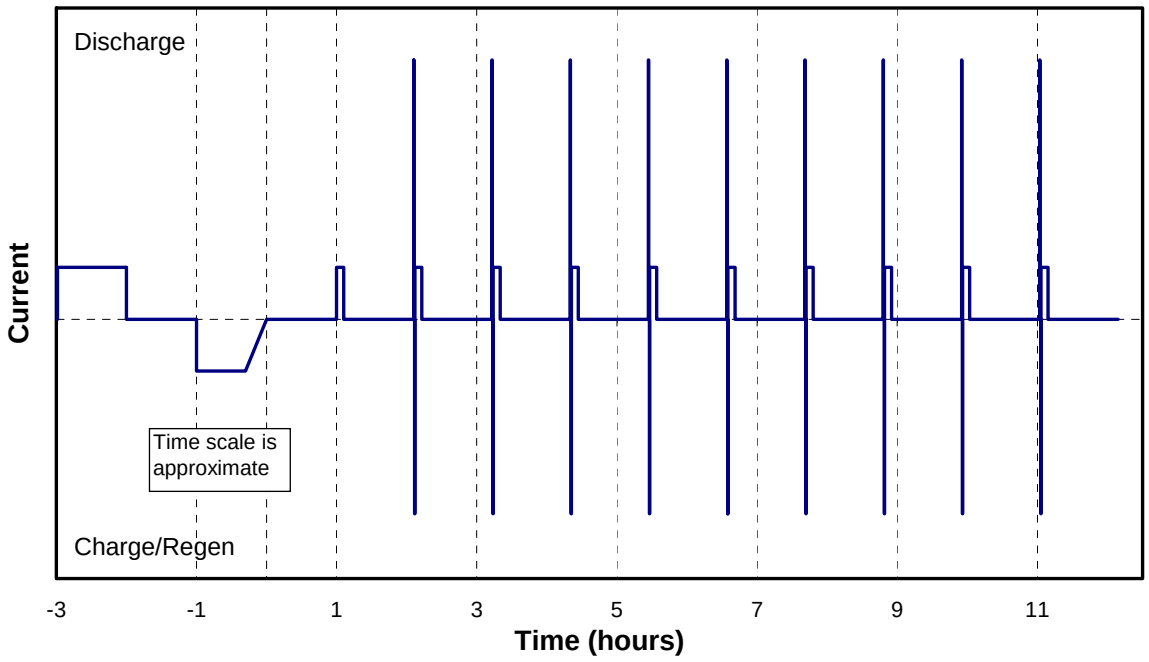

Figure 3.6: Complete hybrid pulse power characterization test

3.1.9 Calendar Life

The objective of the test profile is to demonstrate device life in the calendar life mode when subjected to limited energy use levels and at various temperatures and states of charge. The calendar life test is designed to evaluate degradation in power and capacity of a battery due to the passage of time with minimal usage. In this case only temperature and state of charge are used to accelerate the degradation. The test consists of discharging a fully charged battery to the appropriate state of charge. Once per day, the battery is subjected to the calendar life test profile, shown in Figure 3.7. After the pulse, it is left at open circuit voltage that correlates to the appropriate state of charge for the balance of the 24-hour period. The currents are chosen to correspond to the currents used during the HPPC test. The profile consists of a 10-s 5.3 A discharge pulse, a 50-s rest, a 4.0 A 10-s charge pulse, and a 300-s

taper charge to 3.90 volts (which in this case corresponds to 60% SOC). After the profile is completed, the cell remains at open circuit for the balance of the day. The 10 second discharge and regen resistance during the calendar life test profile can be compared to the HPPC test values at the appropriate DOD. The profile also incorporates a small recharge to return to the original state of charge prior to the implementation of the profile.

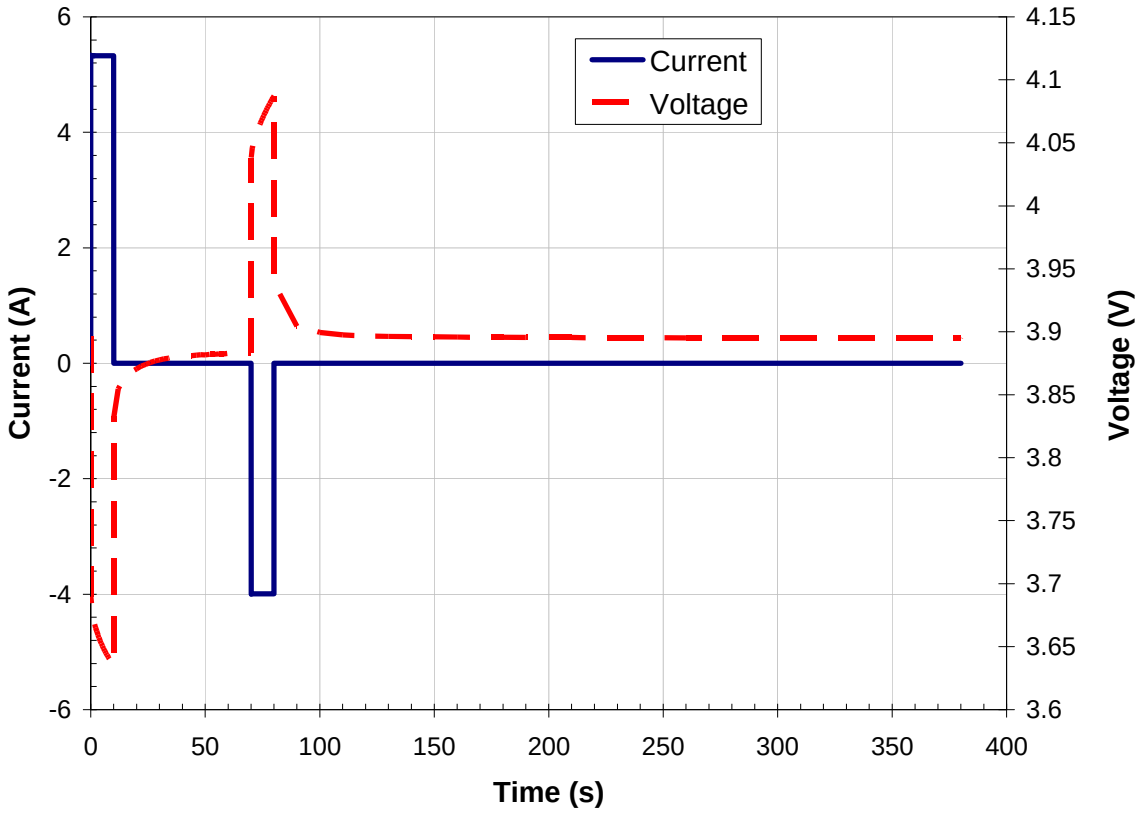

Figure 3.7: Daily pulse current profile (and example voltage profile) used to reset the cell OCV during the calendar aging regime. (Note: in all figures discharge current is shown as positive in sign and charge current is shown as negative in sign with respect to energy being removed from the battery).

3.1.10 Charge Sustaining Cycle Life

The objective of the test profile is to demonstrate device life in the Charge-Sustaining mode when subjected to different energy use levels and patterns appropriate to the targets. The charge-sustaining cycle life test is designed to mimic the hybrid electric vehicle operation of a Plug-In Hybrid electric vehicle. The energy is slowly drained out of the battery during the charge-depleting cycle life type of test at which point the battery operates like a hybrid electric vehicle, providing propulsion assist and regen within a narrow operating band. The cycle life test is performed by repeating the selected test profile at a fixed state-of-charge (i.e, the profile is charge-neutral). 30,000 cycles can be completed over the course of the 32 day test period. With 10 total test periods, 300,000 cycles can be completed. The profile is shown in Figure 3.8.

Each profile is a 90-s pulse profile intended to demonstrate the ability to meet the cycle life target of 300,000 cycles or the equivalent of 150,000 miles with a 3.56 Wh discharge swing, or a scaled a 50-Wh swing. The profile families transfer about 15 million watt-hours (MWh) respectively in and out of the device over 300,000 cycles. The test profiles are all defined at the battery pack level. They are scaled to the appropriate power levels for testing laboratory cells, full-size cells and module designs using the Battery Size Factor.

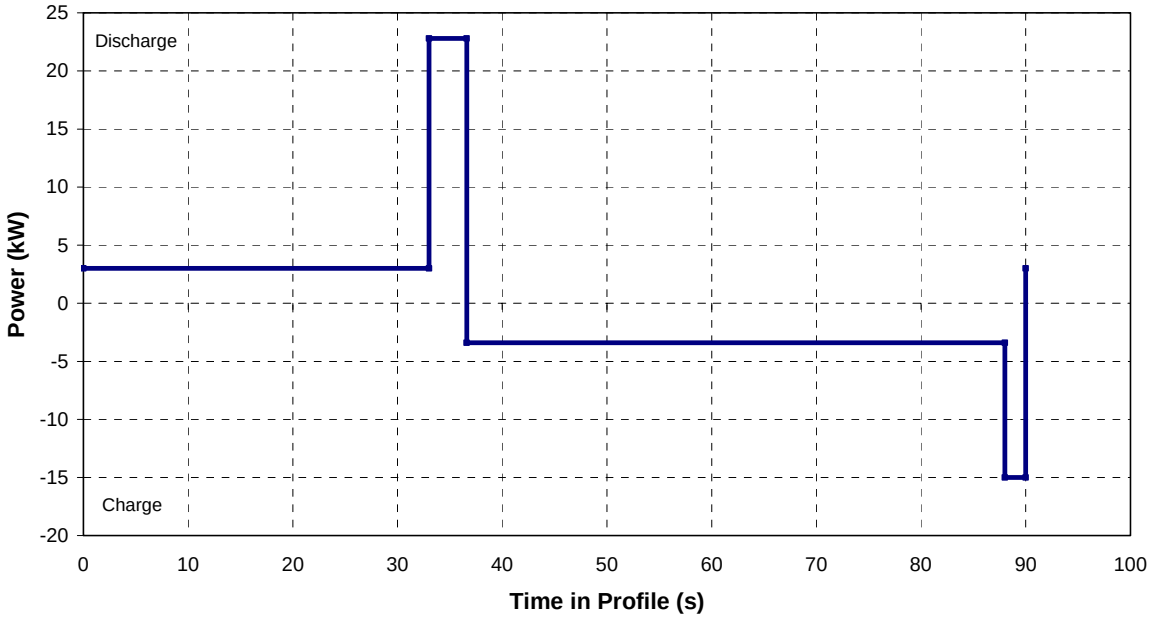

Figure 3.8: Charge-Sustaining cycle life system level test profile

This system level profile consists of a 33 second cruise step at 3.0 kW, followed by a 3 second discharge pulse at 27 kW, followed by a 52 second recharge step at -32 kW, and finally a 2 second recharge pulse at 18 kW. This profile represents the hybrid electric vehicle operation of a PHEV, where the SOC does not dramatically change. However, at the cell level the CS aging is performed by repeating the CS cycle life profile at 60% SOC 30,000 times in between RPTs, and consists of a 33-s low level discharge at 2.1 W, a 3-s discharge pulse at 19.2 W, a 52-s recharge step at 1.3 W (the last 10-s of the step are used to maintain the SOC at 3.89 V), and a 2-s charge step at 12.9 W and shown in Figure 3.10.

Each of the Charge-sustaining (50Wh) cycle life system level test profiles removes 50 Wh on discharge and is nominally charge-balanced (i.e., the profile has more charge than discharge to make up for inefficiencies) for a device that just satisfies the 90% efficiency target.

3.1.11 Charge Depleting Cycle Life

The objective of the test profile is to demonstrate device life in the Charge-Depleting mode when subjected to energy use levels and patterns appropriate to the targets. The charge depleting cycle life test is designed to monitor degradation in power and capacity of a battery due to the passage of time with maximal usage. In this case temperature, recharge rate, rest time, and initial depth of discharge are used to accelerate the degradation. The test consisted of discharging a fully charged battery the appropriate depth of discharge, normally 10% DOD. Multiple repetitions of the Charge-Depleting Cycle Life Test profile are performed

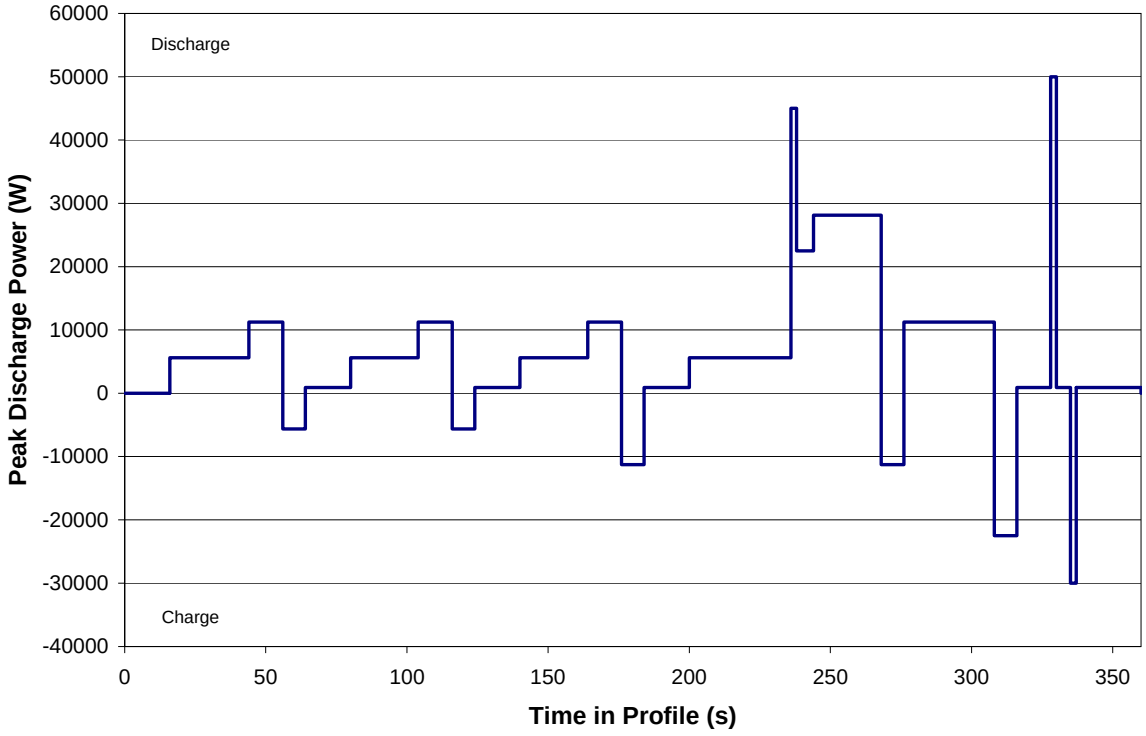

Figure 3.9: Charge-Depleting cycle life system level test profile

until the target energy is reached, i.e. some higher level of DOD. Recharge at the appropriate

recharge rate to the appropriate depth of discharge, normally 10% and repeat the test for 32 days. 500 cycles are completed for each block of 32 day testing until 5000 total cycles are completed.

Each profile is a series of constant power discharge/charge steps with a total duration of 360 seconds. The profile for the Minimum PHEV Battery is intended to demonstrate the ability to meet the Charge-Depleting cycle life target of 5,000 cycles (in sets of ~7 profiles per cycle) with a Charge-Depleting net energy of 3.4 kWh. The profile discharges 17 MWh respectively out of the device over 5,000 cycles.

At the cell level, the CD-aging cycle involves four consecutive steps: (a) repetition of the power profile in Figure 3.10 until 1.95 Wh of discharge[§] is removed (~ 5 profiles); (b) 15 minute rest, (c) recharge to 4.09 V (~90% SOC) using a 1.2 A constant-current charge (d) maintenance of 4.09 V until the current drops below 50 mA; and (e) another 15 minute rest. Steps (a) through (e) are repeated for 32 days (~ 500 cycles) when RPTs are performed and shown in Figure 3.10. Testing is stopped if 2.7 V is reached at any time during any of the aging profiles. The EOL is defined for this work as when aging is terminated, which is after 5 RPTs for CS and CD aging and after 6 RPTs for calendar aging. We define "EOL^{+}" for the cells chosen for reference electrode testing because these cells were put in cold storage (i.e., 0°F) after RPT 6 for approximated 1.5 y before reference electrode insertion. However, the CD-aged cell (i.e., Cell 53) reached 2.7 V the day after RPT 5 and remained in the chamber until RPT 6 was performed.

[§] Note that this corresponds to 80% of the 3.4 kWh for the 1400 cell pack.

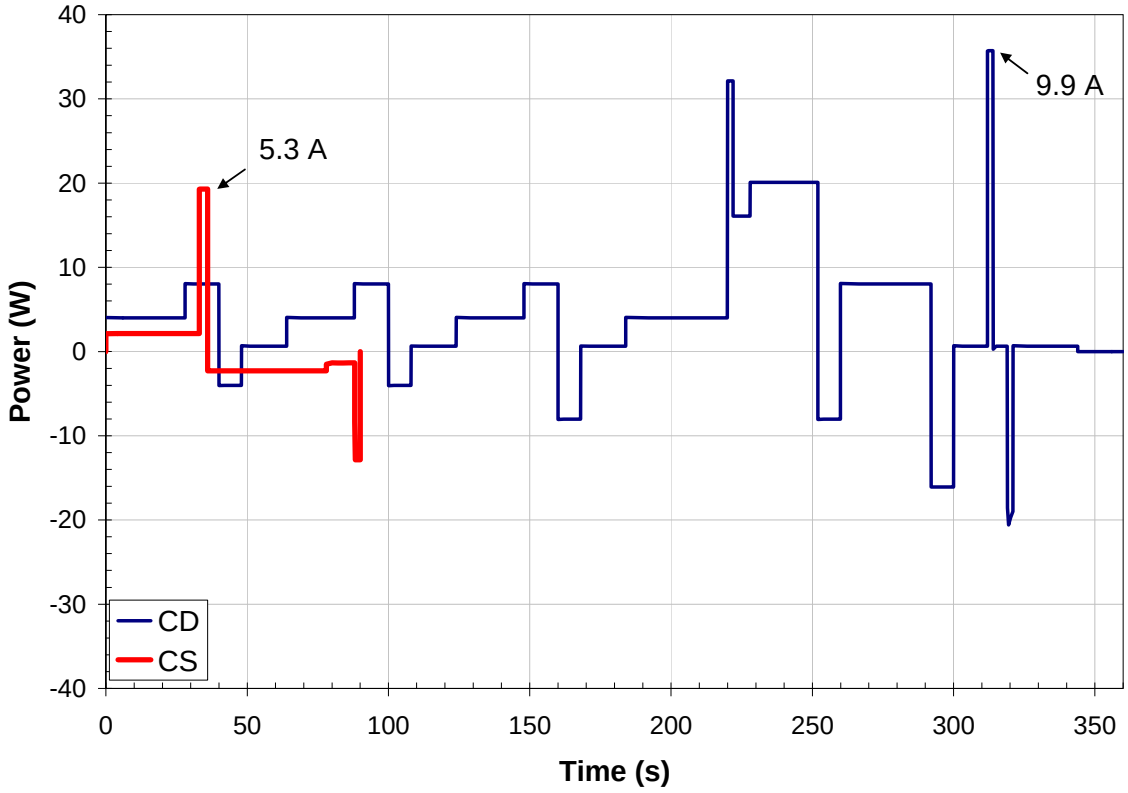

Figure 3.10: The power vs. time profiles used to cycle-age the cells, where the arrows denote the BOL maximum currents attained during the profile. The 90-s CS-aging and 360-s CD-aging profiles, respectively, are shown in red and navy.

3.1.12 Reference Performance Test

RPTs are a group of tests that track the performance, (capacity and resistance) of the battery at periodic intervals, e.g. every 32 days throughout life testing. The RPTs consist of a HPPC-Current constant-current discharge test and the low current HPPC test. These tests measure the capacity, energy, resistance and power throughout life testing [5].

3.2 Task B. Reference Electrode Testing

The improvement in service life of rechargeable lithium-ion batteries has resulted in their widespread adoption. While many aging parameters can affect life, such as depth-of-discharge, discharge or charge rate, and state-of-charge (SOC), increased temperature has been shown to greatly accelerate the aging processes and is very often used to expediently obtain aging information [54, 55, 56]. Aging is generally characterized by measurements of coulombic capacity and power (and/or resistance) at specified reference conditions during temporary interruptions of a certain aging regime. Proposed degradation mechanisms by Liu et al. for capacity loss [48] focus on buildup of a SEI [57] on the negative electrode and for resistance rise focus on decrepitation (micro-cracking, structural disordering, and dissolution) of the active material of the positive electrode [38,39, 40], shown in Figure 3.11. Although the cell voltage (i.e., positive vs. negative electrode) response is typically measured during aging studies, the employment of a reference electrode allows changes in the cell voltage to be ascribed to contributions from the individual electrodes.[**] The use of a reference electrode can therefore add crucial information to the understanding of the degradation mechanisms that lead to cell aging and is the primary focus of this work. The development of an *in situ* lithium-metal reference electrode is described, whereby the electrode is placed within the cell through a perforation and provides direct contact with the liquid electrolytic solution that saturates the cell's components.

A reference electrode provides a potential against which the potentials of the indicator electrode can be measured [29, 58]. The reference electrode also allows the measurement of

[**] Two reference electrodes are not necessary because the voltage of a single reference electrode connected to either the negative or positive electrode and the full cell voltage results in the voltage of the other electrode (vs. reference) by difference.

the potential in the solution. The potential difference between the solution and either electrode can be used to isolate electrode performance. An ideal reference electrode should be reversible (i.e., non-polarizable [58]) and the potential should remain constant during the measurement. However, no electrode can absolutely meet these criteria since no reference electrode is completely reversible or stable. In a lithium-ion system, the lithium metal reference electrode must be sufficiently stable in the electrolytic environment by not contributing to the reaction in the system and provide a known and stable thermodynamic potential over the period of use. Lithium metal with an electrolyte that is similar to the electrolyte in the cell is often the reference electrode of choice in these systems. This reference electrode, while not ideal, is sufficiently reversible and easily produced, and thus used, for this work [58].

Reference electrodes have been used previously in a variety of ways to study lithium-ion cell behavior. Commonly-used reference electrodes are inserted into the cell prior to the sealing of the outer casing material [44, 45, 46, 47]; however, this approach is not amenable to mass production and may alter the performance of the cell relative to one without an inserted reference electrode. Liu et al. [48] utilized a reference electrode by removing the end cap of a cylindrical cell and immersing both the cell and reference electrode in an electrolyte-filled vessel, with the reference electrode located outside of the cell [59], shown in Figure 3.11. These researchers conducted a cycle-aging regime on a cell in this configuration and reported voltage of the negative electrode (vs. Ref.) during several capacity tests as the cell aged. In contrast, in our studies the cells are aged prior to reference electrode insertion in order to minimize the impact of the lithium reference electrode insertion on the chemical processes involved in the cell over the long term. Liu et al. utilized a variety of cell

resistance characterization methods (via full cell voltage measurements) to show that the cell resistance did not increase during any of aging regimes imposed on their graphite/iron phosphate cells. Although the cells in our study employ a different positive-electrode material, a significant increase was observed in cell resistance throughout life that is attributable to the positive electrode through our reference electrode measurements. Other reference electrode designs have focused on the removal of a sample of one of the electrodes, which is introduced into a specially designed cell with a counter electrode and a reference electrode [44, 45]. These designs are capable of quantifying the capacity of the electrode but are inadequate to determine the original resistance contribution of the electrode from the original configuration.

The work reported here focuses on several cells selected for reference electrode measurements before and after aging and is a subset of a larger aging study of over 170 cells [60] conducted at Idaho National Laboratory. In contrast to other studies, the aging regimes in these cell life studies are specifically designed to represent usage in the environment of a plug-in hybrid electric vehicle (PHEV). Three general types of aging regimes are investigated: (1) calendar (i.e., zero-current) aging that minimizes the effects of the chemical and mechanical stresses induced by current throughput, (2) charge-sustaining (CS) cycle aging that would include these additional stresses in a limited range of operation, and (3) charge-depleting (CD) cycle aging which would include further additional stresses due to larger operational ranges. Aging data can aid in the development of improved battery control strategies. The ability to evaluate changes in the performance of the individual electrodes during life studies with a reference electrode will be of particular importance to the

development of computer battery-aging models; elucidation and validation of proposed aging mechanisms will lead to model improvements.

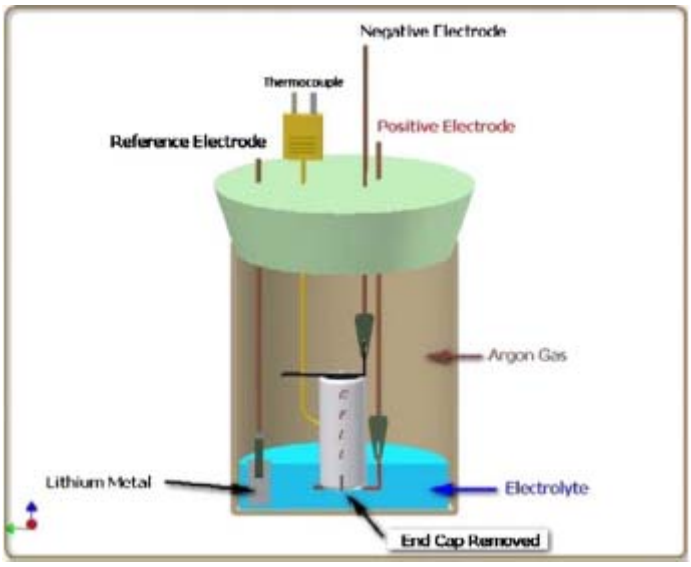

Figure 3.11: In-Situ reference electrode [47]

3.2.1 Reference Electrode Implementation

Since the intrusion of oxygen and water into a cell would result in severe performance degradation, perforation of the cell was accomplished in the confines of an argon-filled glove box as well as all testing after the insertion of the reference electrode. A specifically designed apparatus was used to cut a plug out of the negative end of the cell for reference electrode insertion after the cell was x-rayed to determine the optimal location of the perforation.

3.2.2 X-Ray Imaging

Figure 3.12 gives an X-ray image of the cell focused to show the electrode coatings of the winding, which appear as the whiter annulus-shaped region that fills the can. This figure indicates that it is more appropriate to drill into the negative terminal than the positive because there is less material to drill through. The cell's burst disk resides in the crimped region, which is part of the positive cap shown in the figure.

Figure 3.13 shows an x-ray of the negative end of the cell focused to show the internal tab and the external nickel foil tab that was welded to the negative terminal to assure a low-ohmic connection.[††] The optimal location for perforation (denoted as an "X" in the figure) was chosen based on avoidance of the internal folded metal tab and the external tab and the opportunity to drill into empty gas space. The inset figure superimposed in Figure 3.13 gives an expanded view of the negative end of the cell shown in Figure 3.12, where the feathery, thin gray lines protruding above the winding annulus are the individual sheets of separator between the positive and negative electrode coated foils.

[††] For the same reason, an external nickel foil tab was welded to the positive terminal and may also be discerned in Figure 3.13.

Figure 3.12: X-ray of the 18650 cell focused to show the electrode winding that fills the can. The negative end of the cell is at the top of the figure and the positive terminal is at the bottom.

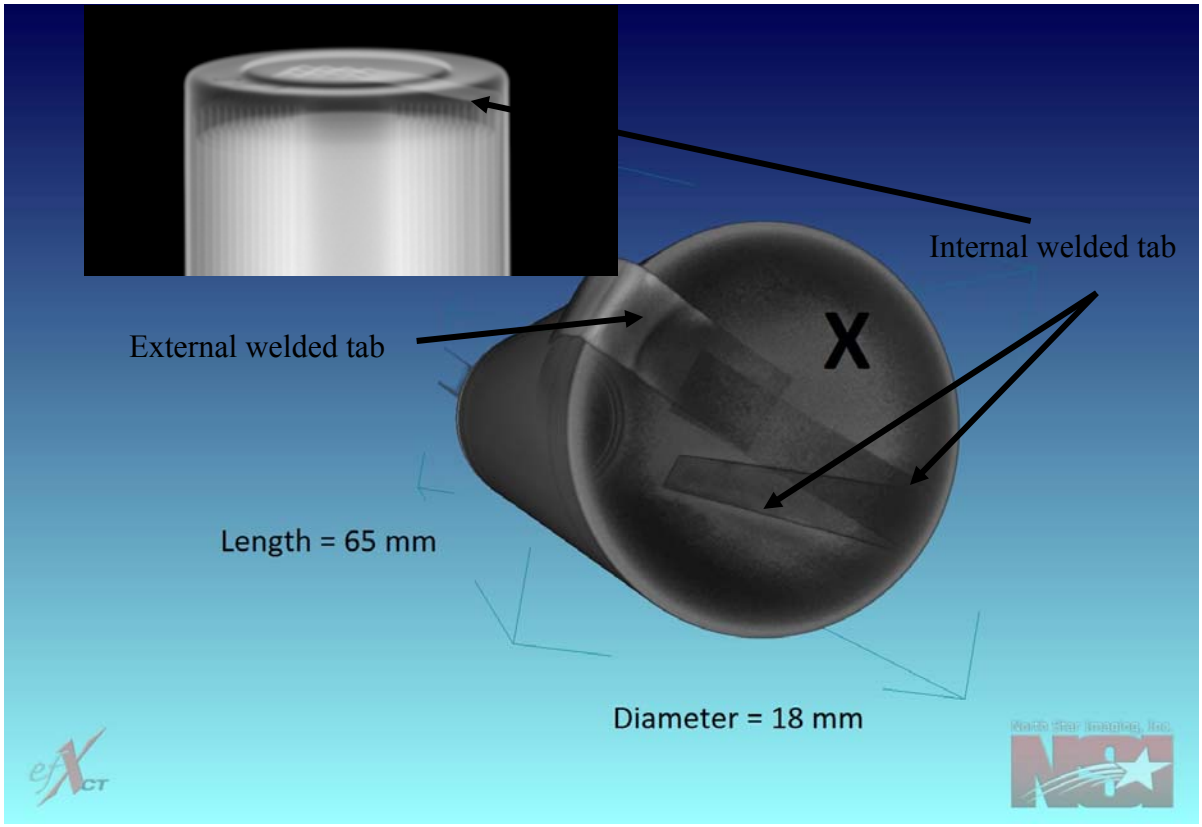

Figure 3.13: X-ray of the negative end of the 18650 cell focused to show the internal and external welded metal tabs. The "X" marks the optimal location for perforation. Insert: expanded view of the negative end of the cell shown in Figure 3.12.

The X-ray in Figure 3.13 also reveals the exterior of the can and the external tab on the outside of the cell and the internal folded metal tab in the interior of the cell, which runs along the inside face and also along the length of the cell wall. This internal folded metal tab running along the length of the cell is also somewhat visible on the right side of the image in Figure 3.12. Note that the external tab is not visible in the insert because the image was taken before the tabs were welded to the cell.

3.2.3 Cell Perforation

Even in an inert atmosphere, perforation of a lithium ion battery can be hazardous because of the risk of shorting. Shorting the electrodes can cause the cell to proceed into a thermal runaway condition that could result in explosion. The use of a traditional drill bit can produce small shavings of metal that can be introduced into the cell during the cutting operation and result in localized shorting. Consequently, cell perforation was performed from the bottom (i.e., with the negative end facing downward) with the customized hole-cutting apparatus shown in Figure 3.14. The apparatus employed a 13/64 inch Brad point drill bit that had the center hollowed out to transform the bit into a plug cutter. This hollowed-out design greatly reduced the risk of shorting by minimizing the production of metal shavings during the perforation process. The cutting head approached the negative end of the metal can from the bottom, so the metal shavings that were produced did not fall back into the hole. The cutting bit was magnetized to collect both the metal plug and the metal shavings as they fell away from the can. The customized hole-cutting apparatus was designed to allow the alignment of the cutter in the horizontal and vertical direction, by moving the cell in relation to the cutting head, while firmly holding the cell. The cutting process was viewable from the side or above via the proper placement of mirrors. The highly accurate controls allowed movement in the thousandths of an inch. Figure 3.14-Figure 3.19 show cell cutter design.

Figure 3.14: Custom-built hole-cutting apparatus.

Figure 3.15: Cell holder front view

Figure 3.16: Cell holder top view

Figure 3.17: Cell with hole cut in the negative end of the can

Figure 3.18: Cell in holder with ampoule

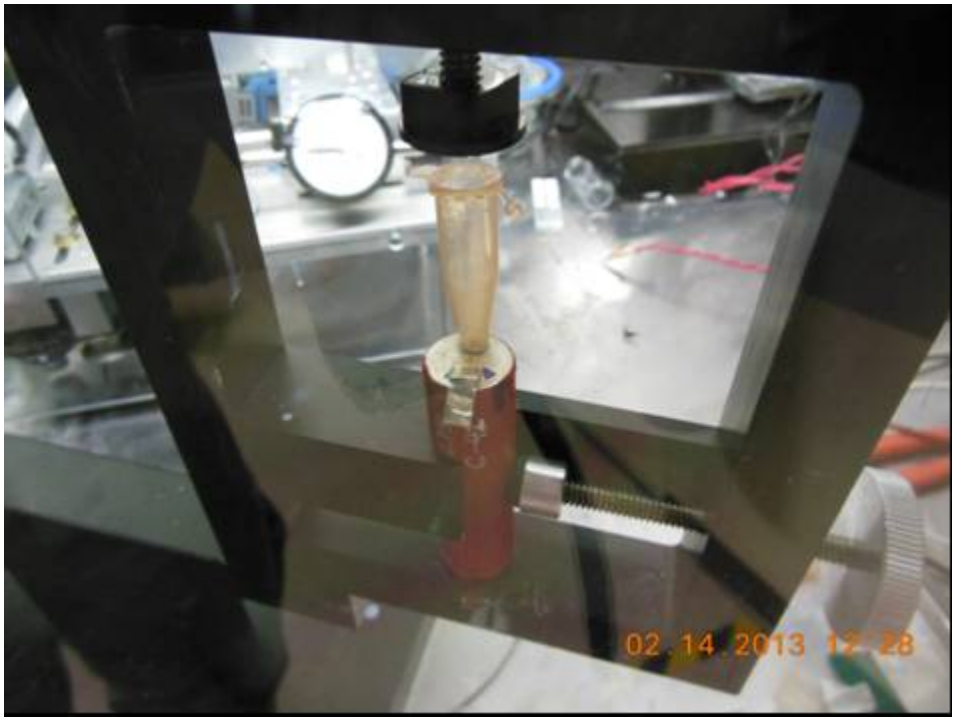

Figure 3.19: Cell in holder with ampoule in place

3.2.4 Reference Electrode Insertion and Construction

Once the hole in the cell was cut, a small plastic ampoule was placed into the hole (see Figure 3.20) and filled with electrolyte. The lithium utilized in the reference electrode consisted of a small piece of lithium metal foil (9.5 mm × 25 mm × 1 mm) that was pressed and flattened onto an 80 mm long, 26 gauge nickel wire. The foil was fed through the ampoule and set on top of the separator layers inside the cell, just past the bottom of the ampoule. The electrolyte was made with LithChem lithium hexaflourophosphate (1.2M $LiPF_6$) in a 2:8 volumetric ratio of ethylene carbonate to ethyl methyl carbonate, which was similar to the electrolyte found in the cell. The process of adding the reference electrode to the cell in its original can is novel in that it places the reference electrode as close as possible to the cell in its original container, which allows the cell resistance and capacity to be measured and compared to test results of cells without the reference electrode. Figure 3.20 shows the specially designed device that firmly holds both the cell and reference electrode during testing. The figure also shows the positive, negative and reference electrode connections to the tester.

Prior to the insertion of a reference electrode, the cells were subjected to a series of capacity and power tests to stabilize performance. Because the aging-study RPTs were all performed at 30°C, these tests were conducted at both 30°C and glove-box temperature (~25°C) to establish a baseline of initial performance. After reference electrode insertion these capacity and power tests were repeated (and in some cases a $C_1/25$ discharge was performed) at ~25°C inside the glove box, which included the voltage data relative to the reference electrode. The reference electrode was placed as close as possible to the electrode

winding within the cell, such that the ohmic potential drop in the measurement was minimized [61] and a resistance measurement of greater accuracy was obtained.

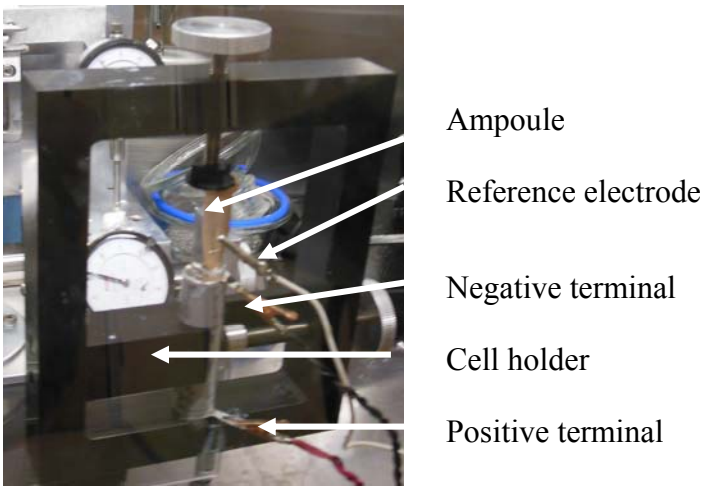

Figure 3.20: Cell in holder with reference electrode, positive, and negative terminals connected to the battery tester.

New and unaged cells were fit with reference electrodes and tested for power and capacity performance to serve as a baseline to measure the performance degradation that occurred after aging; however, cells fitted with reference electrodes were not subjected to the aging regime studies. Reference electrodes were inserted into the cells after aging in order to eliminate the influence of the reference electrode on the aging process and preserve the integrity of the reference electrode itself. This article focuses on reference electrode results of four cells, one not aged and three aged at 60°C, although three other cells aged at 50°C and were tested with reference electrodes as well: the 60°C-aged showed the best resolution for performance degradation and are therefore the primary subject of discussion of results.

3.3 Experimental Test Summary

3.3.1 Summary of Life Testing

The aging studies consisted of testing at four temperatures and three states of charge for cycle and calendar life aging regimes. For calendar life testing, ten cells were tested at 30°C and five cells each were tested at 40, 50, and 60°C. For CD cycle life testing, ten cells were tested at 30°C and five cells each were tested at 40, 50, and 60°C. Five cells were also tested at 60°C for the CS cycle life testing. Additionally at 30°C, five cells were tested during calendar life at each 30% and 90% SOC, with ten cells being tested at 60% SOC. Capacity and resistance changes were tracked with 7.1 W capacity discharge and HPPC tests at 30 day test intervals.

3.3.2 Summary of Reference Electrode Testing

The reference electrode studies concentrated on one new, un-aged cell and one aged cell at 60°C for each calendar, CD life and CS cycle life testing regimes. Each cell was evaluated with multiple 7.1 W capacity discharge and HPPC tests for capacity and resistance changes and for comparison with the results from the aging studies. These tests were performed at 30°C, at room temperature ~25°C and again at ~25°C inside a glove box with a reference electrode inserted into the cell. With these three tests at different temperatures, the test results from the cells with reference electrodes can be directly compared to the last tests performed for the aging studies at 30°C.

3.4 Task C. Life Modeling

Modeling of the data can be accomplished by using a variety of curve fitting tools, such as Excel, Sigma Plot, or a program designed specifically for curve fitting calendar and cycle life data for batteries tested for USABC applications by Argonne National Laboratory called "Battery Life Estimator." Several of these programs were used; however, the Battery Life Estimator program was the best tool for fitting the results. This program not only curve fits the data by providing an appropriate model and initial guesses, but also determines the calendar life of a device at some specified temperature, usually 30°C as well as the upper and lower confidence limits. The upper and lower confidence limits are determined from a Monte Carlo simulation using the estimated error from the experimental data and cell to cell variation.

Chapter Four: Calendar and Cycle Life Results

The average cell Open Circuit Voltage (OCV) at the start of testing was 3.732 Volts with a standard deviation of 0.017 V. If a cell has a measurable voltage, it indicates that the cells is functioning normally and can be subjected to testing. This OCV information, combined with visual inspection, indicated that the cells suffered no significant damage during shipment. The cells were subjected to testing according to the test matrix presented in Table 3.1 is the cell testing matrix. The matrix summarizes the tests that were performed, the number of cells involved in each test, the test condition, the test temperatures, the states of charge, and the testing focus, whether cycle life or calendar life.

A 10 kW Capacity test was performed on the cells during characterization testing. The individual cell capacities were consistent for all the cells. The manufacturer rated the capacity of these cells as 1.2 Ah; however, the measurements showed that the actual cell capacities at the beginning of life were approximately 1.27 Ah with a standard deviation of 0.0034 Ah.

4.1 Capacity

Figure 4.1 illustrates the cell capacities for the RPT results from the beginning of calendar life testing at RPT 0 (beginning of life) to RPT 30. The chart shows the performance of the cells for tests Number 8-11 in Table 3.1. Cells 46 to 50 at 50°C and 56 to 60 at 60°C were taken off test after RPT 6, 192 days because they failed to meet the 45 kW discharge power target. The cells at 60°C failed to meet the target at RPT 3, but testing was

continued to evaluate their performance degradation. These calendar life results in Table 4.1 show increased capacity fade with increasing temperature and time.

A comparison of the capacity fade, power fade, and resistance rise for the four temperatures is shown in Table 4.1 for the Charge Depleting Cycle life tests and the Calendar life tests at the end of testing at each condition. Note that these results do not represent the same time in life, but rather their end of testing results. The resistance rise and power fade correspond well with each other at all temperatures, except for the 15.84% calendar life power fade at 30°C, which is lower than 21% resistance rise for calendar life.

Table 4.1: End of test results summary (Capacity is blue, Power is orange, and Resistance is green)

Performance Degradation	**30°C**	**40°C**	**50°C**	**60°C**
Capacity Fade (%) Results				
CD Cycle	24.71	42.38	46.02	53.86
Calendar	12.02	24.13	22.07	44.79
Power Fade (%) Results				
CD Cycle	45.06	44.48	39.36	49.57
Calendar	15.84	26.94	25.57	51.82
Resistance Rise (%) Results				
CD Cycle	47.77	46.16	37.91	48.86
Calendar	21.00	27.17	25.74	52.10

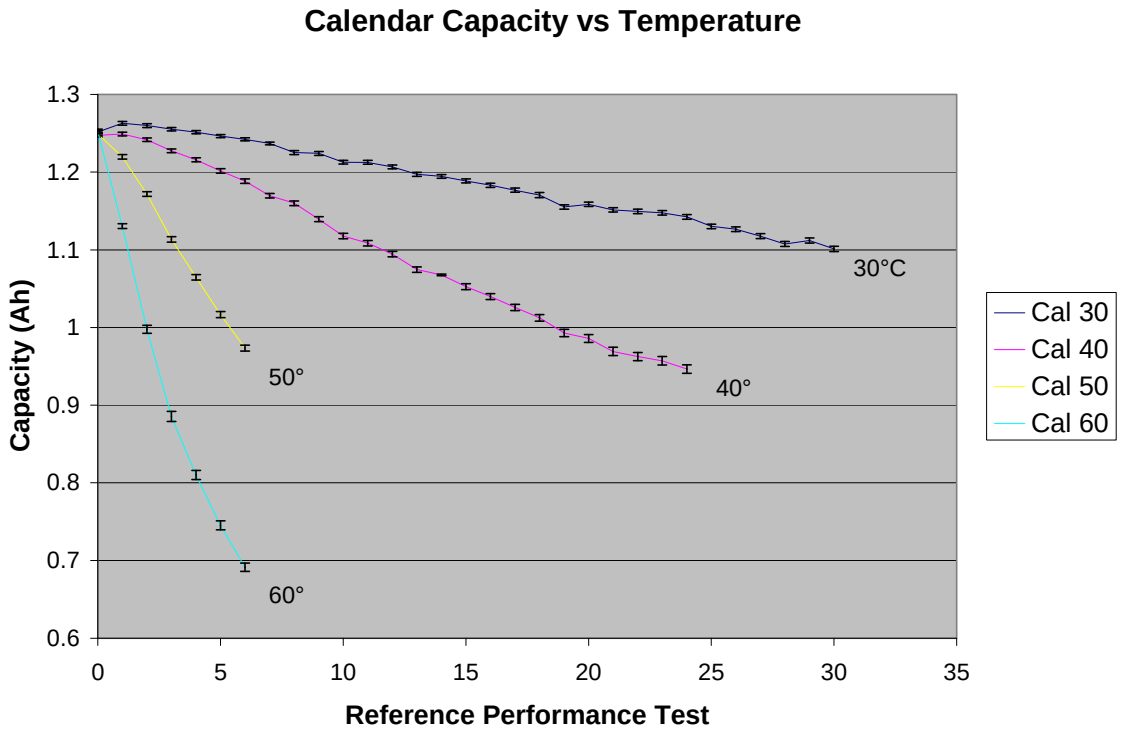

Figure 4.1: Calendar life capacity summary for cells at 30, 40, 50, and 60°C.

Figure 4.2 illustrates the cell capacities for the RPT results from the beginning of calendar life testing at RPT 0 (beginning of life) to RPT 30 at 30%, 60%, and 90% SOC, tests number 5, 6, and 7. The rise in capacity for the cells at 90% SOC is an artifact of the tester (the tester is giving an incorrect value for some unknown reason), not a real value based on the past and post-performance. That same artifact can also be seen in the cells at 30%SOC. These calendar life results show increased capacity fade over time at 60% SOC and 90% SOC compared to the results at 30% SOC.

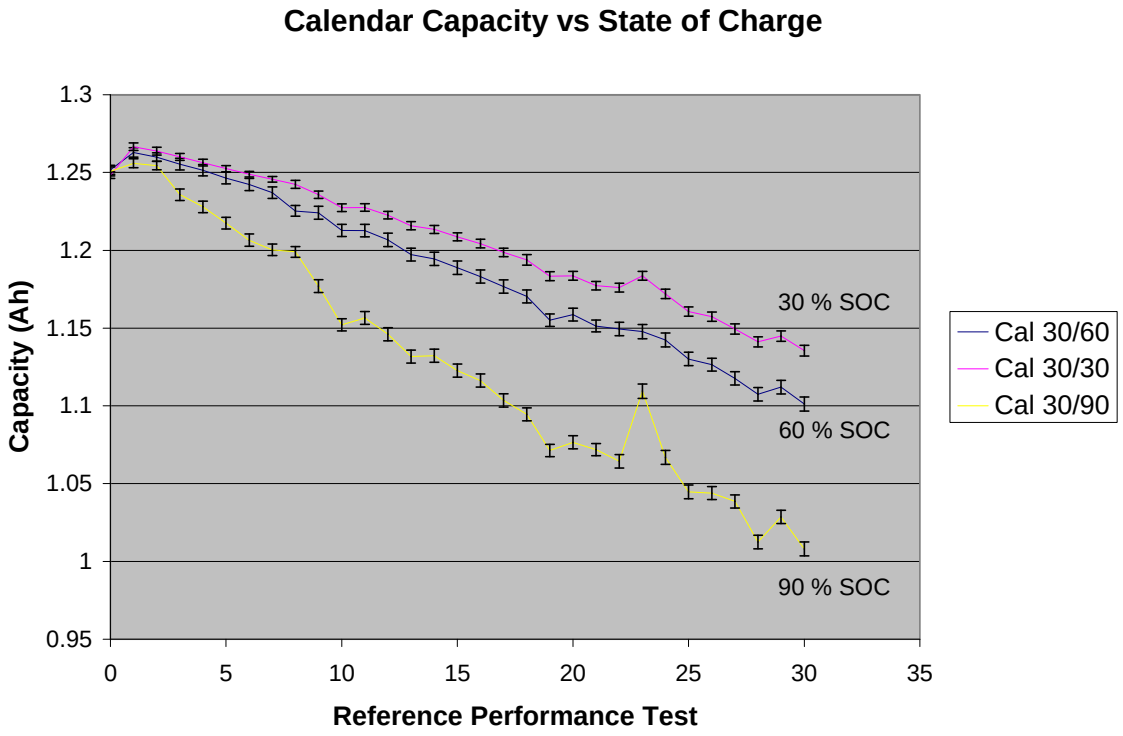

Figure 4.2: Calendar life capacity summary 30%, 60%, and 90% SOC at 30°C

Figure 4.3 illustrates the cell capacities for the RPT results from the beginning of cycle life testing, using the charge depleting cycle life test from the PHEV manual (9) at RPT 0 (beginning of life) to RPT 13 for cells at 30, 40, 50, and 60°C. Cells 41 to 45 at 50°C and 51 to 55 at 60°C were taken off test after RPT 6, 192 days because they failed to meet the 45 kW discharge power target. The cells at 60°C failed to meet the target at RPT 2, but continued testing. These cycle life results show increased capacity fade with increasing temperature and time. This is the same trend as the capacities of the cycle life cells versus temperature.

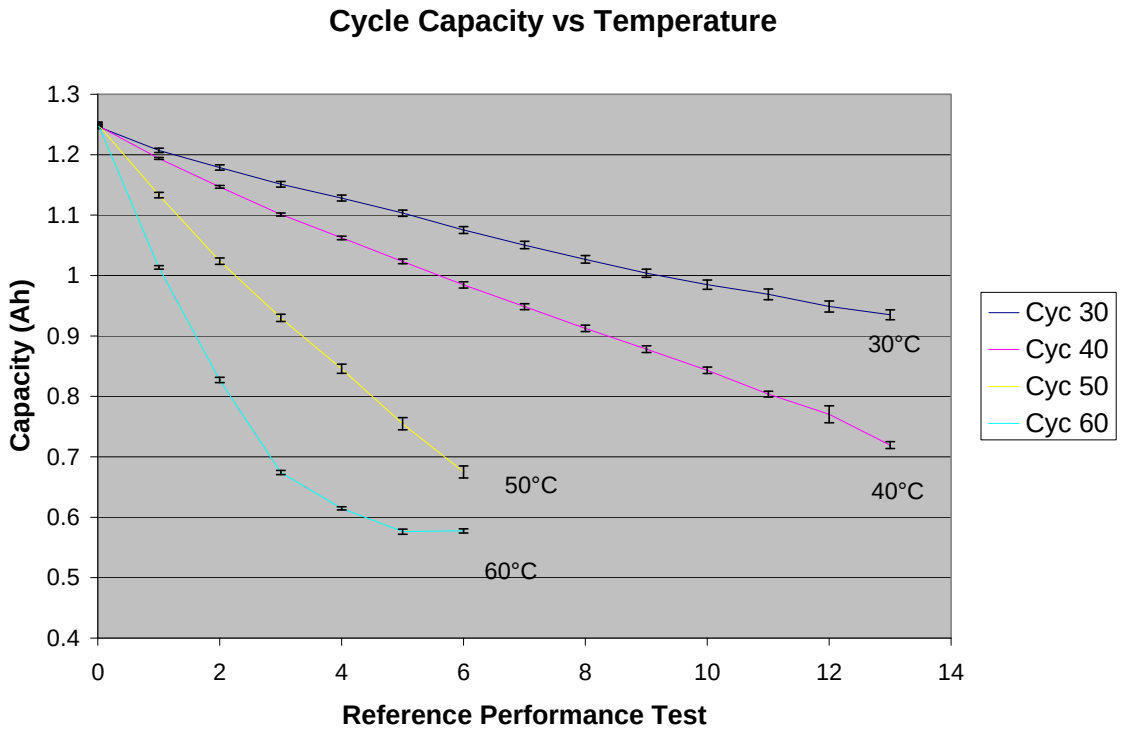

Figure 4.3: Charge Depleting cycle life capacity summary for cells at 30, 40, 50, and 60°C.

Capacity fade is generally associated with a loss of lithium available for intercalation, otherwise known as lithium corrosion, a parasitic loss that occurs between the lithium in the negative electrode and the electrolyte. The lithium corrosion reaction produces several soluble and insoluble products, which are deposited on the surface of the negative electrode. This mechanism may be responsible for the bulk of the capacity fade. The soluble products lead to self-discharge and the insoluble products are responsible for the irreversible capacity loss. A solid electrolyte interphase (SEI) or passivation layer results from the reduction of the electrolyte at the negative electrode. This SEI layer is a good ionic (Li^+) conductor and a poor electronic conductor. The stability of this layer and its ability to reduce lithium oxidation has an effect on the overall capacity fade of the cell during long-term testing [44].

4.2 Power

Figure 4.5 illustrates the discharge and regen resistances and the open-circuit voltage, all versus Depth of Discharge (DOD) for Cell 1 (tested at 30°C for the HPPC test) at the beginning of test. Plotting open-circuit voltage on a linear secondary y-axis shows the linear decrease between cell voltage and DOD. Discharge and regen resistances are determined using a $\Delta V/\Delta I$ calculation for each iteration of the test profile, in accordance with Equations 4.1 and 4.2 and Figure 4.4. Resistances are normally only calculated for completely unabated test profile pulses, i.e., those with full duration and amplitude. The signs of all terms in these equations have been chosen to agree with the PHEV manual convention that discharge current is positive and regen current is negative, thus assuring that the calculated resistance is always a positive quantity. Discharge and Regen resistances are calculated at each DOD using Equations 4.1 and 4.2.

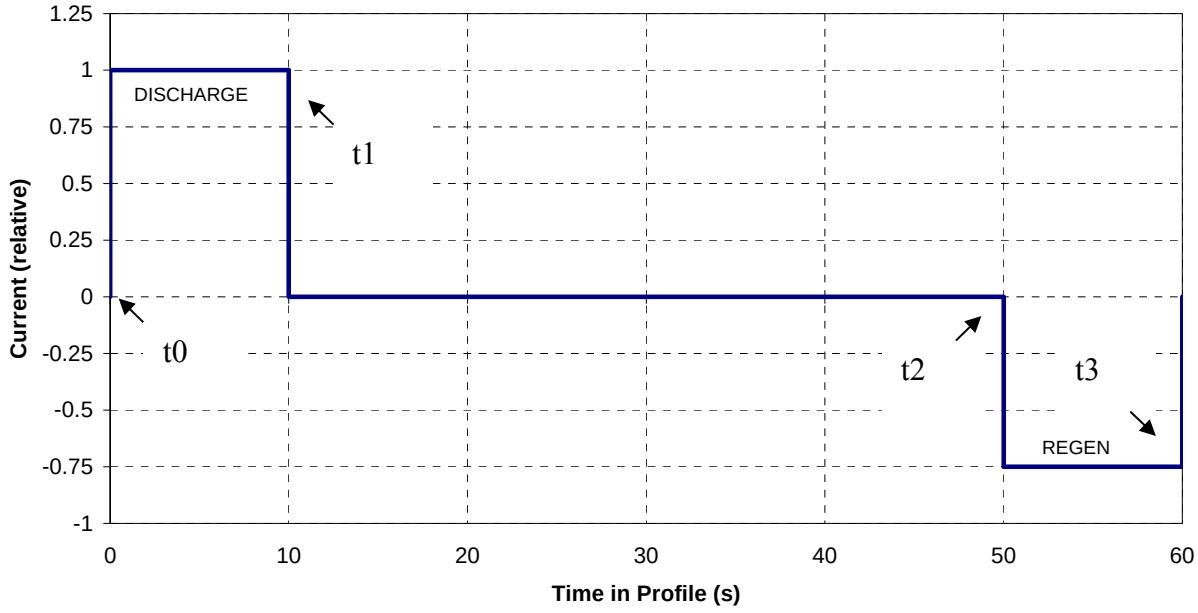

Figure 4.4: Pulse power characterization profile

$$Discharge\ Resistance = \frac{\Delta V}{\Delta I} = \frac{V_{t0} - V_{t1}}{I_{t0} - I_{t1}}$$ Equation 4.1

$$Regen\ Resistance = \frac{V_{t2} - V_{t3}}{I_{t2} - I_{t3}}$$ Equation 4.2

Where t0, t1, t2, t3 are shown in Figure 4.4.

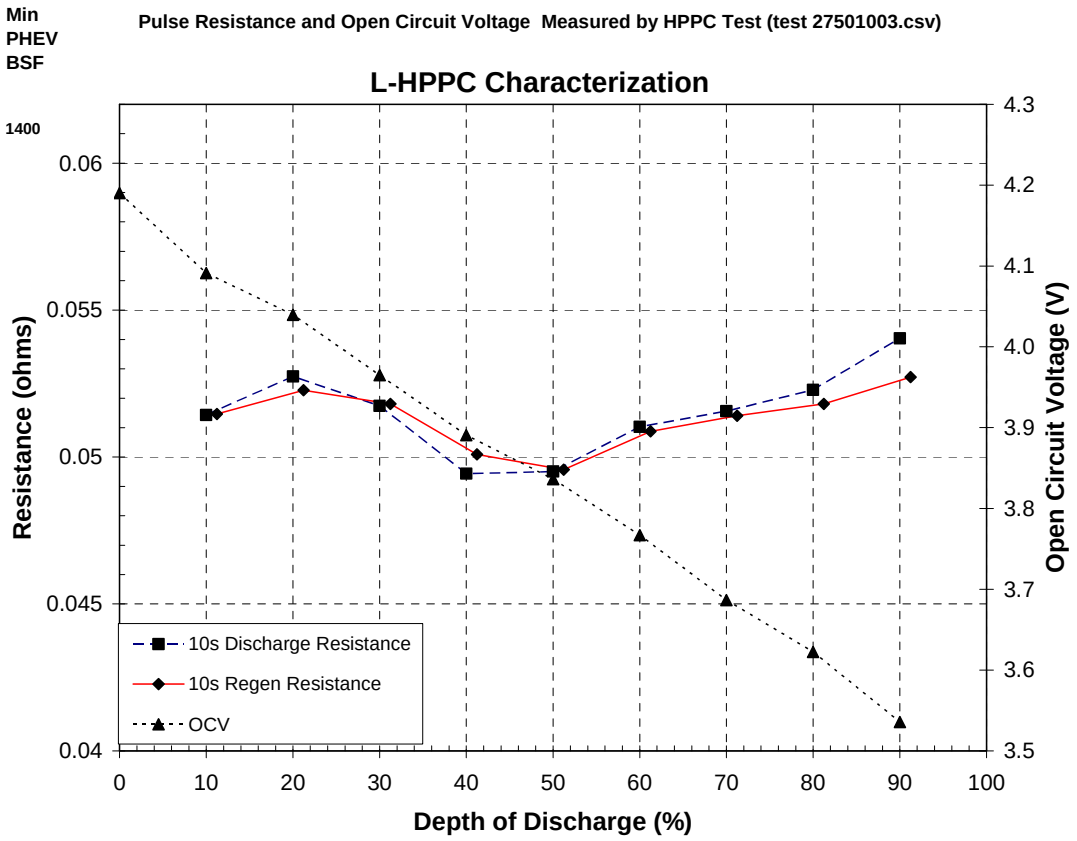

Figure 4.5: Discharge and regen resistance, and the open circuit voltage versus DOD for Cell 1.

Figure 4.6 shows the discharge and regen pulse power capabilities calculated for Cell 1 at the beginning of test. The results show, as one would expect, that discharge power capability is highest at high SOC, while regen power capability is higher at high DOD. Pulse power is calculated from the HPPC results using the discharge and regen resistances and

OCV at each 10% Depth of Discharge increments and is combined with the HPPC voltage limits. Discharge and regen pulse power are calculated using equations 4.3 and 4.4.

$$\text{Discharge Pulse Power Capability} = V_{MIN} \bullet (OCV - V_{MIN}) \div R_{discharge}$$

Equation 4.3

$$\text{Regen Pulse Power Capability} = V_{MAX} \bullet (V_{MAX} - OCV_{regen}) \div R_{regen}$$

Equation 4.4

V_{min} and V_{max} are the minimum pulse voltage limit and the maximum pulse voltage limit respectively. These power capability values are used to determine the total available depth-of-discharge and energy swing that can be used (within the operating voltage limits) for specified discharge and regen power levels based on 10 second pulses. The 10 second pulses represent the pulse duration expected during vehicle operation. For instance, at the point where the power and energy are 78000 Watts and 2000 Watt-hrs, respectively after 2000 Wh are removed, a 10-sec power pulse of 78000 watts can be achieved. This can be seen on Figure 4.7, by the dashed blue line, where x = 2000 Wh and y = 78000 Watts by the large black asterisk. This same point is also represented on Figure 4.7 by the large black asterisk, except the DOD is 31.25% DOD. An example of the power capability versus DOD plot is shown in Figure 4.6. The discharge power versus energy is the red line, while the regen power and energy is the blue line. The black line represents the discharge power level at 45 kW and 30 kW regen power, which represents the PHEV targets.

These and all ensuing calculations were performed in accordance with the methodology described in the PHEV Battery Test Manual [5]. Data reduction was accomplished by an automated software package, HPPCALC, which has undergone rigorous verification and validation [62].

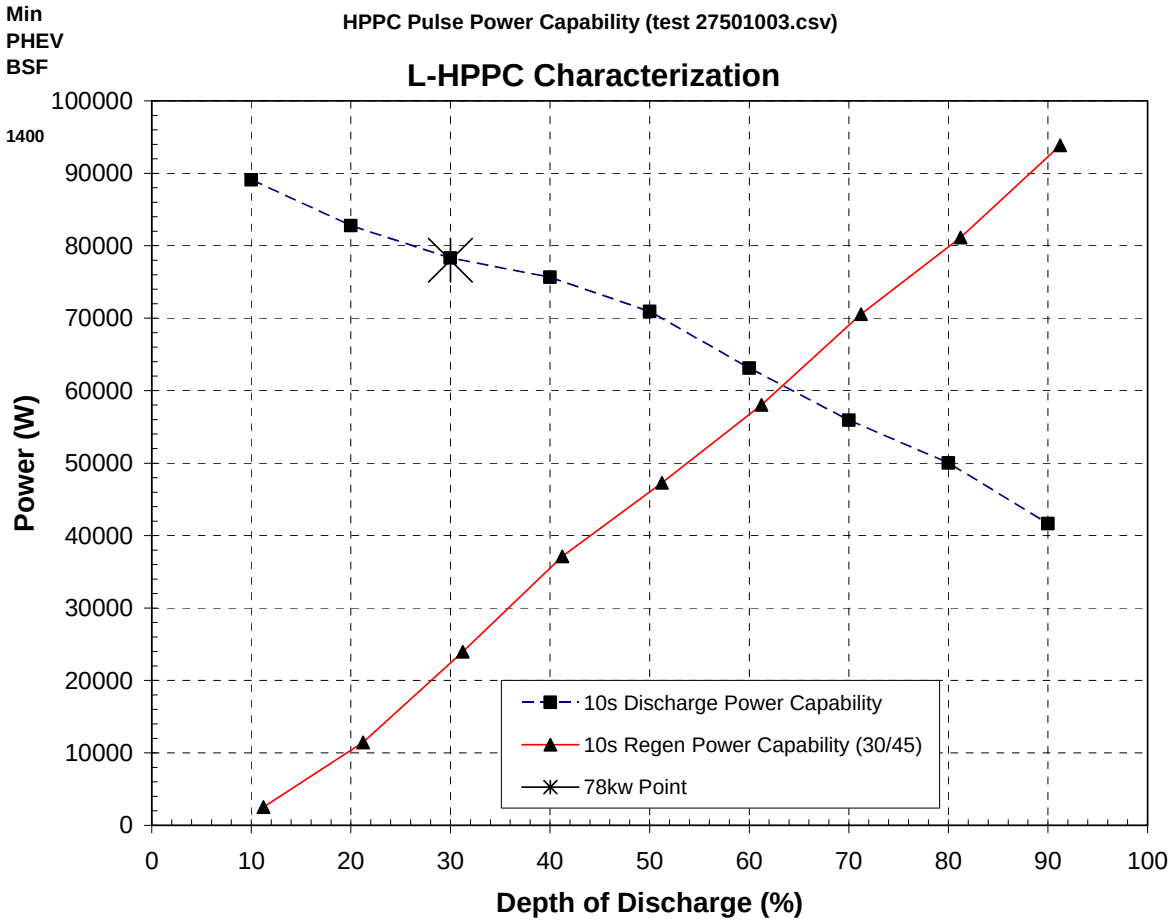

Figure 4.6: Discharge and regen pulse power versus DOD for Cell 1.

From the constant current discharge test data, the Depth of Discharge can be directly related to energy. Figure 4.7 shows discharge and regen pulse power replotted as a function of energy removed. For any given power below the cross over point for the two lines, the area between the discharge and regen power curves; when plotted as a function of discharge energy is the energy available over the associated DOD range, otherwise known as Useable Energy. This Useable Energy as a function of pulse discharge power for Cell 1 at the beginning of test is graphed in Figure 4.8. In order to compare cell performance to pack-

level performance requirements, a scaling factor must be used. The Battery Size Factor (BSF) for these cells was 1400 cells, consistent with their small size.

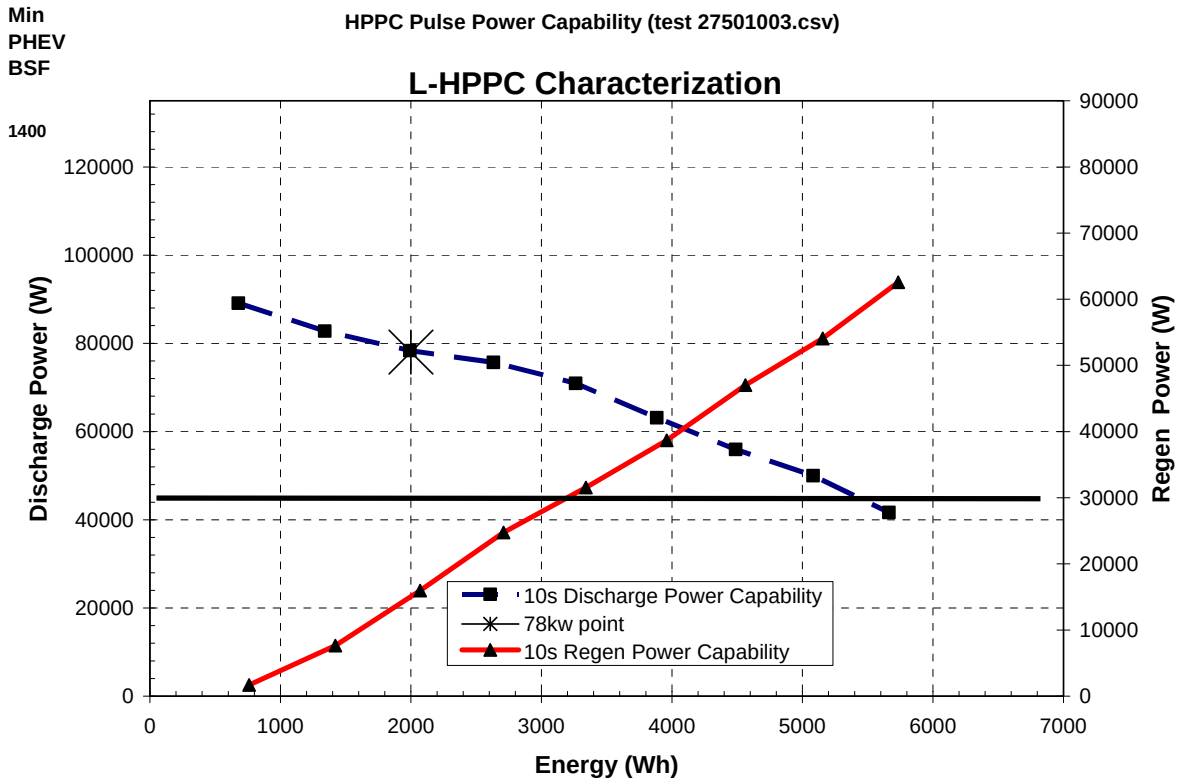

Figure 4.7: Discharge and regen pulse power versus energy for Cell 1.

Scaling both the cell power and cell energy by 1400 a scaled useable energy plot can be developed to directly apply to cell performance to the full-size PHEV battery system performance goals. This approach represents the present method of comparing the cell power and energy capability to the goals. This Scaled Useable Energy as a function of pulse discharge power for Cell 1 at the beginning of test is graphed in Figure 4.9. The bold horizontal and vertical lines represent, respectively, the minimum PHEV battery energy target and power target. The intersection of the useable energy line and the energy target line is the Available Power. To meet the power target, this power value must be greater than or equal to 45,000 W throughout life. Available power is

defined as the maximum power that can be achieved after removing 500 Wh of energy from the device, represented by the round circle. As long as the useable energy curve resides to the right and above the bold goal lines, the cell is capable of simultaneously meeting the power and energy targets. The CD energy, shown by the asterisk at 4700 Wh, exceeds the target of 3400 Wh.

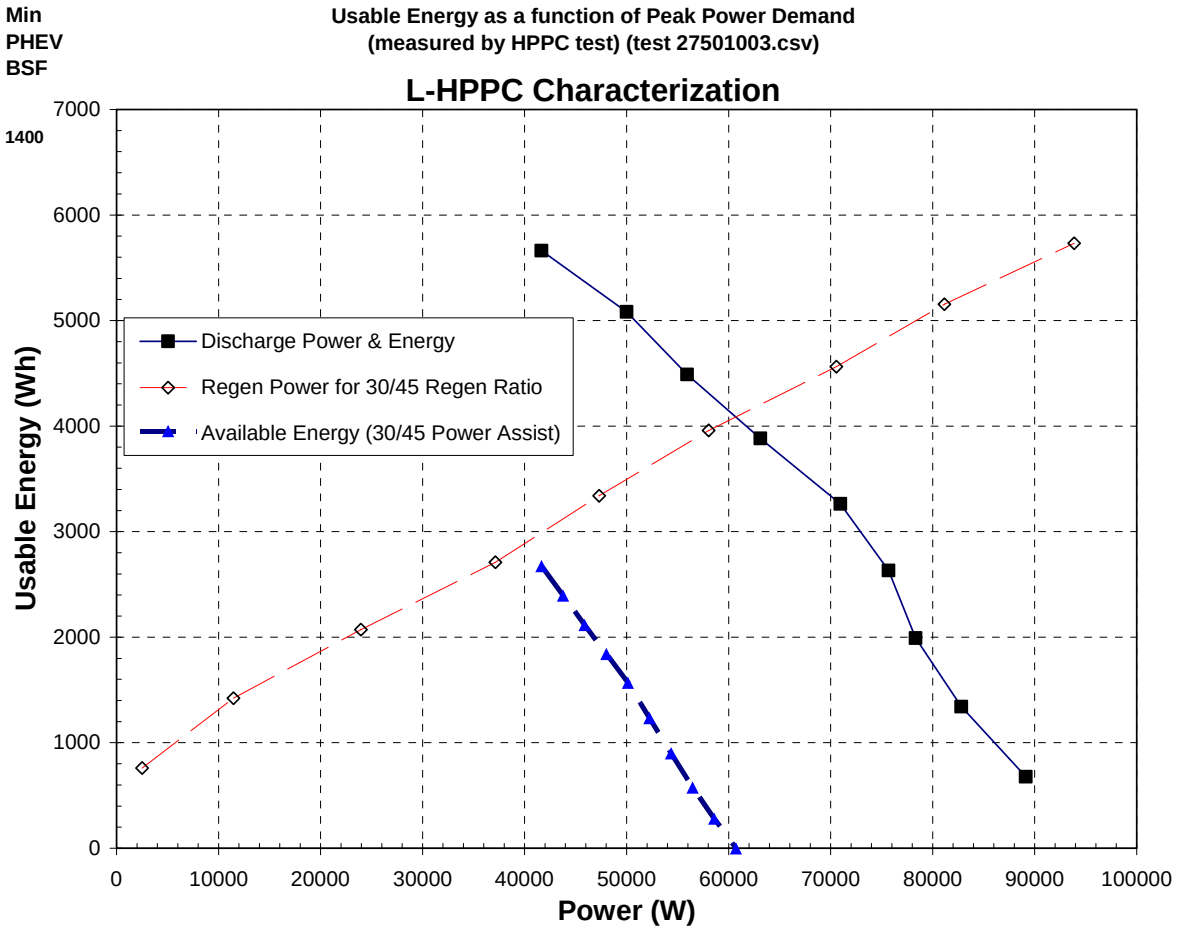

Figure 4.8: Useable Energy versus discharge pulse power for Cell 1.

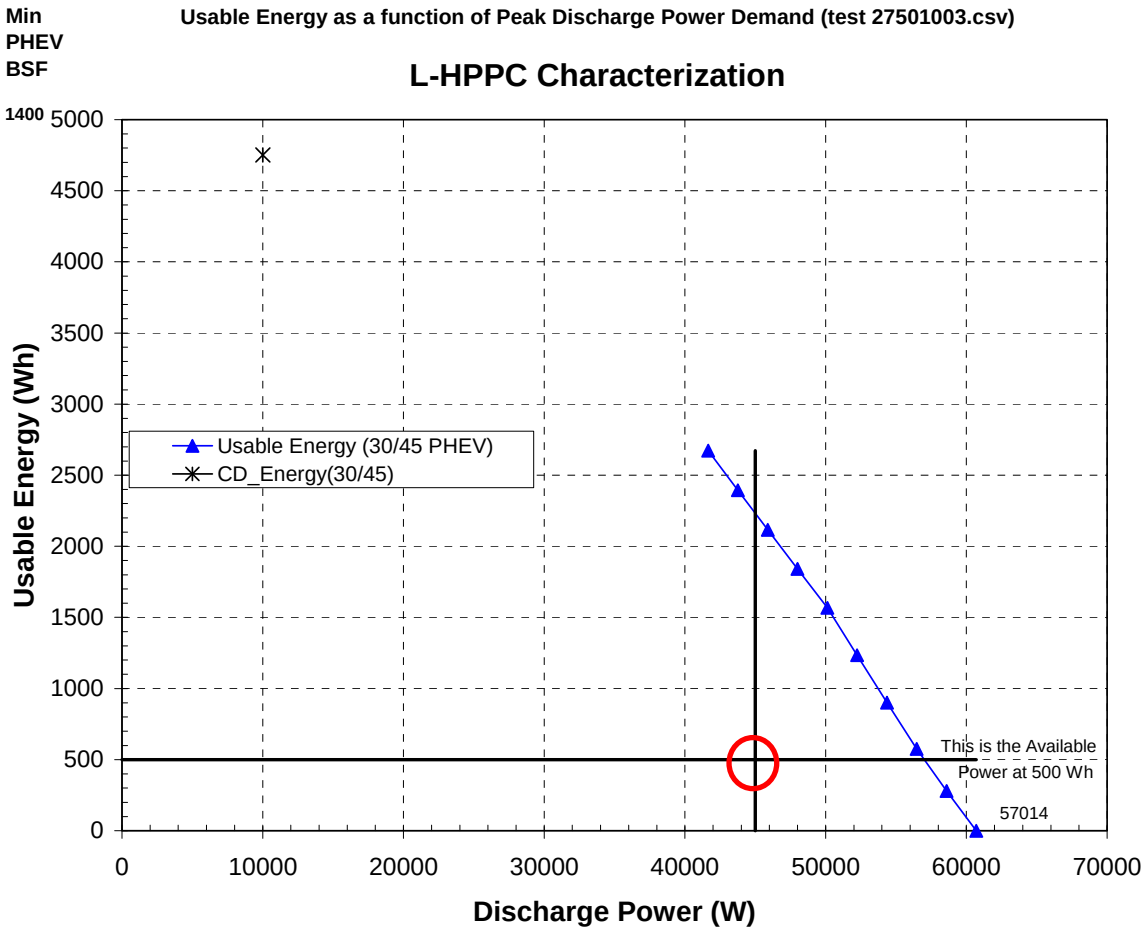

Figure 4.9: Scaled Useable Energy versus discharge pulse power for Cell 1.

The average beginning of life power capability for all cells was 58.0 kW with a standard deviation of 674 W, exceeding the FreedomCAR discharge power goal of 45 kW. Figure 4.10 illustrates the cell Available Powers for the RPT results from the beginning of calendar life testing at RPT 0 (beginning of life) to RPT 30 at 30, 40, 50, and 60°C. Cells 46 to 50 at 50°C and 56 to 60 at 60°C were taken off test after RPT 6 at 192 days because they failed to meet the 45 kW discharge power target. The cells at 60°C failed to meet the target at RPT 3, but testing was continued to evaluate their performance degradation. The sharp drop in power at RPT 15 and 20 for the cells at 30°C is an artifact of the tester, not a real

value based on the past and post-performance. These calendar life results show increased power fade with increasing temperature and time.

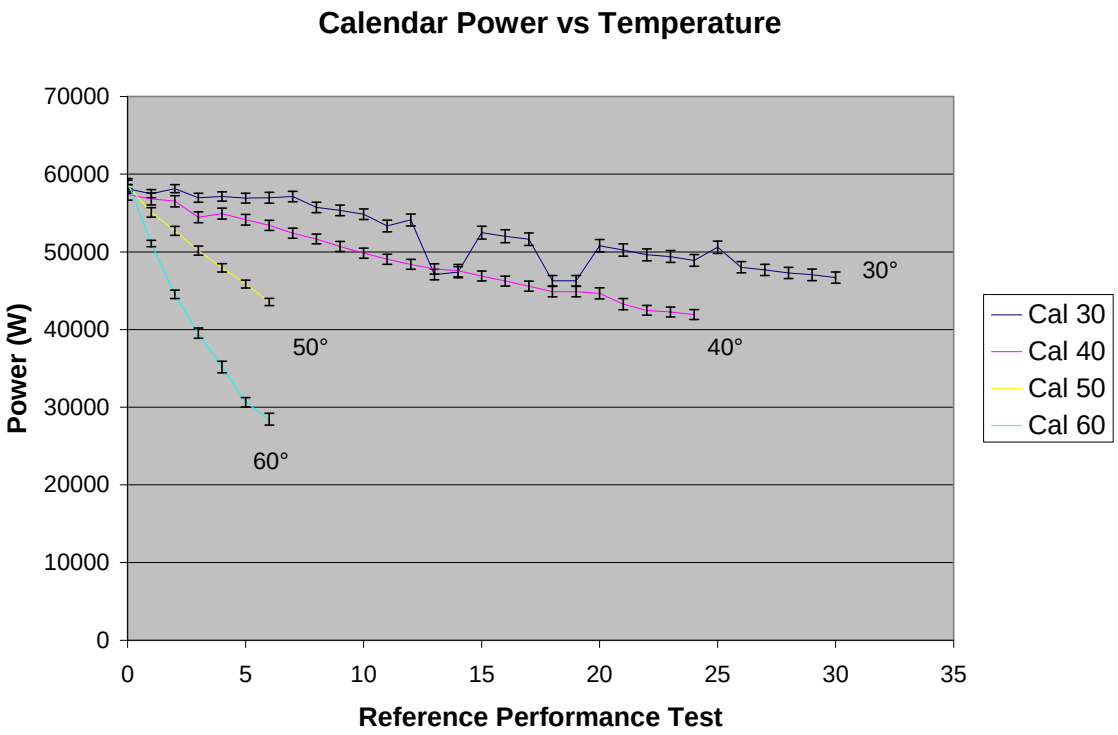

Figure 4.10: Calendar life available power summary for cells at 30, 40, 50, and 60°C.

Figure 4.11 illustrates the cell Available Powers for the RPT results from the beginning of calendar life testing at RPT 0 (beginning of life) to RPT 30 at 30%, 60%, and 90% SOC. These calendar life results show increased power fade over time at 60% SOC and 90% SOC compared to the results at 30% SOC.

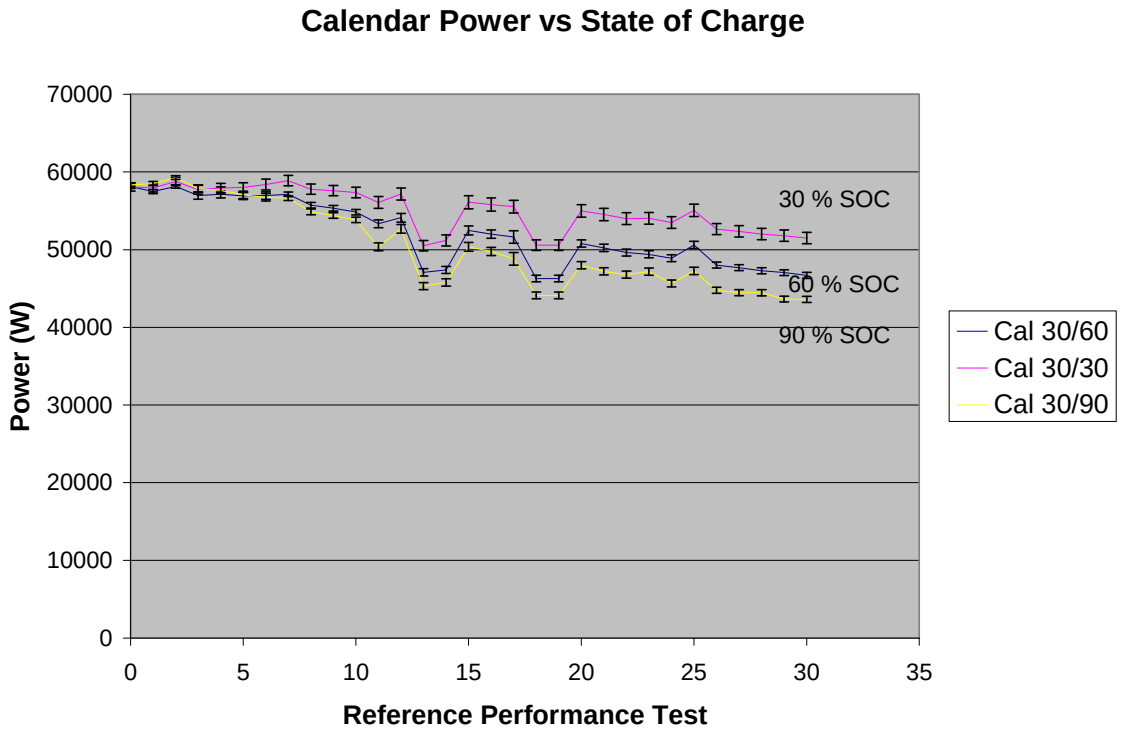

Figure 4.11: Calendar life available power summary for cells 30%, 60%, and 90% SOC at 30°C

Figure 4.12 illustrates the cell Available Powers for the RPT results from the beginning of cycle life testing at RPT 0 (beginning of life) to RPT 13 for cells at 30, 40, 50, and 60°C. Cells 41 to 45 at 50°C and 51 to 55 at 60°C were taken off test after RPT 6 at 192 days because they failed to meet the 45 kW discharge power target. The cells at 60°C failed to meet the target at RPT 2, but continued testing to evaluate their performance degradation. These cycle life results show increased power fade with increasing temperature and time. This is the same trend as the powers of the cycle life cells versus temperature.

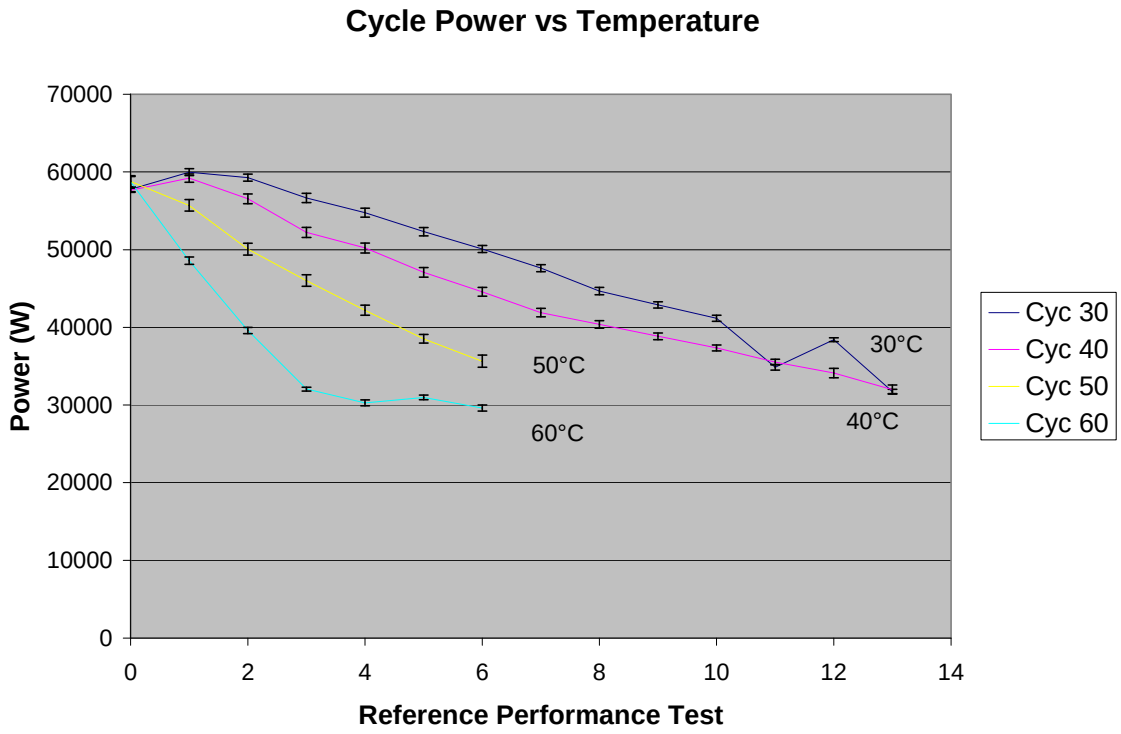

Figure 4.12: Charge Depleting cycle life available power summary for cells at 30, 40, 50, and 60°C.

The cause of the power fade is believed to be a result of the increased resistance due to the build-up of the solid-electrolyte-interface (SEI) layer with aging on the negative electrode and an increase in resistance on the positive electrode from phase transformations as a result of lithium insertion and a loss of electronic conductivity that results from deposits of insoluble salts and polycarbonates on the surface of the electrode [12].

4.3 Resistance

All cells have beginning of life resistance measurements less than 50 milliohms, an average of 48.7 milliohms and a standard deviation of 0.000646 milliohms. Figure 4.13 illustrates the cell Resistances for the RPT results from the beginning of calendar life testing

at RPT 0 (beginning of life) to RPT 30. Cells 11 to 20 were calendar life tested at 30°C, 60% SOC. Cells 36 to 40 were calendar life tested at 40°C, 60% SOC. Cells 46 to 50 were calendar life tested at 50°C, 60% SOC. Cells 56 to 60 were calendar life tested at 60°C,

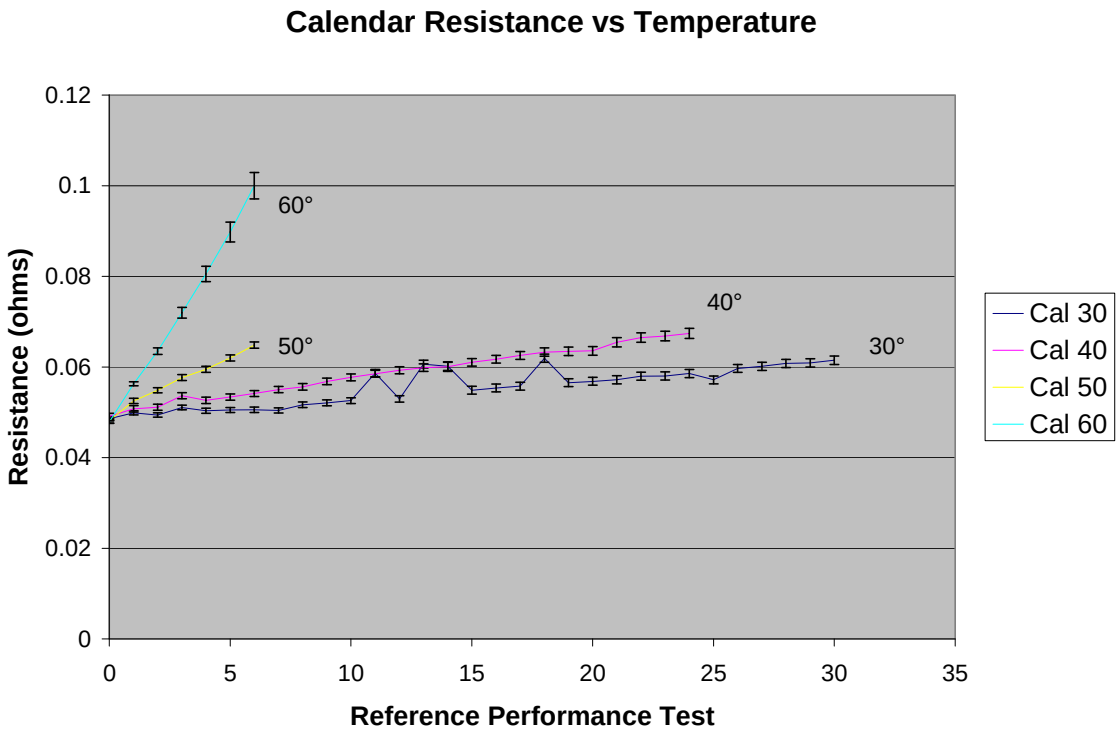

Figure 4.13: Calendar life resistance summary for cells at 30, 40, 50, and 60°C.

60% SOC. Cells 46 to 50 at 50°C and 56 to 60 at 60°C were taken off test after RPT 6 at 192 days because they failed to meet the 45 kW discharge power target. The cells at 60°C failed to meet the target at RPT 3, but continued testing to evaluate their performance degradation. These calendar life results show increased resistance rise with increasing temperature and time.

Figure 4.14 illustrates the cell Resistances for the RPT results from the beginning of calendar life testing at RPT 0 (beginning of life) to RPT 30, at 30%, 60%, and 90% SOC.

The sharp rise in resistance at RPT 9, 15, and 30 for the cells at 30°C is an artifact of the tester, not a real value based on the past and post-performance. This is the same artifact mentioned before, where the tester provided erroneous results. These calendar life results show increased power fade over time at 60% SOC and 90% SOC compared to the results at 30% SOC.

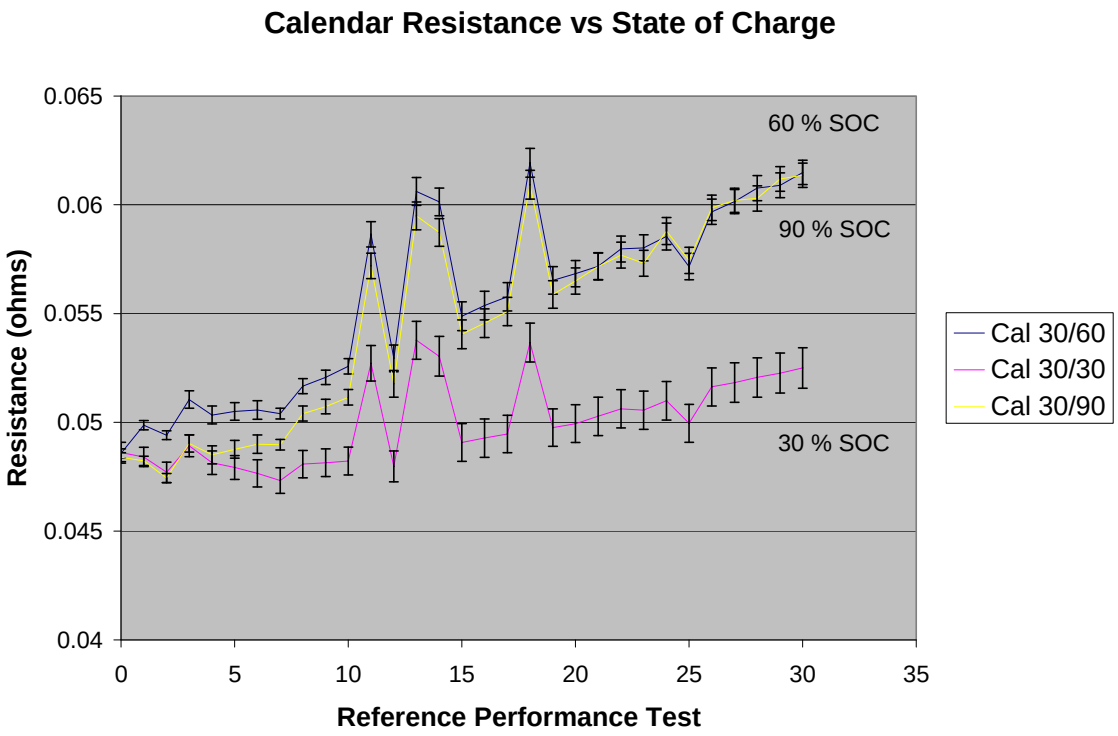

Figure 4.14: Calendar life resistance summary for cells at 30, 60 and 90% SOC at 30°C

Figure 4.15 illustrates the cell Resistances for the RPT results from the beginning of cycle life testing, using the charge depleting cycle life test from the PHEV manual (9) at RPT 0 (beginning of life) to RPT 13 for cells at 30, 40, 50, and 60°C. Cells 41 to 45 at 50°C and 51 to 55 at 60°C were taken off test after RPT 6 at 192 days because they failed to meet the 45 kW discharge power target. The cells at 60°C failed to meet the target at RPT 2, but

testing was continued to evaluate their performance degradation. These cycle life results show increased resistance rise with increasing temperature and time. This is the same trend as the power and capacity of the cycle life cells versus temperature.

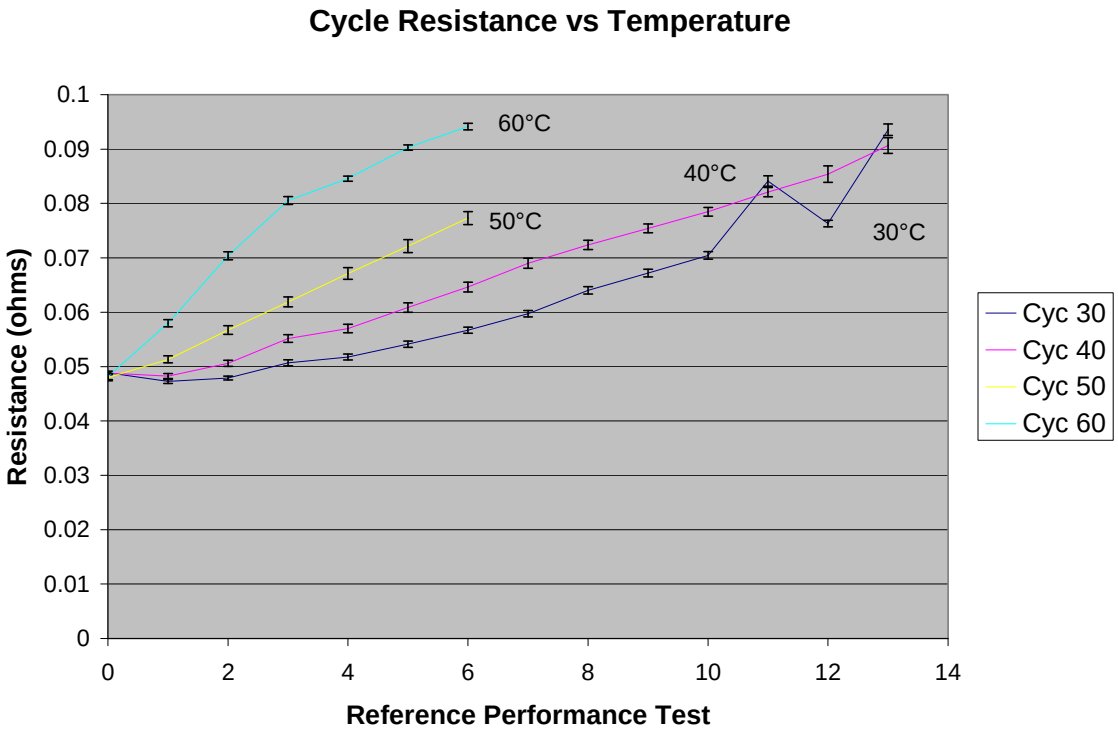

Figure 4.15: Charge Depleting cycle life resistance summary for cells at 30, 40, 50, and 60°C.

4.4 Results Summary

Temperature is the primary variable of degradation for these cells. The higher the temperature, the larger the capacity fade, power fade, and resistance rise for both calendar and cycle life conditions. Charge Depleting cycle life testing results in more degradation (capacity, power and resistance) than calendar life testing at each temperature. State of Charge during calendar life testing had the smallest effect on degradation compared with temperature and the calendar versus cycle life testing.

A comparison of the capacity fade, power fade, and resistance rise is shown in Table 4.2 for the Charge Depleting Cycle life tests and the Calendar life tests at the RPT 6, or 192 days. The comparison at the same point in time shows similar fade rates for CD cycle life testing and capacity fade, power fade, and resistance rise, at each temperature, showing that the temperature trends are consistent. Calendar life fade rates are also similar for each temperature. At 30°C, the effects of CD cycle life testing compared to the effects of calendar life testing are 3.5 times higher for resistance rise, 6.7 times higher for power fade, and 18 times higher for capacity fade. This trend continues at a diminishing rate through 40°C, 50°C, and 60°C, where the fade rates are almost the same.

Results from the three different States of Charge are shown in Table 4.3. The fade rates at 30% SOC are the smallest, followed by 60% SOC and finally 90% SOC. This is consistent with potential driven reactions. At the higher states of charge, 60 and 90%, the potential is higher than at 30% state of charge. The higher the potential, the faster the rate of the degradation reaction will occur within the cell.

Table 4.2: Test results summary at RPT 6 (Capacity is blue, Power is orange, and Resistance is green)

Performance Degradation	**30°C**	**40°C**	**50°C**	**60°C**
Capacity Fade (%) Results				
CD Cycle	13.73	21.12	46.02	53.86
Calendar	0.75	4.73	22.07	44.79
Power Fade (%) Results				
CD Cycle	13.32	22.68	39.36	49.57
Calendar	1.98	6.92	25.57	51.82
Resistance Rise (%) Results				
CD Cycle	13.80	24.51	37.91	48.86
Calendar	3.94	9.29	25.74	52.10

Table 4.3: End of test state of charge results summary (Capacity is blue, Power is orange, and Resistance is green)

Results	**60% SOC**	**30% SOC**	**90% SOC**
Capacity Fade %	12.02	9.04	19.40
Power Fade%	15.84	7.91	21.73
Resistance Rise%	21.00	7.41	21.12

Consequently, at higher temperatures the faster the degradation reaction will be. At low temperatures, calendar life testing results in lower degradation than cycle life testing. At the higher temperatures, very little difference exists between the calendar and cycle life results. The state of charge results indicate that the higher the state of charge the greater will be the degradation.

Chapter Five: Reference Electrode Testing Results

5.1 In Situ Reference Electrode

A select number of cells were subjected to in situ reference cell testing. Focused destructive analysis was performed with half-cell testing utilizing a lithium reference electrode to understand the mechanisms that affect resistance rise and capacity fade in the path dependence studies of commercial Lithium Ion cell testing. Cells were evaluated using a novel in situ reference electrode method at the end of testing to determine the progress of fade mechanisms over time under the effect of cycling, calendar life, temperature, and various states of charge. This method quantifies not only the capacity of the cell but also the cell, negative electrode and positive electrode resistances. The in situ reference electrode was instrumental in separating the effects of the positive electrode and the negative electrode from the total performance of the cell. Prior to inserting a reference electrode into the cell, the cells were subjected to a series of 5-10 HPPC tests to condition the cells at both 30°C and room temperature, especially if the cells had been in storage at low temperature for greater than a month. This established a baseline of initial performance. After the reference electrode was inserted into the cell, another HPPC test was performed, with additional voltage data collected from the positive electrode/reference and the negative electrode/reference at room temperature inside of an argon filled glovebox. Comparison of end of life results to results gathered from new cells at the beginning of their life identified which electrode is limiting performance for path dependent life testing. A single cell from the group of cells tested at 60°C CD cycle life and calendar life was performance tested using the HPPC test. The reference electrode, used to isolate the negative and positive electrode

from the overall cell performance was placed as close as possible to the electrodes in the cell, such that the ohmic overpotential in the measurement was minimalized [61], which allowed greater accuracy of the resistance measurement. Utilizing the in situ reference electrode methodology, battery manufacturers can devise new strategies or materials based on which electrode is limiting cell performance to increase life, improve performance, or reduce cost.

5.2 Cell Capacity from Reference Performance Testing

The curves in Figure 5.1 indicate capacity loss throughout calendar aging as measured by 7.1 W (dashed) and $C_1/25$ (solid) discharge capacity tests (Cell 60) prior to reference electrode insertion. Figure 5.2 gives the 7.1 W and $C_1/25$ data for CD-aging (Cell 53) prior to insertion. Both cells encountered six RPTs and were therefore aged for the same time period (~ 6 months). The green diamonds in Figure 5.1 give the OCVs obtained from the BOL HPPC test. The $C_1/25$ maximum capacity is reflective of the theoretical maximum capacity of Cell 60 because the BOL $C_1/25$ voltages are in good agreement with these OCV values. Calendar aging resulted in the cell retaining only 53% of the BOL capacity, as measured by the $C_1/25$ test. The capacity retention after CD aging of 42% indicates the additional reduction in the theoretical maximum capacity due to cycling. Comparison of the dashed curves (~ 2-hour discharge) voltages to those of the solid curves (~ 25-hour discharge) indicates the voltage losses that are typically associated with the transport and kinetic irreversibilities[‡‡] that are absent in the nearly equilibrated $C_1/25$ discharge.

[‡‡] Overvoltage has been associated with ohmic and mass transport in the solid and liquid phases as well as charge transfer, for example [63].

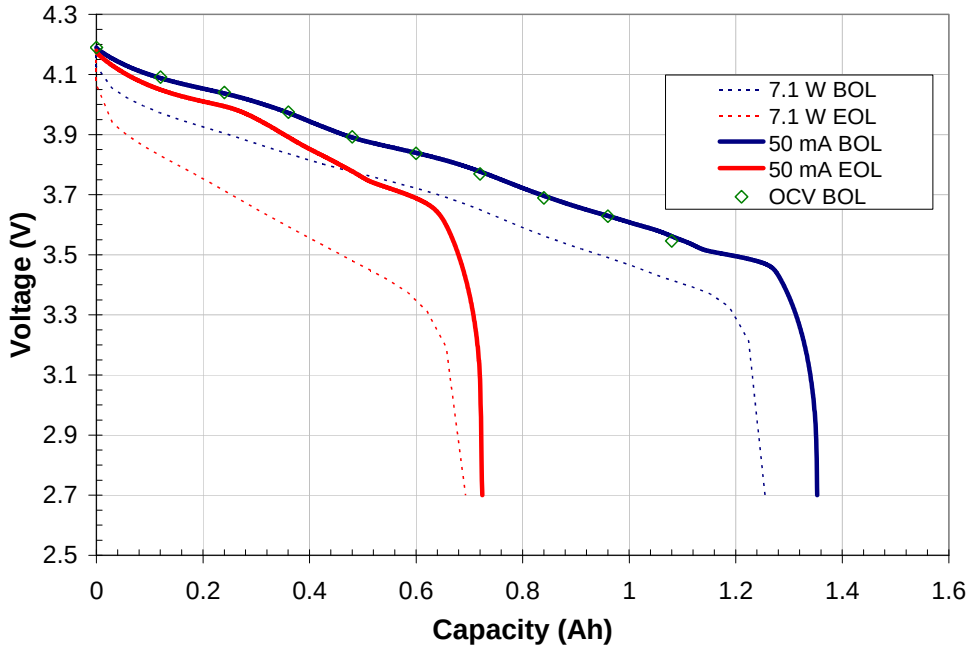

Figure 5.1: Capacity test data before and after calendar-aging (60°C, 60% SOC): 7.1 W test (dashed) and $C_1/25$ (solid) test for Cell 60 prior to reference electrode insertion. The green diamonds are OCVs from the BOL HPPC test.

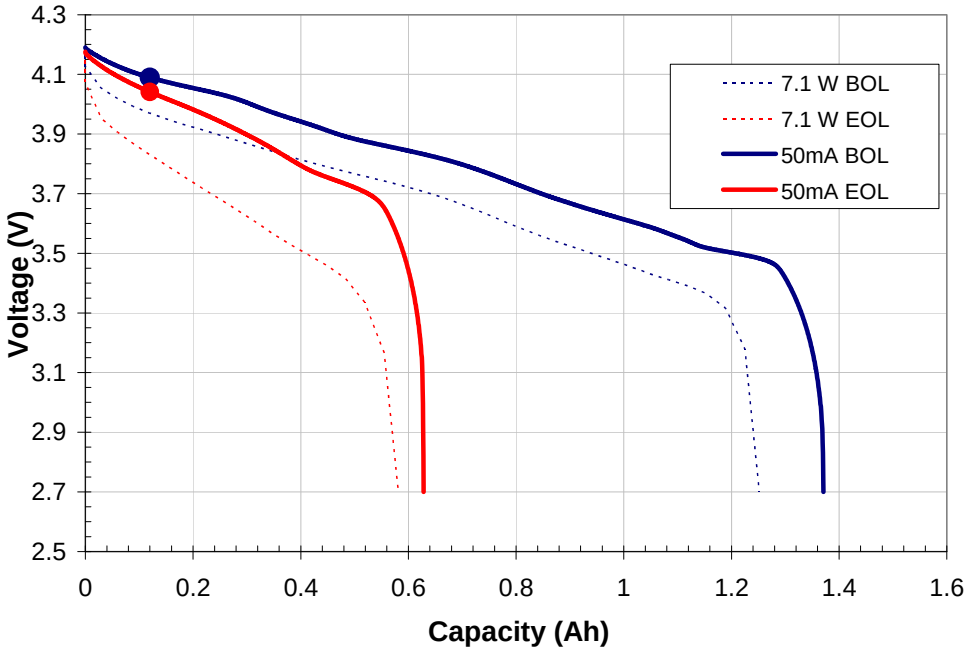

Figure 5.2: Capacity test data before and after CD-aging (60°C): 7.1 W test (dashed) and $C_1/25$ test (solid) for Cell 53 prior to reference electrode insertion. The dots denote 10% DOD.

Figure 5.3 shows the voltage vs. time data during the full 7.1 W capacity test at EOL$^+$ for the CD-aged cell (Cell 53) after reference electrode insertion. These data indicate that the cell voltage excursions throughout the test (i.e., over 1.5 V) can be attributed to the positive rather than the negative electrode. An expanded ordinate for the negative vs. Ref. is shown to highlight those of the negative, which varies less than 100 mV throughout the test. The discharge capacity was measured to be 0.54 Ah, which indicates that the cell further lost 7% its capacity during cold storage (i.e., compared to 0.58 Ah in Figure 5.2). The variations (± 5 mV) in electrode voltages vs. Ref. in Figure 5.3 during the 1 hour rest periods before discharge and after charge demonstrate the stability of the reference electrode. The

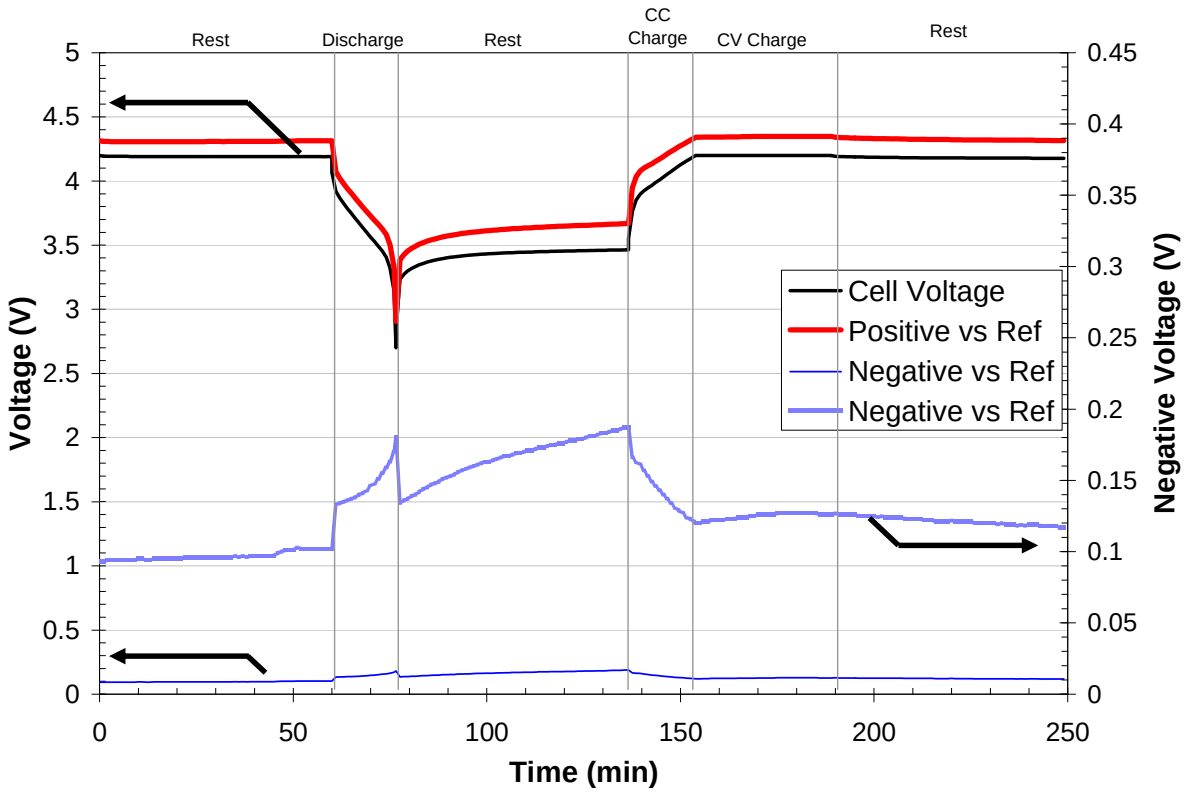

Figure 5.3: Voltage vs. time data during the full 7.1 W capacity test at EOL$^+$ for Cell 53 (i.e., CD-aged at 60°C) after reference electrode insertion.

precipitous drop in the positive voltage vs. Ref. during the discharge at 76 minutes and the lack of response in the negative voltage vs. Ref. indicates that the positive electrode limits the available capacity of the cell in this test. In contrast, differential voltage analysis [48] of the C_1/25 EOL discharge in Figure 5.2 would indicate that the cell's capacity is limited by the negative electrode. The lower electronic conductivity of the positive electrode active material relative to that of the negative [63] is the likely explanation the apparent higher resistance of the positive electrode than that of the negative and will be discussed further in the next section. The electrode voltages vs. Ref. during the rest period between discharge and charge show that the cell voltage relaxation behavior after interruption of discharge also is dominated by the positive electrode. The cell voltage after interruption is within 20 mV of the 1 hour cell OCV after 30 min. The positive electrode is also responsible for the rise in cell voltage during charge to the 4.2 V lid.

Figure 5.4 shows the 7.1 W capacity results for representative cells subjected to the three aging regimes. Relative to cycle aging, we would expect a lesser degree of capacity decay via calendar aging because the minimized flow of current would greatly limit the effects of parasitic chemical processes and mechanical stresses induced by current throughput. The lithium insertion and extraction that accompanies current flow is associated with particle swelling and shrinking, cracking, and perhaps loss of electrical connectivity or increased area of polarization to drive parasitic electrochemical reactions. Thus, relative to CD aging, the CS-aging regime would result in a lesser degree of capacity decay because of the lower average current and the smaller average changes in the electrode degrees of lithiation associated with the cell not being swept through the full range of available capacity.

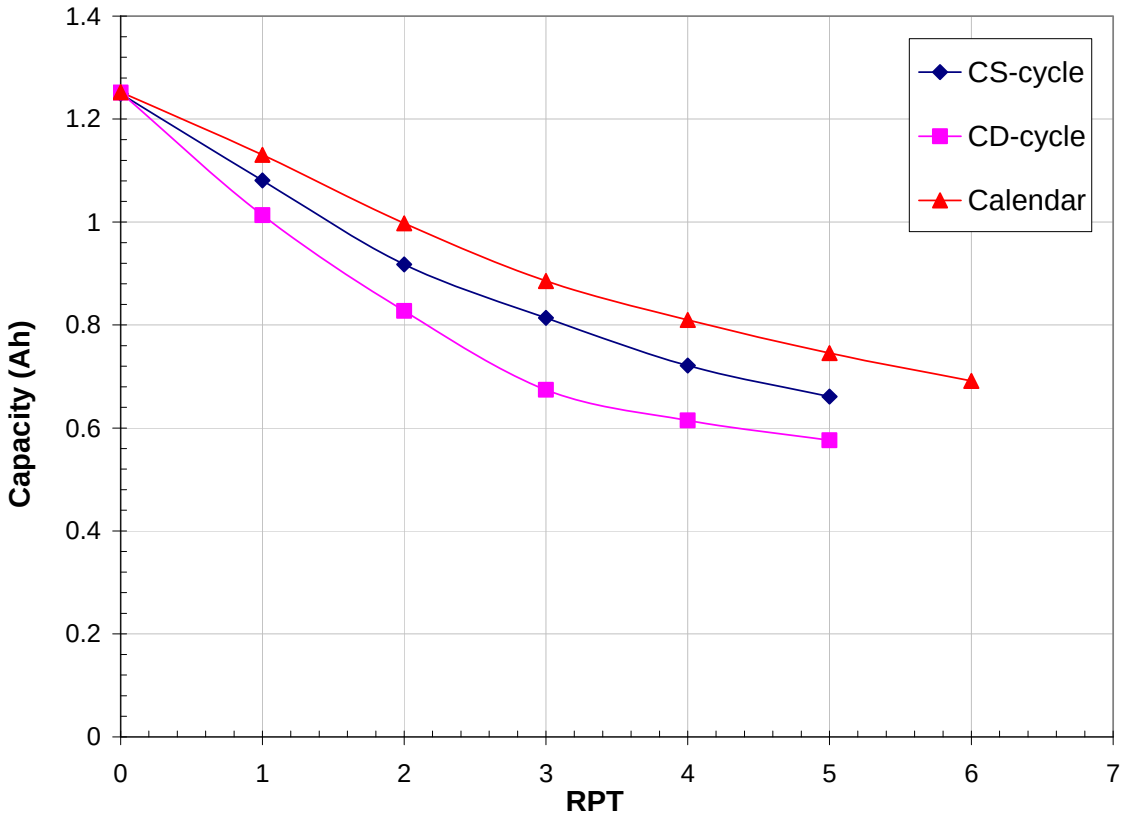

Figure 5.4: Capacity comparison of CS (blue), CD (pink), and Calendar Life (red) results at 60°C as measured by the 7.1 W discharge capacity tests at each RPT.

5.3 Stability of the Reference Electrode

Figure 5.5a and Figure 5.5b show voltage and current profiles, respectively, during the 7.1 W capacity tests and HPPC test for a representative BOL cell (i.e., Cell 111). The reference electrode used with Cell 53 (see Figure 5.3) was brand new and showed more stability during the rest periods (from 0 to 60 minutes and 190 to 250 minutes) than the reference used with Cell 111 in Figure 5.5 (from 75 to 135 minutes and 1140 to 1200 minutes), which had been used several times. After the discharge in both cases, (Figure 5.3, from 76 to 136 minutes and Figure 5.5, from 172 to 232 minutes) the reference electrode shows less stability which can be attributed to the equilibration of the system after the

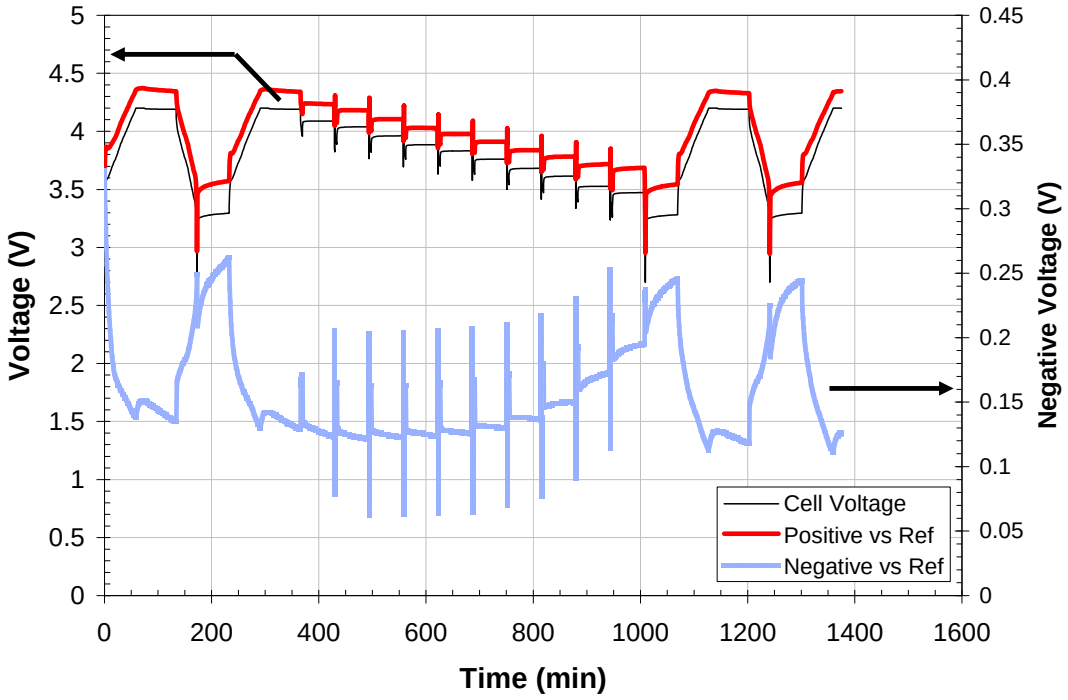

a)

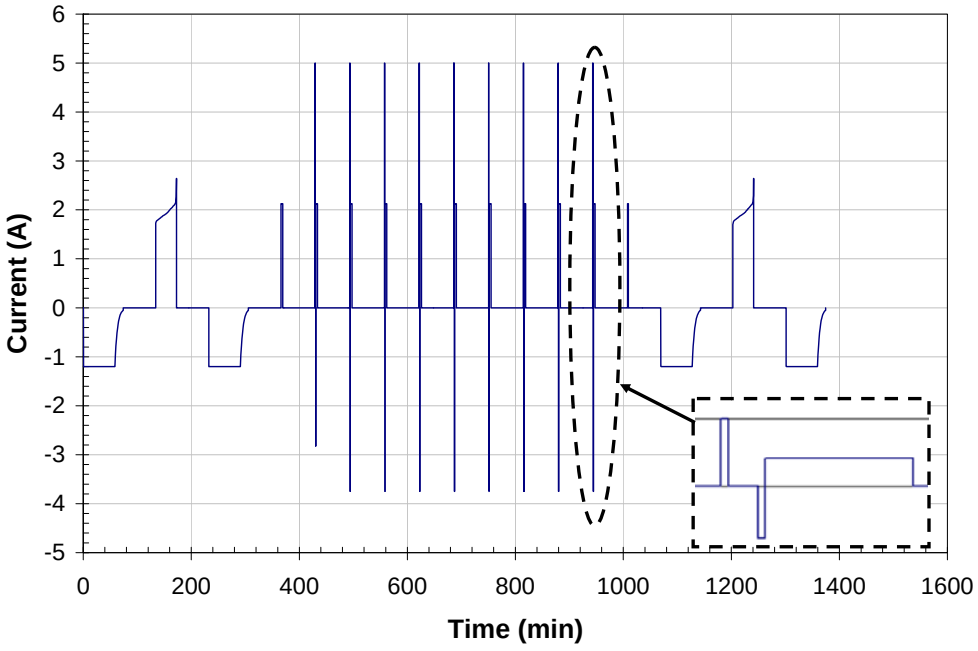

b)

Figure 5.5: Voltage (a) and current (b) profiles during the RPT for Cell 111 prior to aging (i.e., RPT 0). Insert: expanded view of the 90% DOD 10-second discharge pulse, 40-second rest, 10-second charge pulse, and initial portion of the 2.13 A discharge to 100% DOD.

discharge. However, it was observed that the reference electrode would develop a surface layer which would dull the original shiny lithium surface after a period of use. This surface layer could be scraped off. Although the same drift (on the order of a couple of millivolts) was noticed during the discharged condition, the fully charged condition showed little drift in the reference electrode voltage.

5.4 Resistances from Reference Performance Testing

Calculations of cell and electrode resistances (designated as *RdisPos* or *RdisNeg*) can be made from the HPPC results. Figure 5.5a shows the overall cell voltage, the positive electrode vs. Ref. (shown in red) and the negative electrode vs. Ref. (shown in blue) that were used for the calculations. The resistance is calculated to be the difference between the 1 hour OCV and the 10-s voltage divided by the HPPC pulse current. For example the discharge resistance at 40% DOD for Cell 111 is calculated from the following values: (3.887 V-3.608 V)/5.0 A = 0.0558 Ω. However, instead of using the voltage between the positive and the negative electrode, either the voltage difference between the positive and the reference electrode is used, or between the negative and the reference electrode is used. Every cell that was tested with a reference electrode had at least two sets of 5 sequential HPPC tests performed at ~25°C before and after the insertion. Table 5.1 shows there is good agreement between the results of two of the first two sets of 5 sequential HPPC tests for Cell 53 at EOL^{+}. The resistance (3^{rd} col.) from the HPPC that was performed before reference electrode insertion was ~6% larger than the HPPC test (5^{th}col.) after the insertion. These values, observed to be close to the measured cell resistance, which is separately measured between the positive terminal and the negative terminal as expected. The OCV values in column 2 and column 4, between the two tests match, indicating that in terms of OCV, the pulses were performed at the same SOC. The *RdisNeg*

is ~5 times smaller than the *RdisPos*. Consequently, the information in Table 5.1 shows that inserting the reference electrode in the cell decreases the resistance measured 5.6% after the insertion due to the increased electrolyte added to the system. These results provide confidence for a comparison between the reference electrode results of other cells.

Table 5.1: Resistances of CD-aged cell (Cell 53) at EOL^+ before and after reference electrode insertion (Positive electrode is red and Negative electrode is blue).

Before Insertion			**After Insertion**				
DOD	OCV	Cell Resistance	OCV	Cell Resistance	RdisPos + RdisNeg	RdisPos	RdisNeg
%	(V)	(Ω)	(V)	(Ω)	(Ω)	(Ω)	(Ω)
0	4.175		4.178				
10	4.044	0.1067	4.045	0.1006	0.1006	0.0840	0.0166
20	3.943	0.1082	3.944	0.1018	0.1022	0.0854	0.0168
30	3.809	0.1085	3.810	0.1018	0.1022	0.0856	0.0166
40	3.717	0.1146	3.716	0.1093	0.1098	0.0930	0.0168

Figure 5.6 shows the voltage during the 7.1 W capacity test and subsequent four HPPC discharge and charge pulses with a reference electrode for Cell 53 at EOL^+. (Calculated resistances associated with the results in these three figures are shown in Figure 5.8.) Note that the discharge and charge portions up through 250 minutes in Figure 5.6 were shown previously in Figure 5.3. A new cell with no capacity loss (e.g., Figure 5.5) would have 9 pulses, while and an aged cell would have fewer pulses, such as the four pulses shown in Figure 5.6. Figure 5.7 gives the HPPC discharge resistances for the full cell, positive-, and negative-electrodes as a function of DOD before and after calendar aging (60°C, 60% SOC,

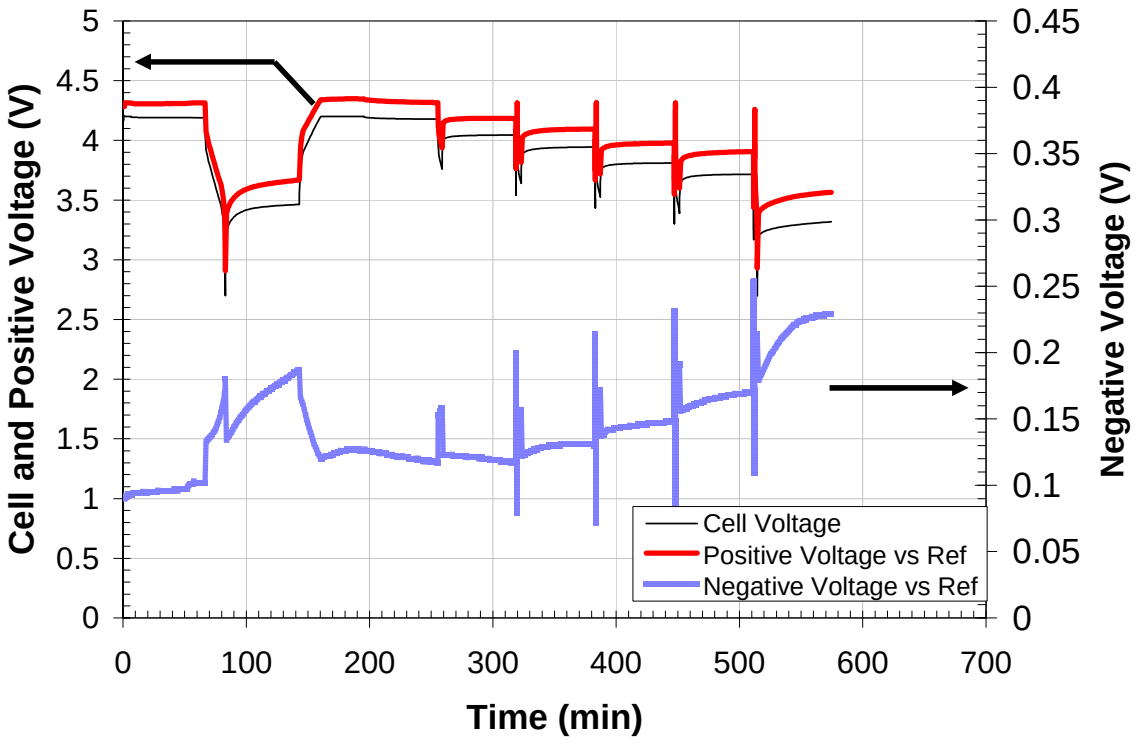

Figure 5.6: Voltage profiles of Cell 53 during RPT 6 after CD aging (60°C).

Cell 60) and Figure 5.8 gives these resistances before and after CD-aging (Cell 53). Both figures show increased full cell resistance from BOL to EOL^{+} for both calendar and CD aging. The data in Figure 5.8 show that the resistance of the negative electrode rises 6% and the resistance of the positive electrode rises 148% after CD aging. Figure 5.7 shows that after calendar aging the resistance of the negative electrode rises 19% and the positive electrode rises 165%. Both figures show little to no change in the resistance of the negative electrode from the BOL to EOL^{+} in comparison to the positive electrode. The large change in cell resistance from BOL to EOL^{+} is the direct result of the large change in the positive

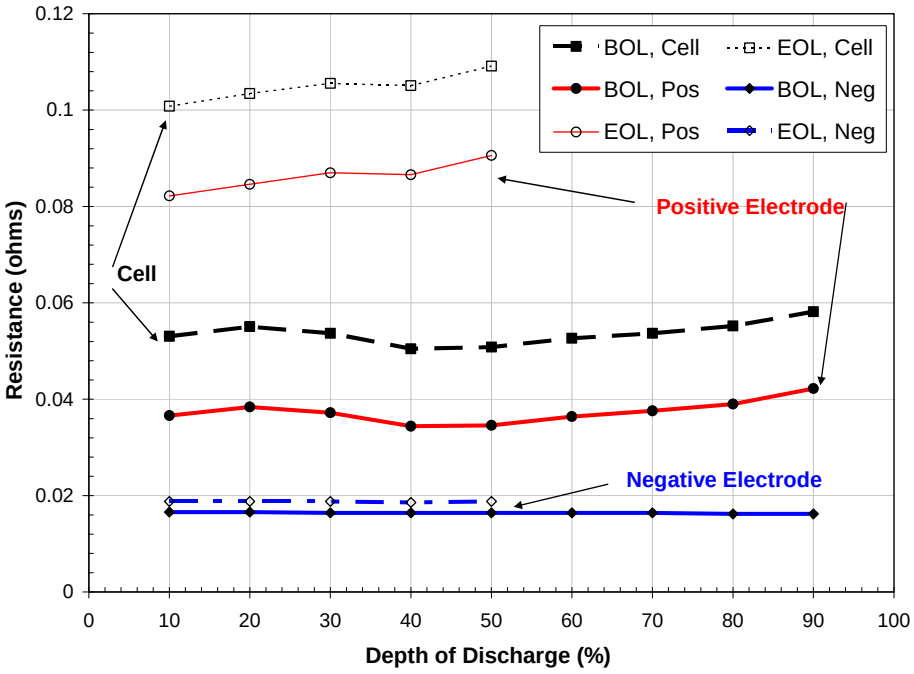

Figure 5.7: HPPC discharge resistances (10-s) for the full cell (black), positive- (red), and negative- (blue) electrode before and after calendar-aging (60°C, 60% SOC) for Cell 60.

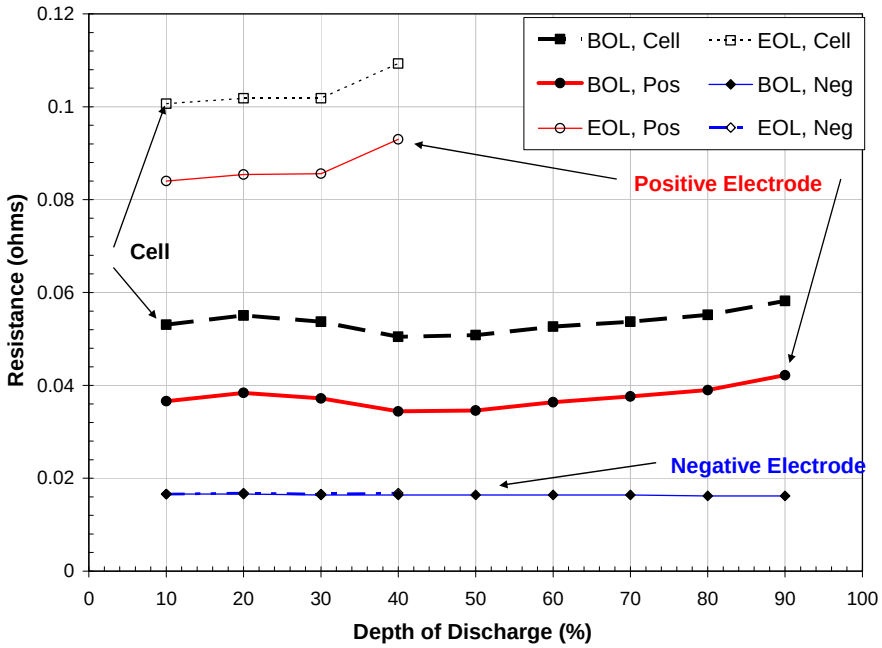

Figure 5.8: HPPC discharge resistances (10-s) for the full cell (black), positive- (red), and negative- (blue) electrode before and after CD-aging (60°C) for Cell 53.

electrode resistance.

Figure 5.9 shows the positive and negative electrode voltages vs. reference electrode during the 10% DOD (i.e., 0.12 Ah removed) HPPC discharge pulse at BOL and after CD aging (EOL^{+}), from which the first set of resistances in Figure 5.8 were obtained. At the onset of current, for the negative electrode data (bottom) in Figure 5.9 both before and after CD aging, a value of *initial* polarization is exhibited. "Initial" electrode polarization is defined as the magnitude of the difference between the OCV vs. Ref. and the electrode voltage (vs. Ref.) measured at 50 ms (i.e., the first data point after current onset) and likewise for "initial" cell polarization. This polarization is maintained throughout the 10-s pulse, and then rapidly (i.e., within 1s) the voltage returns to the open-circuit condition after the current interrupt. The increase in the BOL negative OCV vs. Ref. of ~ 25 mV with aging (from 130 to 155 mV vs. Ref.) may represent reference electrode drift, but is more likely due to the carbonaceous negative residing in a lower state of lithiation [48, 63]. Another potential advantage of these types of reference electrode measurements is the ability to map the degree of lithiation of the electrode from the OCV data if the electrode OCV vs. degree of lithiation relationship is known *a priori*. Since the negative electrode polarization remains constant during the pulse after the initial polarization may indicate that the electrode material resides on a voltage plateau throughout the pulse [63]. The negative-electrode BOL polarization (above open circuit) is ~ 90 mV and increases slightly (to ~ 100 mV) after CD aging, perhaps due to decreased electronic conductivity resulting from particle fracture.

In contrast, the positive electrode (top portion of Figure 5.9) exhibits a certain value of initial polarization. The polarization increases throughout the pulse, but the voltage vs. Ref. slowly returns to the open-circuit condition (within several minutes) after the

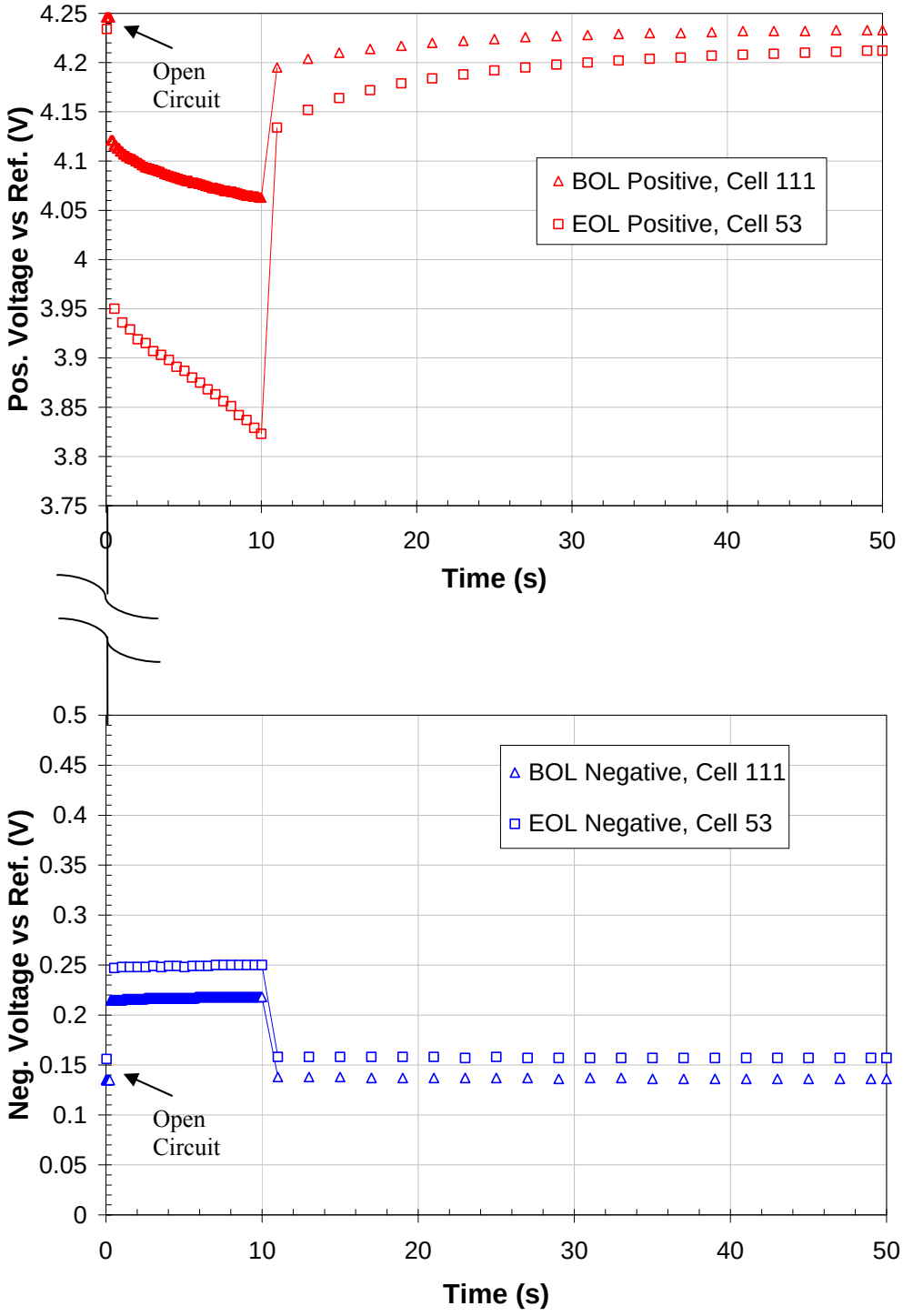

Figure 5.9: Electrode voltage vs. time during the 10-s 10% DOD HPPC discharge pulse before (Δ) and after (□) CD aging (60°C): positive vs. Ref (top, red) and negative vs. Ref. (bottom, blue).

current interrupt. The initial polarization of the positive electrode is ~ 35% greater than that of the negative prior to aging and is nearly triple that of the negative after aging. Since the initial polarization in these types of cells has been associated primarily with the electronic conductivity of the solid active material [63], it is postulated that the increase with aging may be due to the loss of electrical connectivity resulting from particle fracture. The buildup of positive-electrode polarization after the presentation of the initial value and relaxation after current interrupt has been attributed to the generation and dissipation, respectively, of solid-state lithium concentration variations throughout the positive electrode particles [63]. This buildup of polarization after aging is nearly triple that of the BOL values may indicate lowered ease of solid-state lithium transport through the degraded active material. Reasons for the decrease in the BOL positive OCV vs. Ref. of ~ 10 mV after aging may be the preferential degradation of the high-voltage component of the blended material, or the positive active material residing in a higher state of lithiation. As expected, the full cell OCV (by difference in figure) prior to the onset of current is lower after CD aging than at the BOL. These BOL and EOL^{+} OCVs are more clearly denoted by the navy and red dots, respectively, in Figure 5.2, which show ~ 30 mV decrease with CD aging.

Table 5.2 shows a summary of the reference electrode tests resistance results for representative cells subjected to the three different aging regimes. The BOL capacity results in Table 5.2 show a significant difference between the 7.1 W capacity and $C_1/25$ capacity, as expected. The EOL^{+} 7.1 W and $C_1/25$ test results do not show the same significant difference that was seen in the beginning of life results. These results indicate that the loss of either available lithium for intercalation within the specified voltage limits or the loss of intercalation sites is more significant than the effects of diffusion at the beginning of life.

Additionally, the capacity loss from the charge depleting cycle life test is 18% larger than the average calendar and charge sustaining cycle life 7.1 W and 22% larger for the $C_1/25$ measurements. These results show that the CD cycle life results in slightly more capacity degradation than the calendar life and CS cycle life testing, (see Figure 5.1 and Figure 5.2).

Table 5.2: Capacity and resistance summary of BOL (without reference electrode) and EOL$^+$ Cells (with and without reference electrode) (Positive electrode is red and Negative electrode is blue).

Beginning of Life								
Cell	Test Cond. (°C)	7.1 W (Ah)	C1/25 (Ah)	Cell Resistance (Ω)	Cell Resistance (Ω)	RdisPos + RdisNeg (Ω)	RdisPos (Ω)	RdisNeg (Ω)
111	new	1.257		0.057			0.035	0.016
53	CD 60°C	1.252	1.371	0.049				
60	Cal 60°C	1.255	1.353	0.048				
84	CS 60°C	1.250	1.290	0.049				
End of Life								
53	CD 60°C	0.581	0.581	0.095	0.109	0.110	0.093	0.017
60	Cal 60°C	0.693	0.724	0.101	0.109	0.109	0.091	0.019
84	CS 60°C	0.673	0.674	0.106	0.107	0.107	0.087	0.020

Table 5.2 also demonstrates the rise in resistance for the positive electrode tested. Comparison of the HPPC resistance at 40% DOD shows the same consistency as Table 5.1 before and after the insertion of the reference electrode. The rise of resistance in all cases from the BOL to the EOL$^+$ is expected. However, the bulk of the rise in resistance is concentrated at the positive electrode. While there is some difference in the negative electrode resistance, it tends to be much smaller, (6 % to 25%), than the difference in the positive electrode resistance (148% to 165%). The rise in negative electrode resistance is either the effect of measurement error or the solid-electrolyte interphase, a nanometer scale

buildup of solvent reaction products on the negative electrode. However, the significant rise in resistance of the positive electrode can be attributed to either a similar buildup of solid-electrolyte interphase and/or a decrepitation (micro-cracking and structural disordering) of the positive electrode. The decrepitation mechanism accounts for the rise in resistance and loss of capacity through the loss of intercalatable lithium/lithium intercalation sites. As the structure changes, portions of the electrode will become electronically disconnected, creating an increasingly tortuous path of electron conduction and trapping lithium ions within the structure at the same time. This same phenomenon could also be affecting the negative electrode in a less pronounced way.

5.5 Summary

Due to the long term nature of life testing, it is important to identify which electrodes are limiting performance under various life conditions, rather than haphazardly modifying one or both electrodes to improve life. The *in situ* reference electrode can be used to quantify the electrode capacity, consistent with past work but also be expanded to evaluate the resistance contributions from each electrode.

While some of the capacity loss during the 7.1 W constant power discharge test between BOL and EOL can be attributed to the rise in resistance, virtually none of the corresponding capacity loss during the $C_1/25$ discharge can be attributed to the rise in resistance. The $C_1/25$ capacity loss is the direct result of the rise in resistance that was identified in the end of life reference electrode tests. As the resistance of the positive rises, it is presumed that this is the result of the main degradation mechanisms of the positive

electrode such as; micro-cracking and structural disordering, which can cause a loss of available sites for lithium intercalation.

Utilizing the *in situ* reference electrode methodology, battery manufacturers can devise new strategies or materials based on which electrode is limiting cell performance to increase life, improve performance, or reduce cost. This work has shown that insertion of a reference electrode into the original container is feasible with proper precautions. Additionally, performance testing with a reference electrode identifies which electrode limits performance during aging.

The work done with reference electrodes shows the degradation on the positive electrode is responsible for the performance degradation of the cell. Consequently, in order to further improve lithium ion technology, reference electrodes coupled with long term testing must be used to identify which electrodes limit overall cell capacity and resistance performance. This work clearly points to the positive electrode as the cause of the resistance rise.

Chapter Six: Mathematical Model

6.1 Model development

The fundamental physical process occurring during the battery operation involves movement of the lithium ions between the positive and the negative electrodes. Lithium intercalated in the negative electrode in a charged cell deintercalates, travels across the separator and intercalates into the positive electrode during discharge. The reverse reaction takes place during the charging operation. The chemical reactions occurring in this process can be represented by the following equation.

$$Li^{+} + e^{-} + \theta_s \Leftrightarrow \left\{Li^{+\delta} - \theta_s^{-\delta}\right\} \qquad \text{Equation 6.1}$$

θ_s represents the vacant sites available for lithium ions to intercalate into the host material. $\left\{Li^{+\delta} - \theta_s^{-\delta}\right\}$ represents the intercalated species, and δ represents the charge of the species after intercalation. [64]

The cell potential (voltage) is a function of the concentration of the intercalated species, and the Nernst equation takes the following form, assuming ideality which allows the activities to be replaced by concentrations.

$$V = V^0 - \frac{RT}{nF}\ln\left[\frac{[Li^{+}][\theta_s]}{[Li^{+\delta} - \theta_s^{-\delta}]}\right] \qquad \text{Equation 6.2}$$

V is the potential at the temperature of interest, with V^0 as the standard potential

R is the gas constant

T is the temperature in Kelvin

N is the number of equivalents per mole involved in the reaction

F is Faradays constant, [64, 65]

The current (I) in A is related to the cell capacity (Q) in Ah by:

$$\frac{dQ}{dt} = I \qquad \text{Equation 6.3}$$

The cell energy (E) in Wh is related to the current and voltage:

$$\frac{dE}{dt} = IV \qquad \text{Equation 6.4}$$

The performance of any cell deteriorates over time, as observed by a decrease in the cell voltage, capacity and energy. The decrease in the voltage can be explained on the basis of a decrease in the number and concentration of the vacant sites, θ_s. As fewer sites are available for the intercalation of lithium ions, the concentration of the intercalated species also goes down. As a result, the cell voltage decreases as governed by equation 6.2. It should be noted that this decrease in vacant sites takes place over several of charge and discharge cycles (cycle life) or extended period of zero duty (calendar life). The concentration of the sites can be assumed to be constant during any single charge or discharge cycle. In other words, there is only a negligible change in the number and concentration of the vacant sites as the cell goes from a fully charged to fully discharged state.

The cell voltage and hence the cell energy are functions of the concentration of the vacant sites. A rigorous mathematical model for the performance of the cell will involve these concentrations, which cannot be measured, but are time-dependent. A simplified model

can be developed by expressing the concentrations as a time function that decreases over time, leading to the following equation:

$$\frac{dE}{dt} = kf(t) \qquad \text{Equation 6.5}$$

Where, k is the rate constant. The decrease in cell energy over time can be modeled by a time dependent function. Further, the temperature dependence of the degradation can be incorporated in the model through the rate constant, which can be assumed to have Arrhenius-type dependence on temperature.

$$kA(T) = A\exp(-\frac{E}{RT}) \qquad \text{Equation 6.6}$$

kA(T) = specific reaction rate or calendar life (yr^{-1})

A_o = preexponential factor or frequency factor (yr^{-1})

E = activation energy, J/mol

It has been observed that the rate of cell degradation rises exponentially with temperature, and the above equation 6.6, can be used to model the performance degradation of cell (energy fade, capacity fade, etc.) as a function of time and temperature. While Celsius was used to describe the testing in previous sections, Kelvin will be used for the temperature with the modeling chapter. Equation 6.6 is typically written in the forms shown below.

$$\frac{dE}{dt} = -B_1 E_1 \exp(B_o + \frac{B_2}{Temp}) * t^{(B_1 - 1)} \qquad \text{Equation 6.7}$$

$$\frac{dE}{dt} = -B_1 E_1 A_0 \exp(\frac{B_2}{Temp}) * t^{(B_1 - 1)} \qquad \text{Equation 6.8}$$

E is the energy. E_1 is the energy in Wh at RPT 0 (beginning of testing, RPT 0). $B_1\exp(B_0)$ is the frequency factor with units of time [yr^{-B1}] raised to the $-B_1$ power, B_2*R is the Activation Energy, and B_1 is the exponent of time. Equation 6.8 shows a modified version of Equation 6.7, where A_0 is $\exp(B_0)$ with units of time raised to the $-B_1$ power.

The following equations (6.9, 6.10, and 6.11) are used for life models for capacity, resistance and power, respectively. These equations are similar nature to the energy equation 6.4 discussed previously. Relative capacity is defined as initial capacity, C_0 at time = 0 divided by the capacity at time = a, C_a. Relative resistance as shown in Figures 6.8, and 6.10 is defined as Resistance at time = a, R_a divided by the initial resistance, R_0 at time = 0. Relative power as shown in Figure 6.12 and 6.14 is defined as initial power, P_0 at time = 0 divided power at time = a, P_a.

$$\frac{dC}{dt} = -B_1 C_1 A_0 \exp(\tfrac{B_2}{Temp}) * t^{(B_1 - 1)} \qquad \text{Equation 6.9}$$

$$\frac{dR}{dt} = -B_1 R_1 A_0 \exp(\tfrac{B_2}{Temp}) * t^{(B_1 - 1)} \qquad \text{Equation 6.10}$$

$$\frac{dP}{dt} = -B_1 P_1 A_0 \exp(\tfrac{B_2}{Temp}) * t^{(B_1 - 1)} \qquad \text{Equation 6.11}$$

In all cases, the values that were modeled were normalized, i.e. relative capacity, relative resistance and relative power. Modeling of the data was accomplished by program designed specifically for curve fitting calendar and cycle life data for batteries by Argonne National Laboratory called "Battery Life Estimator." [67] This program not only curve fits the data by providing an appropriate model and initial guesses, but also predicts the calendar life of a device at some specified temperature, usually 30°C or 303K as well as the upper and lower confidence limits. The upper and lower confidence limits are determined from a

Monte Carlo simulation using the estimated error from the experimental data and cell to cell variation.

The proposed model can be used to construct a mathematical relation of fade as a function of temperature and time and to predict life at normal operating conditions, nominally 30°C or 303K. Accelerated testing at elevated temperature can be used to obtain data for parameter estimation and model validation. The main caveat is the elevated temperatures must not introduce any new degradation mechanisms that do not otherwise occur at normal operating conditions.

6.2 Capacity Results

6.2.1 Calendar Life

Figure 6.1 shows the model and relative capacity during calendar aging at 303, 313, 323, and 333 K. The results at 303, 323, and 333 K show the best agreement with the model. The results for 313K show an increasing discrepancy between the experimental data and model after 1 yr. Capacity fade of 20 % (relative capacity of 1.2) was used for the EOL for the life estimate. When the cell fails to meet the 45 kW Available Power target, this is defined as EOL. The model predicts the cells at 303K will reach EOL at 2.85 years, see Figure 6.2. UCL and LCL are the upper and lower confidence limits for the estimates. Confidence limits are the upper and lower boundaries for the confidence interval, which indicates the reliability of the estimate.

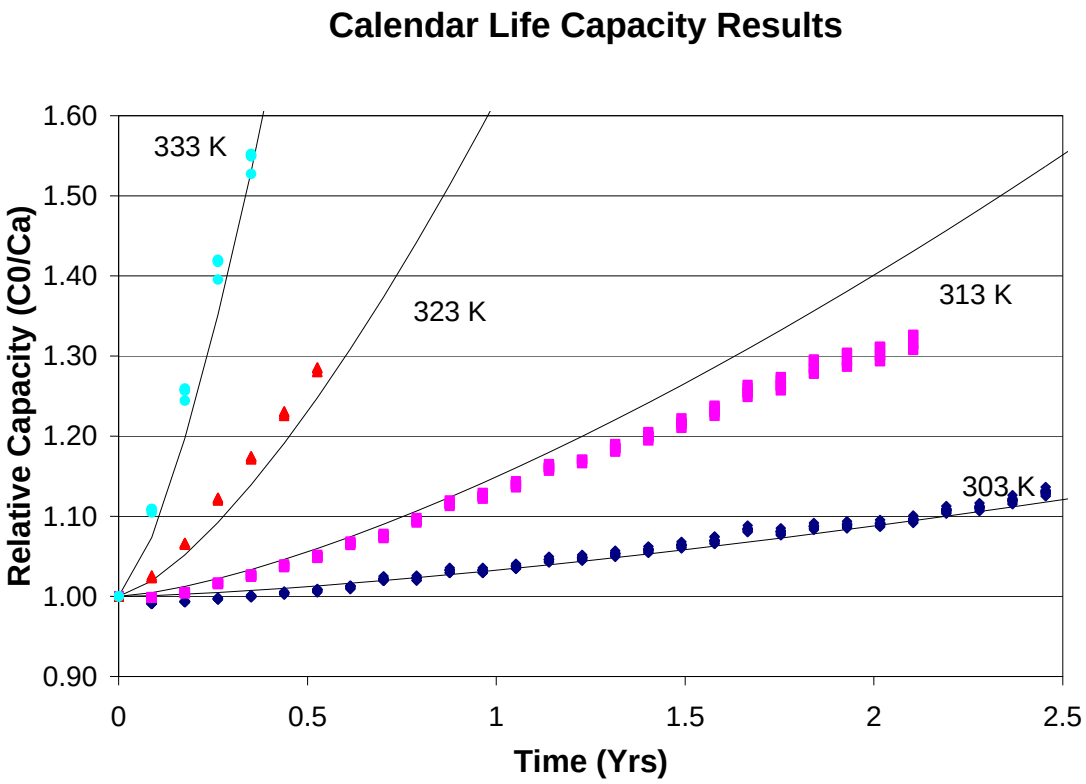

Figure 6.1: Capacity model results for calendar life versus time and temperature (K)

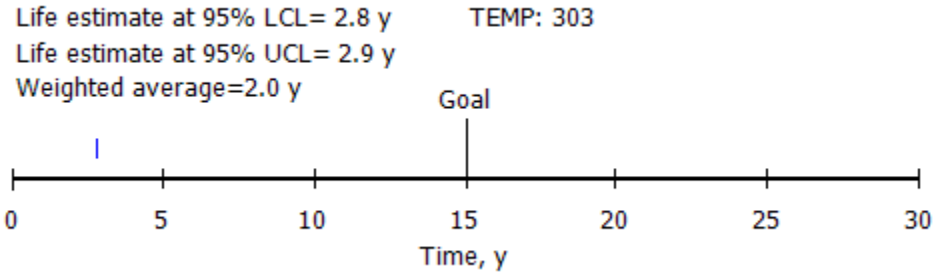

Figure 6.2: Life estimate for capacity model results for calendar life versus time and temperature (K)

6.2.2 Cycle Life

Figure 6.3 shows the model and relative capacity during CD aging at 303, 313, 323, and 333 K. The results at 303, 323, and 333K show agreement with the model predictions over the 1.1 yr time period. The results at 313 show a continuous gap between prediction

and performance after the 1st RPT. The cells at 303K fail to meet the 45kW EOL target (1.2 relative capacity) after 0.6 yrs, or 3500 CD cycles, see Figure 6.4.

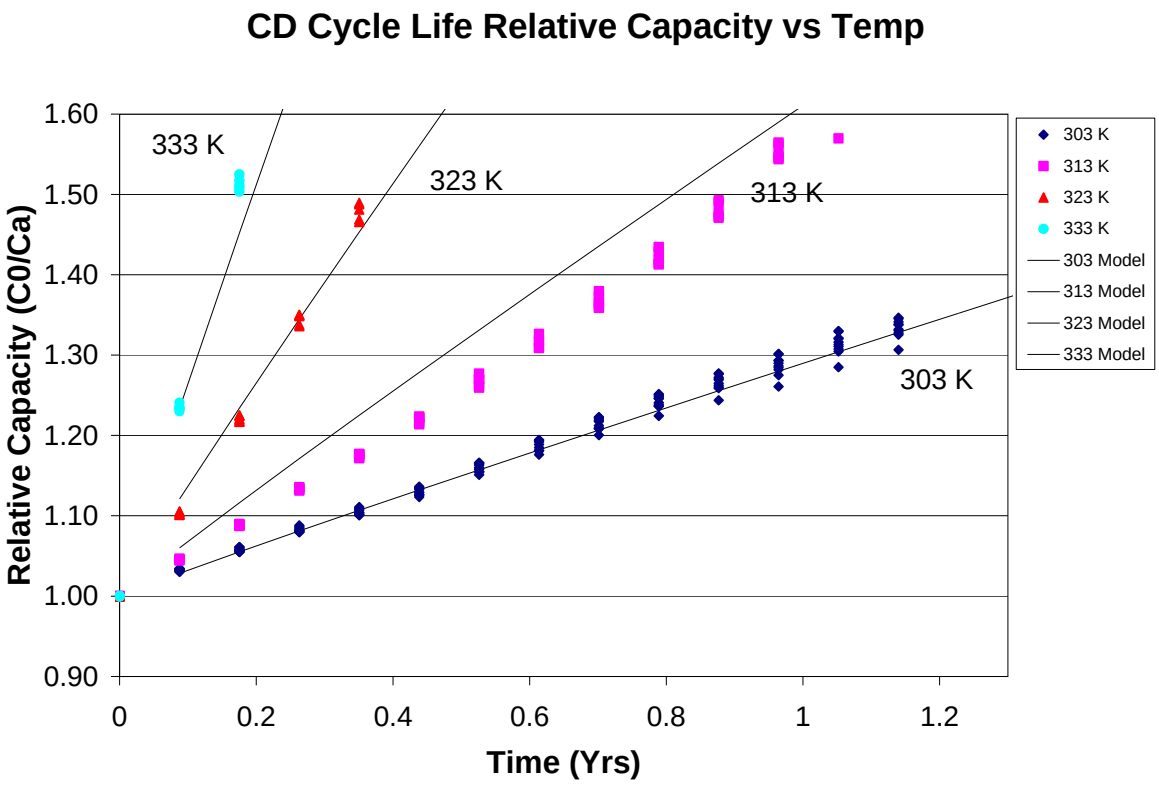

Figure 6.3: Capacity model results for CD cycle life versus time and temperature (K)

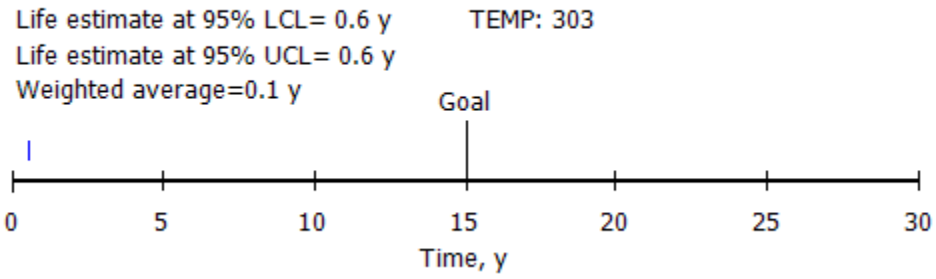

Figure 6.4: Life estimate for capacity model results for CD cycle life versus time and temperature (K)

6.2.3 Calendar Life SOC

The same EOL criteria for Figure 6.4 used for the results in Figure 6.5, the model and relative capacity results during calendar aging at 30, 60, and 90% SOC. Thus, the life estimate, shown in Figure 6.6 is the same. While the 30 and 60 % SOC results agree with the model, the results at 90% SOC do not agree as well due to the noise in the data from 2 yrs onward.

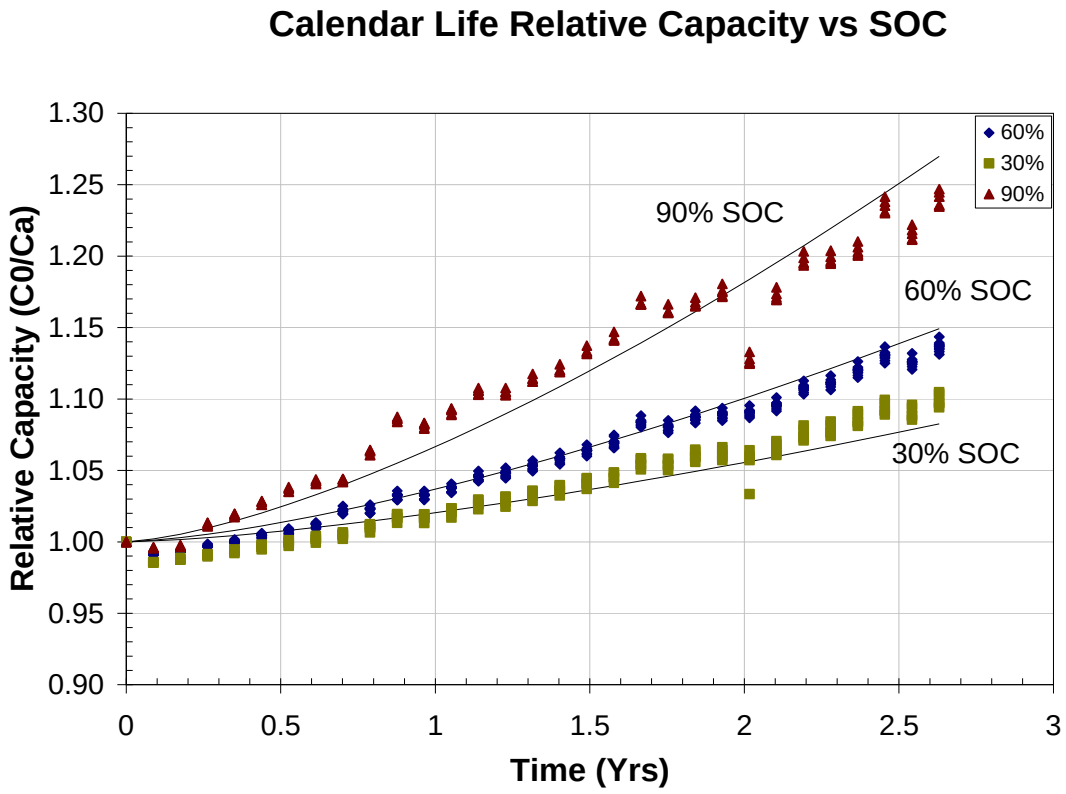

Figure 6.5: Capacity model results for calendar life versus time and state of charge

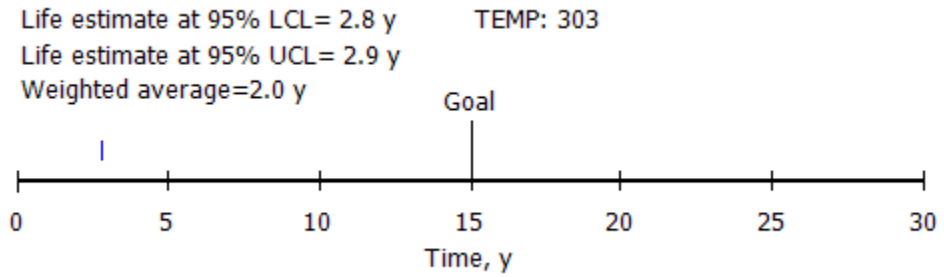

Figure 6.6: Life estimate for capacity model results for calendar life versus time and state of charge

6.3 Resistance

6.3.1 Calendar Life

Figure 6.7 shows the model and relative resistance for calendar aging at 303, 313, 323, and 333 K. The model agrees with the 303 and 323K results, but diverges from the 313

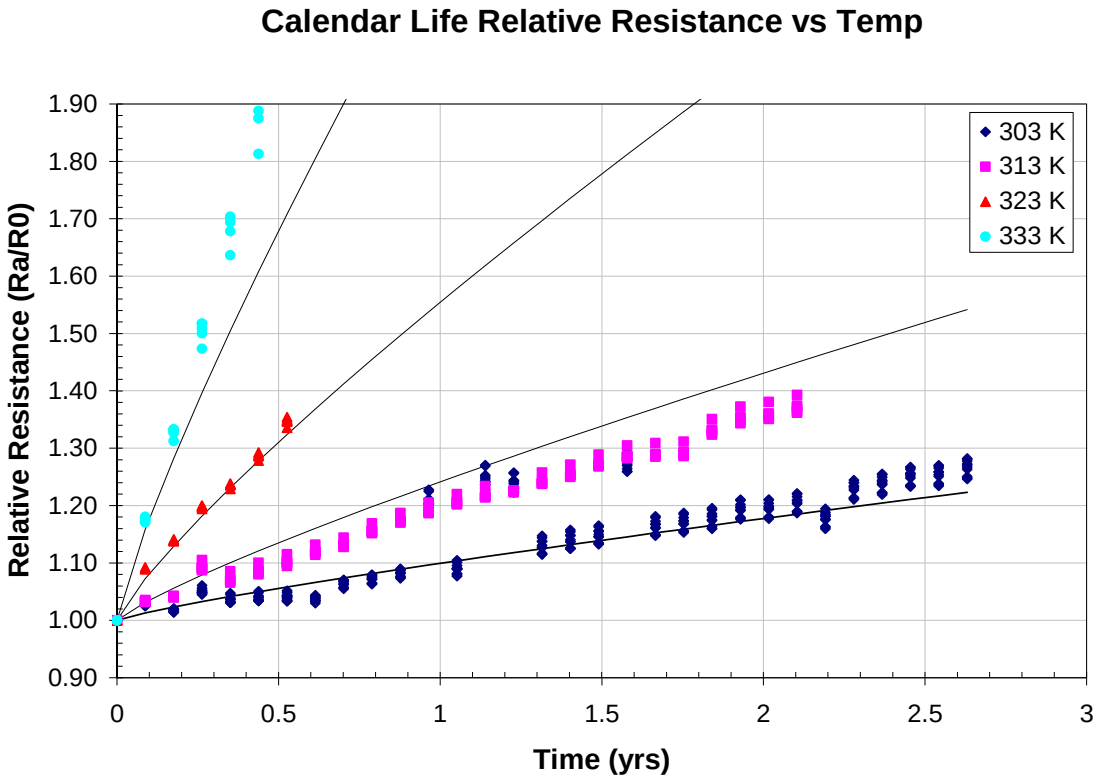

Figure 6.7: Resistance model results for calendar life versus time and temperature (K)

and 333 K results as time progresses. The life estimate, shown in Figure 6.8 of 3.1 years is based on a relative resistance of 1.3, where the cells at 313K were estimated to be unable to meet the 45kW EOL Available power target.

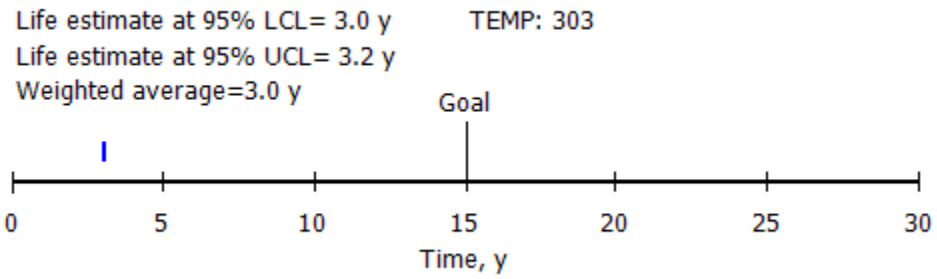

Figure 6.8: Life estimate for resistance model results for calendar life versus time and temperature (K)

6.3.2 Cycle Life

Figure 6.9 shows the model and relative resistance for CD aging at 303, 313, 323, and 333K. The model fits for 313 and 303K are poor and indicate another mechanism early in life that reduces resistance. The model fits get worse for the last few data sets at each of the temperatures, indicating yet another competing mechanism compared to just the Arrhenius kinetics mechanism. The life estimate, shown in Figure 6.10 of 0.8 years shows the cells at 303K did not meet the Available Power targets, 45kW after 4500 CD cycles and a relative resistance of 1.3. The tapering effect in the 60°C data is the result of an inability of the cells to complete the full CD cycle life profile, resulting in a reduced level of degradation after RPT 3 due to the large amount of capacity fade of the cells at the high temperature.

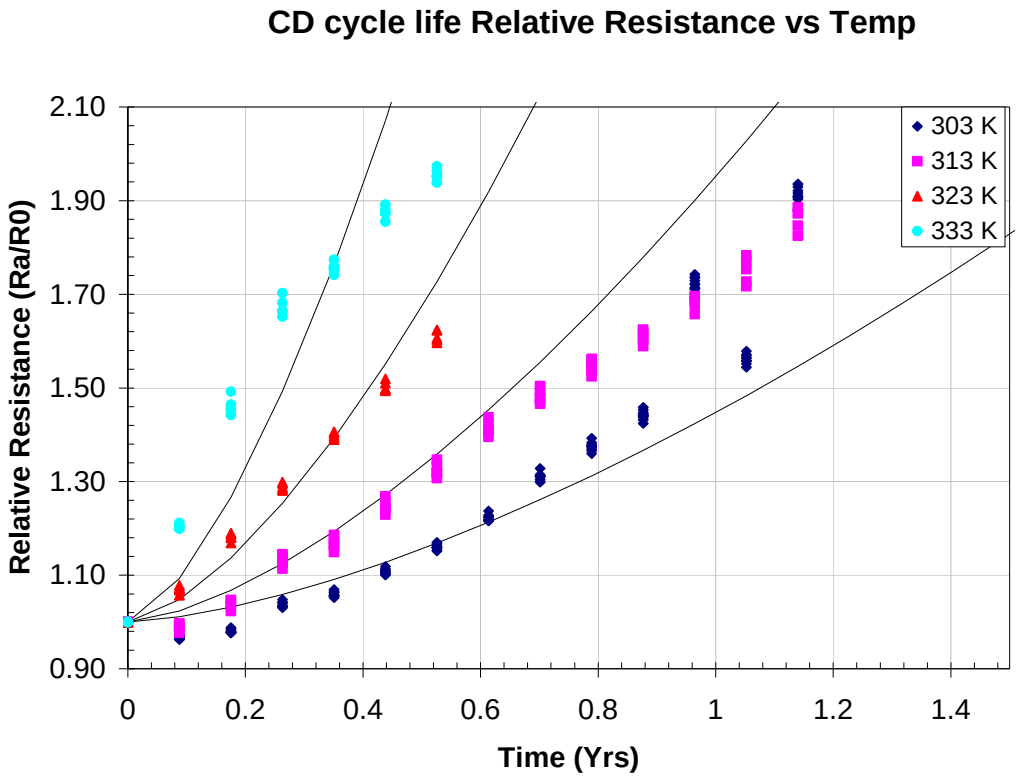

Figure 6.9: Resistance model results for CD cycle life versus time and temperature (K)

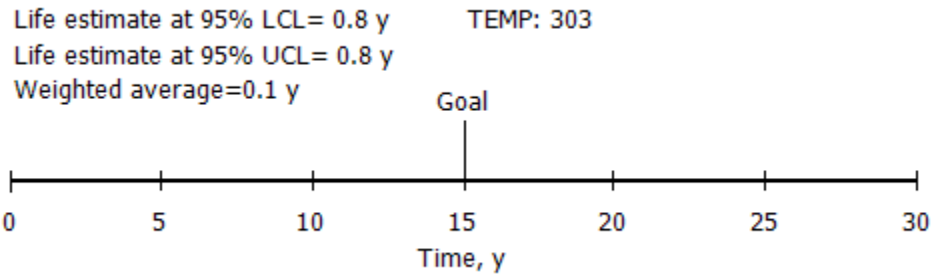

Figure 6.10: Life estimate for resistance model results for CD cycle life versus time and temperature (K)

6.4 Power

6.4.1 Calendar Life

Figure 6.11 shows the model and relative power for calendar aging at 303, 313, 323, and 333 K. The model shows the same effects as the relative resistance for calendar aging but with a lower life estimate, shown in Figure 6.12, 2.55 years based on EOL relative power of 1.3.

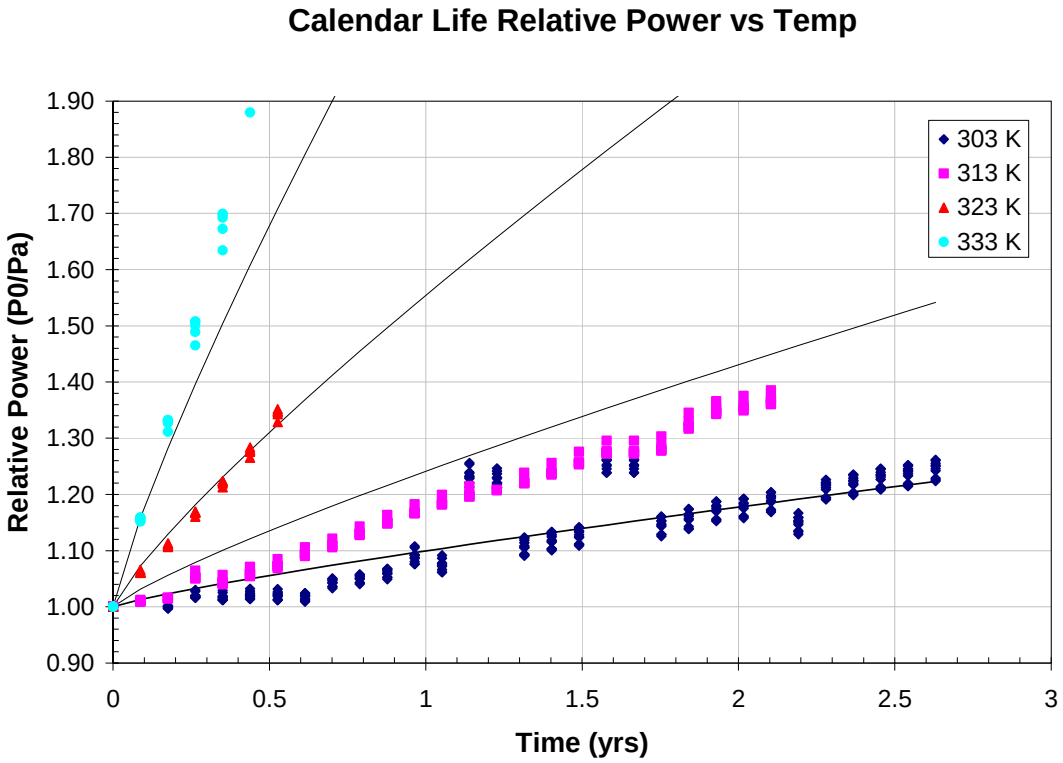

Figure 6.11: Power model results for calendar life versus time and temperature (K)

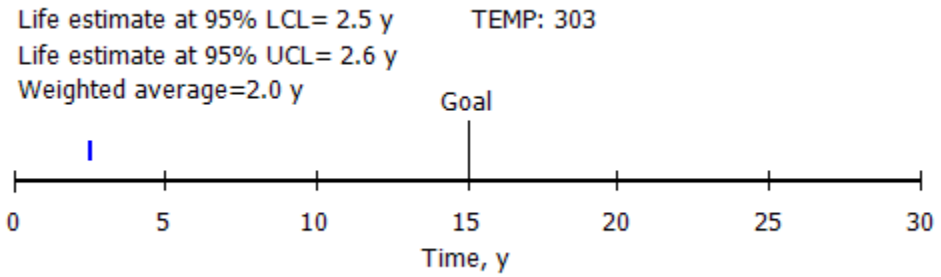

Figure 6.12: Life estimate for power model results for calendar life versus time and temperature (K)

6.4.2 Cycle Life

Figure 6.13 shows the model and relative power for CD cycle aging at 303, 313, 323, and 333 K. The model shows the same effects as the relative resistance for CD cycle aging

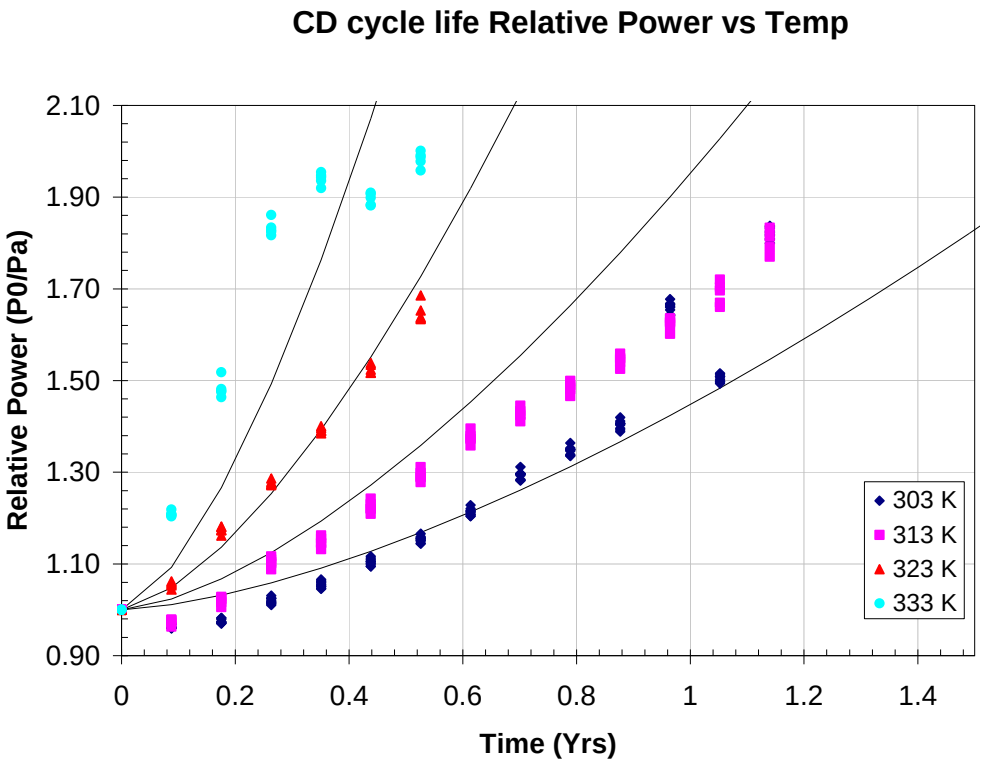

Figure 6.13: Power model results for CD cycle life versus time and temperature (K)

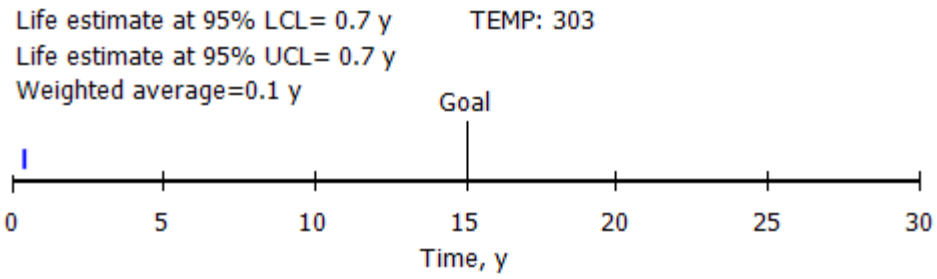

Figure 6.14: Life estimate for power model results for CD cycle life versus time and temperature (K)

but with a lower life estimate, shown in Figure 6.14, 0.7 years based on EOL relative power of 1.3. Due to an inability of the cells to complete the full CD cycle life profile, similar to the resistance data there is a tapering effect in the 60°C data. Thus a reduced level of degradation after RPT 3 is seen as a result of the large amount of capacity fade of the cells at the high temperature.

6.5 Model Parameter Summary

The model fits for the testing conditions discussed previously are shown in Table 6.1. The model parameters A_0, B_1, B_2, and the R^2 values are shown in the table. The initial capacity, resistance, and power are the initial values at the beginning of life, RPT 0 for each cell, approximately 1.27 Ah for the capacity, 48.7 milliohms for the resistance, and 58.0 kW for the power. A_0 represents the frequency factor, which is a representation of the number of collisions that contribute to the reaction in the system. B_1, represents the reaction order and B_2/R, where R is the gas constant, represents the activation energy in an Arrhenius type of equation. R^2, is the sum of the squares or coefficient of determination, which represents the goodness of fit.

Table 6.1: Model parameters (Capacity is blue, Resistance is green, and , Power is orange)

Test Condition	A_0	B_1	B_2	R^2
Capacity Model Results				
Calendar (Time, Temperature)	$1.37 \times 10^{19}\ yr^{-1.425}$	1.425	-14388 K	92.4%
CD Cycle (Time, Temperature)	$3.96 \times 10^{9}\ yr^{-0.952}$	0.952	-7071 K	94.1%
Resistance Model Results				
Calendar (Time, Temperature)	$1.12 \times 10^{11}\ yr^{-0.836}$	0.836	-8408 K	82.0%
CD Cycle (Time, Temperature)	$8.01 \times 10^{9}\ yr^{-1.523}$	1.523	-7153 K	73.9%
Power Model Results				
Calendar (Time, Temperature)	$7.52 \times 10^{13}\ yr^{-1.105}$	1.105	-10474 K	83.6%
CD Cycle (Time, Temperature)	$2.89 \times 10^{10}\ yr^{-1.532}$	1.532	-7565 K	71.9%

While the R^2 values for the capacity indicates a good fit, the R^2 values for the resistance and power (derived from the resistance) are not as good, with values in the 70 to 84% range. Some of this lack of fit is due to the increased noise in the raw resistance data compared to the capacity data. Since the capacity is an integrated value with time, there are less outliers. However, since the resistance data is based on voltage and current measurements that are taken at a very fast rate, over a 10 second period, and they depend on a small difference in voltage measurement to calculate the resistance, there tend to be more significant outliers in the resistance and power results. This lends to a poorer fit. Additionally, the poor fit also indicates that these models could be refined or improved upon to fit the data better and represent the degradation mechanism better.

Table 6.2 shows the life estimates from the models. The life estimates from calendar life testing range from 2.55 yr to 3.1 yr, while the CD cycle life estimates are between 0.6 and 0.8 yr. High A_o values yield high calendar life as opposed to the lower A_o values for CD cycling.

Table 6.2: Life estimate from models (Capacity is blue, Resistance is green, and, Power is orange)

Test Condition	Life Estimate
Capacity Model Results	
Calendar (Time, Temperature)	2.85 yr
CD Cycle (Time, Temperature)	0.6 yr
Resistance Model Results	
Calendar (Time, Temperature)	3.1 yr
CD Cycle (Time, Temperature)	0.8 yr
Power Model Results	
Calendar (Time, Temperature)	2.55 yr
CD Cycle (Time, Temperature)	0.7 yr

6.6 Temperature Dependence

The temperature dependence of the reaction rate is supported by thermodynamics, collision theory, and transition-state theory. As the temperature increases, the reaction rate increases or reactions that cause fade occur faster. The greater the fade, the shorter will be the calendar life of a battery. The model predicts that the rate of energy loss decreases as expected. This model accommodates testing results from multiple temperatures. It is an adaptation of earlier Arrhenius based empirical models that were used by the author to model lithium ion battery life. [54]

This model is capable of predicting performance (capacity fade, energy fade, power fade, or resistance rise) at any temperature in the range of investigation. In theory, the model will predict the performance over whatever temperature range that the mechanism operates. Additionally, the activation energy is an indicator of the speed of the degradation mechanism. A low activation energy is indicative of a high rate of degradation and thus a short calendar/cycle life. Conversely, a high activation energy is indicative of a low rate of degradation and thus a long calendar/cycle life.

The values in Table 6.3 are consistent with the range of values in Table 6.4 for the activation energies from reaction in battery systems. The values in Table 6.4 range from 23 to 130 kJ/mol, which are in the range of the values from Table 6.3. The activation energy is

Table 6.3: Activation energies from model parameter (Capacity is blue, Resistance is green, and, Power is orange)

Test Condition	**Ea**		**B_2**
Capacity Model Results			
Calendar (Time, Temperature)	119.6 kJ/mol		-14388 K
CD Cycle (Time, Temperature)	58.8 kJ/mol		-7071 K
Resistance Model Results			
Calendar (Time, Temperature)	69.9 kJ/mol		-8408 K
CD Cycle (Time, Temperature)	59.4 kJ/mol		-7153 K
Power Model Results			
Calendar (Time, Temperature)	87.0 kJ/mol		-10474 K
CD Cycle (Time, Temperature)	62.9 kJ/mol		-7565 K

the minimum energy required to initiate a chemical reaction. The higher the value, the slower would be the reaction. The lower values ~60 kJ/mol are consistent with the lower estimates for CD cycle life, while the higher value of 119.6 kJ/mol is consistent with the much higher estimates for calendar life. The fits for the capacity life models were 12 to 30% higher than the resistance and power models.

In the case of the commercially available cells, the activation energy is 119.6 kJ/mole based on the capacity fade model during calendar aging. This value is fairly high and correlates with the low calendar life of 2.85 years. This value is consistent with the range of activation energies for reactions that occur within the electrochemical cell. Following is a list of activation energies for various reactions, Table 6.4:

Table 6.4: Activation energies in battery reactions

Reaction	**Activation Energy**	**Reference**
Thermal decomposition of $Li_{0.81}CoO_2$	130 kJ/mole	[68]
Thermal decomposition of $Li_{0.65}CoO_2$	97 kJ/mole	[68]
Capacity loss of $LiMn_2O_4$ and $LiCoO_2$	83.2 kJ/mole	[69]
Capacity loss of $Li_xNi_{0.8}Co_{0.15}Al_{0.05}O_2$	50-55 kJ/mole	[23]
Interfacial lithium-ion transfer reaction in aqueous electrolyte	23-25 kJ/mole	[70]
Interfacial lithium-ion transfer reaction in propylene carbonate electrolyte	50 kJ/mole	[70]

A low activation energy is indicative of a high rate of degradation and thus a short calendar/cycle life. Conversely, a high activation energy is indicative of a low rate of degradation and thus a long calendar/cycle life. The reaction modeled by the equations below are considered to be the result of a decrepitation of the active material in the positive electrode or a loss of the vacant sites available for lithium intercalation and a buildup of the solid electrolyte interface on the positive electrode to increase the resistance of the positive electrode and the cell overall. This reaction causes the structure of the positive electrode to fall apart, making the spaces where lithium can be inserted too small, and hence unavailable for lithium intercalation. The buildup of the solid electrolyte interface is the result of side reactions that occur in the cell and deposit the products on the surface of the positive electrode, increasing the resistance therein.

6.7 Summary

The models and life estimates presented above for capacity, resistance and power for calendar and cycle life conditions are based on the semi-empirical results from the testing. These models can be used to predict end of life at any temperature between 30 and 60°C or

(303 to 333K) for calendar and CD cycle life operation. The model forms follow the recognized and accepted Arrhenius kinetics for performance degradation. The highest life estimate at 3.1 years is far below the automotive target of 15 years, however these cells were not designed for automotive use but rather for use with consumer electronics. Nevertheless, the methodology presented herein is applicable for life evaluation of most lithium ion battery technologies. The results also show the limitations of these cells for cycle life aging. Calendar life estimates compared to cycle life are 4.75 times larger for the capacity results, 3.9 times larger for the resistance results, and 3.6 times larger for the power results.

Chapter Seven: Conclusions

Seventy-one commercially-available, 1.2-Ah cells were tested to evaluate calendar life and Charge Depleting cycle-life performance over the course of 2.5 years with respect to the Plug-In Hybrid Electric Vehicle Battery Test Manual procedures and targets. The effects of temperature on calendar life and on Charge Depleting cycle life; and the effects of State of Charge on calendar life showed a dependence on Arrhenius kinetics across the temperatures tested. The results indicated that the performance decline in the cells was less in calendar life testing than CD cycle life testing, as expected. Increased temperature increased degradation during calendar and cycle life testing in accordance with their dependence on Arrhenius kinetics. The results at 30% SOC showed less degradation than 60% SOC, which was showed less degradation than 90% SOC. Consequently, these cells are chemically more stable at low states of charge than at higher states of charge.

This work has shown that inserting a reference electrode into the original cell container is achievable and does not disturb the voltage and current characteristics. Cell perforation inside a glove box under the guidance of x-ray allows the placement of a reference electrode that is in electrolytic contact with the cell is also feasible. This novel approach demonstrates the methodology and apparatuses necessary to minimize the risk of shorting and disruption of cell performance. While only metal can cells were used in this study, the same process could be implemented with pouch cells with some modifications. Not only can the electrode performance be isolated, but the degree of lithiation of the individual electrodes can be mapped to cell state of charge; this mapping cannot be done once the cell is disassembled.

It is recommended that the cells not be aged with an inserted reference electrode because of the evaporation of the solvent through the perforation in the glove box environment. This will also cause the buildup that was observed on the reference electrode foil to be most likely exacerbated. However, with some additional effort, after insertion, the plug could be re-welded and sealed for additional testing.

The capacity loss from BOL to EOL as measured by the 7.1 W capacity test can be attributed to the rise in resistance. It is presumed that the rise in positive electrode resistance is the result of the main degradation mechanisms of the positive electrode such as micro-cracking and structural disordering, which can cause a loss of available sites for lithium intercalation.

The work done with reference electrodes shows the degradation on the positive electrode is responsible for the performance degradation of the cell. Even with a large capacity loss, consistent with a thick, non-electronically conducting SEI layer, only a small resistance was rise was observed for the negative electrode. The most common theory of battery degradation is the buildup of the solid-electrolyte interphase on the negative electrode. However, this work clearly points to the positive electrode as the cause of the resistance rise.

Utilizing the *in situ* reference electrode methodology, battery manufacturers can devise new strategies or materials based on which electrode is limiting cell performance to increase life, improve performance, or reduce cost. Additionally, performance testing with a reference electrode identifies which electrode limits performance during aging.

These long term tests were designed to age cells under various conditions and provide a greater understanding of how temperature, SOC, calendar and cycle life can degrade the

performance of lithium ion cell. While these results are chemistry specific, many of the general trends apply to most lithium ion technologies.

The results show that higher temperatures accelerate the degradation reactions consistent with Arrhenius kinetics. At low temperatures, calendar life testing results in lower degradation than cycle life testing. At the higher temperatures, there is very little difference between the calendar and cycle life results; the high temperature reaction rates overshadow the differences between calendar and cycle life. The state of charge results indicate that the higher the state of charge the greater will be the degradation. However, in all cases, the life estimates based on cycle life to reach the end of life targets were always much lower than for calendar life. Thus, cycle life degradation is 3-4 times faster than the degradation of calendar life.

The life modeling methodology discussed herein can be applied to automotive grade batteries after 1 year of accelerated testing to determine the efficacy of the 10-15 year warranty claims. Although the calendar life of the cells in this study was only 3.1 years, this methodology is effective for batteries with calendar lives that exceed 10 years.

The model results, while being chemistry specific show not only how performance degrades, but also estimates calendar and cycle life under a range of temperature and SOC conditions. These methods show the discrepancy in the results if life estimates are only based on capacity results and ignore the life estimates from resistance or power measurements. Since calendar life estimation is crucial for electrified vehicle development warranties and battery sizing, these methodologies can be used to characterize the performance degradation of cells for use in automotive applications.

References

1. Annual Energy Review 2004. DOE/EIA-0384(2004), August 2005.

2. S. Davis, S. Diegel, Transportation Energy Data Book: Edition 25. Oak Ridge National Laboratory, ORNL-6974, 2006.

3. "FreedomCAR Partnership Plan," April 1, 2003, www.uscar.org. (August 2006).

4. URL:http://www.eere.energy.gov/vehiclesandfuels/pdfs/basics/jtb_fuel_cell.pdf, (Aug 2006).

5. J. Belt, Battery Test Manual For Plug-In Hybrid Electric Vehicles. INL/EXT-07-12536, (http://www.inl.gov/technicalpublications/Documents/3952791.pdf), *A.* Revision 0, March 2008. B. Revision 2, December 2010

6. L. Wang, J. Li, X. He, W. Pu, C. Wan, and C. Jiang, "Recent advances in layered $LiNi_xCo_yMn_{1-x-y}O_2$ cathode materials for lithium ion batteries," *J. Solid State Electrochem.*, 13 (2009), 1157-1164.

7. D.J. Jang, Y.J. Shin, and S.M. Oh, "Dissolution of Spinel Oxides and Capacity Losses in 4 V $Li/Li_xMn_2O_4$ Cells," *J. Electrochem. Soc.*, 143 (1996), 2204-2211.

8. K.W. Nam, W.S. Yoon, H. Shin, K.Y. Chung, S. Choi, and X.Q. Yang, "*In situ* X-ray diffraction studies of mixed $LiMn_2O_4$–$LiNi_{1/3}Co_{1/3}Mn_{1/3}O_2$ composite cathode in Li-ion cells during charge–discharge cycling," *J. Power Sources*, 192 (2009), 652-659.

9. Y. Xia, Y. Zhou, and M. Yoshio, "Capacity Fading on Cycling of 4 V $Li/LiMn_2O_4$ Cells,"*J. Electrochem. Soc.*, 144 (1997), 2593-2600.

10. Y. Xia and M. Yoshio, "Studies on Li-Mn-O spinel system (obtained from melt-impregnation method) as a cathode for 4 V lithium batteries Part IV. High and low temperature performance of $LiMn_2O_4$,"*J. Power Sources*, 66 (1997), 129-133.

11. R.J. Gummow, A. de Kock, and M.M. Thackeray, "Improved capacity retention in rechargeable 4 V lithium/lithium-manganese oxide (spinel) cells," *Solid State Ionics*, 69(1994), 59-67.

12. J. Fergus, "Recent developments in cathode materials for lithium ion batteries," *J. Power Sources*, 195 (2010), 939-954.

13. S.K. Jeong, J.S. Shin, K.S. Nahm, T.P. Kumar, and A.M. Stephan, "Electrochemical studies on cathode blends of $LiMn_2O_4$ and $Li[Li_{1/15}Ni_{1/5}Co_{2/5}Mn_{1/3}O_2]$," *Materials Chemistry and Physics*, 111(2008), 213-217.

14. A. Manthiram and W. Choi," Suppression of Mn Dissolution in Spinel Cathodes by Trapping the Protons within Layered Oxide Cathodes ," *J. Electrochem. Solid-State Letters* 10 (2007), A228-A231.

15. J. Goa and A. Manthiram, "Eliminating the irreversible capacity loss of high capacity layered $Li[Li_{0.2}Mn_{0.54}Ni_{0.13}Co_{0.13}]O_2$ cathode by blending with other lithium insertion hosts," *J. Power Sources*, 191 (2009), 644-647.

16. I. Bloom, B.W. Cole, J.J. Sohn, S.A. Jones, E.G. Polzin, V.S. Battaglia, G.L. Henriksen, C. Motloch, R. Richardson, T. Unkelhaeuser, and H.L. Case, "An accelerated calendar and cycle life study of Li-ion cells ,"*J. Power Sources* 101 (2001), 238–247.

17. J. Belt, C. Ho, C. Motloch, T. Miller. T. Duong, "A capacity and power fade study of Li-ion cells during life cycle testing," *Journal of Power Sources,* 123, 2, 241-246, 2003.

18. R.B. Wright, C.G. Motloch, J.R. Belt, J.P. Christophersen, C.D. Ho, R.A. Richardson, I. Bloom, S.A. Jones, V.S. Battaglia, G.L. Henriksen, T. Unkelhaeuser, D. Ingersoll, H.L.Case, S.A. Rogers, and R.A. Sutula, " Calendar- and cycle-life studies of advanced technology development program generation 1 lithium-ion batteries ," *J. Power Sources*, 110 (2002), 445-470.

19. I. Bloom, S.A. Jones, V.S. Battaglia, G.L. Henriksen, J.P. Christophersen, R.B. Wright, C.D. Ho, J.R. Belt, and C.G. Motloch, "Effect of cathode composition on capacity fade, impedance rise and power fade in high-power, lithium-ion cells ,"*J. Power Sources*, 124 (2003), 538.

20. I. Bloom, A.N. Jansen, D.P. Abraham, J. Knuth, S.A. Jones, V.S. Battaglia, and G.L. Henriksen, "Differential voltage analyses of high-power lithium-ion cells: 2. Applications," *J. Power Sources*, 139 (2005), 295.

21. I. Bloom, B.G. Potter, C.S. Johnson, K.L. Gering, and J.P. Christophersen, "Effect of cathode composition on impedance rise in high-power lithium-ion cells: Long-term aging results,"*J. PowerSources*, 155 (2006), 415.

22. I. Bloom, L.K. Walker, J.K. Basco, D.P. Abraham, J.P. Christophersen, and C.D. Ho, "Differential voltage analyses of high-power lithium-ion cells. 4. Cells containing NMC," *J.Power Sources*, 195 (2010), 877-882.

23. B. Liaw, E. Roth, R. Jungst, G. Nagasubramanian, H. Case, D. Doughty, "Correlation of Arrhenius behaviors in power and capacity fades with cell impedance and heat generation in cylindrical lithium-ion cells," Journal of Power Sources, 119-121, pg 874-886, 2003

24. N. Nakayama, T. Nozawa, Y. Iriyama, T. Abe, Z. Ogumi, K. Kikuchi, "Interfacial lithium-ion transfer at the LiMn2O4 thin film electrod/aqueous solution interface," Journal of Power Sources, 174, pg 695-700, 2007

25. R. Morse, "Franklin and Electrostatics- Ben Franklin as my Lab Partner", Sept 2004 URL:http://www.tufts.edu/as/wright_center/fellows/bob_morse_04/franklin_electricity_screen.pdf.

26. C. Vincent, F. Bonino, M. Lazzari, B. Scrosati, Modern Batteries. London, Edward Arnold Publishers Ltd, 1984.

27. URL: http://inventors.about.com/library/inventors/blbattery.htm (April 2006).

28. URL: http://www.sparkmuseum.com/VOLTA.HTM (April 2006).

29. D. Linden, T. Reddy, Handbook of Batteries 3rd edition. McGraw-Hill, New York, 1995.

30. M. Broussely, P. Biensan, B. Simon, "Lithium Insertion into Host Materials: the Key to Success for Li-Ion Batteries," Electrochimica Acta, 45, (1999), 3-22.

31. E. Gileadi, Electrode Kinetics for Chemists and Chemical Engineers, and Materials Scientists. Wiley, New York, 1993.

32. K. Takei, K. Kumai, Y. Kobayashi, H. Miyashiro, N. Terada, T. Iwahori, T. Tanaka, "Cycle Life Estimation of Lithium Secondary Battery by Extrapolation Method and Accelerated Aging Tests," Journal of Power Sources, 97-98, (2001), 697-701.

33. W. Bogel, J. Buchel, H. Katz, "Real-Life EV Battery Cycling on the Test Bench," Journal of Power Sources, 72, (1998), 37-42.

34. K. Takeno, M. Ichimura, K. Takano, J. Yamaki, "Influence of Cycle Capacity Deterioration and Storage Capacity Deterioration on Li-Ion Batteries Used in Mobile Phones," Journal of Power Sources, 142, (2005), 298-305.

35. B. Popov, G. Ning, B. Haran, "Capacity Fade Study of Lithium-Ion Batteries Cycled at High Discharge Rates," Journal of Power Sources, 117, (2003), 160-169.

36. K. Striebel, J. Shim, E. Cairns, R. Kostecki, Y. Lee, J. Reimer, T. Richardson, P. Ross, X. Song, G. Zhuang, " Diagnostic Analysis of Electrodes from High-Power Lithium-Ion Cells Cycled Under Different Conditions," Journal of The Electrochemical Society, 151, (2004), A857-A866.

37. K. Asakura, M. Shimomura, T. Shodai, "Study of Life Evaluation Methods for Li-Ion Batteries for Backup Applications," Journal of Power Sources, 119-121, (2003), 902-905.

38. J. Vetter, P. Novak, M. Wagner, C. Veit, K. Moller, J. Besenhard, M. Winter, M. Wohlfahrt-mehrens, C. Vogler, A. Hammouche, "Ageing Mechanisms in Lithium Ion Batteries," Journal of Power Sources 147, (2005), 269-281.

39. M. Broussely, S. Herreyre, P. Biensan, P. Kasztejna, K. Nechev, R. Staniewicz, "Aging Mechanism in Li-Ion Cells and Calendar Life Predictions," Journal of Power Sources 97-98, (2001), 13-21.

40. G. Sarre, P. Blanchard, M. Broussely, "Aging of Lithium-Ion Batteries," Journal of Power Sources 127, (2004), 65-71.

41. M. Broussely, P. Blanchard, P. Biensan, J. Planchat, K. Nechev, R. Staniewicz, "Properties of Large Li-Ion Cells Using a Nickel Based Mixed Oxide," Journal of Power Sources 119-121, (2003), 859-864.

42. M. Broussely, F. Perton, P. Biensan, J. Bodet, J. Labat, A. Lecerf, "Li_xNiO_2, a Promising Cathode for Rechargeable Lithium Batteries," Journal of Power Sources, 54, (1995), 109-114.

43. M. Broussely, P. Biensan, F. Bonhomme, P. Blanchard, S. Herreyre, K. Nechev, R. Staniewicz, "Main Aging Mechanisms in Li-Ion Batteries," Journal of Power Sources, 146, (2005), 90-96.

44. M. Wu, P. Chiang, J. Lin, "Electrochemical Investigations on Advanced Lithium-Ion Batteries by Three-Electrode Measurements," J. Electrochem Soc., 152, A47-A52, 2005

45. C. Wang, A. Appleby, F. Little, "Criteria for Reliable Electrochemical Impedance Measurements on Li-Ion Battery Anodes**,"**J. Electrochem Soc., 150, A143-A148, 2003

46. M. Verbrugge, B. Koch, "Electrochemical Analysis of Lithiated Graphite Anodes,"J. Electrochem Soc., 150, A374-A384, 2003

47. Q. Wu, W. Lu, J. Prakash, "Characterization of a commercial size cylindrical Li-ion cell with a reference electrode," Journal of Power Sources, 88, 2000, 237-242

48. P. Liu, J. Wang, J. Garner, E. Sherman, S. Soukiazian, M. Verbrugge, H. Tataria, J. Musser, P. Finamor, "Aging Mechanisms of LiFePO4 Batteries Deduced by Electrochemical and Structural Analyses," J. Electrochem Soc., 157, A499-A507, 2010

49. D.P. Abraham, S.D. Poppen, A.N. Jansen, J. Liu, D.W. Dees, Electrochim Acta 49 (2004) 4763.

50. Uncertainty Study of INEEL EST Laboratory Battery Testing Systems, Volume 1, INEEL/EXT-01-00505, December 2001.

51. Uncertainty Study of INEEL EST Laboratory Battery Testing Systems, Volume 2, INEEL/EXT-01-00505, March 2003.

52. J. Belt, "Test Plan for Commercial cells Phase II", EHV-TP-238, Idaho National Laboratory document, 2010.

53. G. Hunt, FreedomCAR Battery Test Manual For Hybrid Electric Vehicles. Revision 0, DOE/ID-11069, October 2004.

54. J. Belt, C. Motloch, K. Nechev, G, Chagnon, T. Miller, "Calendar Life Modeling Methodology for High-Power PNGV Saft Batteries," Abstract presented at 200th Electrochemical Society Meeting, San Francisco, September 6, 2001. (http:/www.electrochem.org/dl/ma/200/pdfs/0129.pdf)

55. J. Belt, C. Ho, M. Habib, T. Miller. T. Duong, "The effect of temperature on capacity and power in cycled lithium ion batteries," *Journal of Power Sources,* 142, 354-360, 2005.

56. J. Belt, C. Ho, "Long Term Combined Calendar and Cycle Life Testing," Abstract presented at 214th Electrochemical Society Meeting, October 2008

57. P. B. Balbuena and Y. Wang, *Lithium-Ion Batteries: Solid-Electrolyte Interphase*, Imperial College Press, Covent Garden, London, 2004.

58. J. Newman and K. E. Thomas-Alyea, *Electrochemical Systems*, 3rd ed., Hoboken, N. J., Wiley-Interscience, 2004.

59. J. Wang, S. Soukiazian, M. Verbrugge, H. Tataria, D. Coates, D. Hall, P. Liu, "Active lithium replenishment to extend the life of a cell employing carbon and iron phosphate electrodes," *Journal of Power Sources*, 196, 2011, 5966-5969.

60. J. Belt, V. Utgikar, I. Bloom, "Calendar and PHEV Cycle Life Aging of High-Energy, Lithium-Ion Cells Containing Blended Spinel and Layered-Oxide Cathodes," *Journal of Power Sources*, 196, 10213-10221, December 2011.

61. U. Landau, N. Weinberg, E. Gileadi, "Three-Electrode Measurements in Industrial Cells," Journal of Electrochemical Society, pg 396-403, February 1988.

62. J. Belt, Validation of HPPCALC. INL/EXT-06-11848, February 2001.

63. D. M. Bernardi and J. Y. Go, "Analysis of pulse and relaxation behavior in lithium-ion batteries," *Journal of Power Sources,* 196, 412-427 (2011).

64. D. K. Karthikeyan, G. Sikha, R. E. White, "Thermodynamic model development for lithium intercalation electrodes," Journal of Power Sources, 185, p1398-1407, 2008

65. J. Christensen, J. Newman, "Stress generation and fracture in lithium insertion materials," Journal Solid State Electrochem, 10, 293-319, 2006

66. G. Prentice, Electrochemical Engineering Principles. Prentice-Hall, NJ 1991

67. Battery Calendar Life Estimator Manual Modeling and Simulation. Revision 1, INL/EXT-08-15136, October 2012. (http://www.inl.gov/technicalpublications/Documents/5516217.pdf)

68. Y. Furushima, C. Yanagisawa, T. Nakagawa, Y. Aoki, N. Muraki, "Thermal stability and kinetics of delithiated $LiCoO_2$," Journal of Power Sources, 196, pg 2260-2263, 2011

69. R. Yazami, Y. Ozawa, "A kinetic study of self-discharge of spinel electrodes in Li/LixMn2O4 Cells," Journal of Power Sources, 153, pg 251-257, 2006

70. E. Gileadi, Electrode Kinetics for Chemists and Chemical Engineers, and Materials Scientists. Wiley, New York, 1993.

Appendix 1: Glossary

CS Available Power –the discharge pulse power at which the useable energy is equal to the Charge-Sustaining Available Energy target for a given mode (Minimum, Medium, or Maximum PHEV).

Battery Size Factor (BSF) – for a particular cell or module design, an integer which is the minimum number of cells or modules expected to be required to meet all the performance and life targets. If this value cannot be determined prior to testing, the Battery Size Factor is chosen as the minimum number of cells or modules that can both satisfy the CS energy target with a 30% power margin and provide a 20% energy margin for Charge Depleting Available Energy at beginning-of-life . Battery Size Factor is determined separately for each mode.

Beginning-of-Life (BOL) – the point at which life testing begins. A distinction is made in this manual between the performance of a battery at this point and its initial performance, because some degradation may take place during early testing prior to the start of life testing. Analysis of the effects of life testing is based on changes from the BOL performance.

C_1/1 Rate – a current corresponding to the manufacturer's rated capacity (in ampere-hours) for a one-hour discharge at 30°C. For example, if the battery's rated one-hour capacity is 40Ah, then $C_1/1$ is 40A.

Charge – any condition in which energy is supplied to the device rather than removed from the device. Charge includes both recharge and regen conditions. Charge is indicated in this manual as a negative value (from the perspective of the battery)

Charge-Depleting Available Energy –the discharge energy available at a 10-kW constant power discharge rate between an arbitrarily defined upper limit (nominally 10% DOD) and the minimum DOD. (See Section 4.3.4)

Charge-Sustaining Available Energy –the discharge energy available over the DOD range where both the discharge and regen pulse power targets for a given mode (Minimum, Medium, or Maximum PHEV) are precisely met. This energy is measured using a 10-kW discharge rate, and the limiting power conditions are calculated using the procedure defined in this manual (section 4.3.4).

Depth-of-Discharge (DOD) – the percentage of a device's rated capacity removed by discharge relative to a fully charged condition, normally referenced to a constant current discharge at the HPPC-Current rate.

Device – a cell, module, sub-battery or battery pack, depending on the context. The generic term "device" is normally used in test procedures except where a specific type of device is meant. (Most test procedures are intended to apply to any of these types).

Discharge – any condition in which energy is removed from the device rather than supplied to the device. Discharge is indicated in this manual as a positive value (from the perspective of the battery)

End-of-Life (EOL) – a condition reached when the device under test is no longer capable of meeting the targets. This is normally determined from HPPC Test results scaled using the Battery Size Factor, and it may not coincide exactly with the ability to perform the life test profile (especially if cycling is done at elevated temperatures). The number of test profiles executed at end of test is not necessarily equal to the cycle life per the targets.

End of Test – a condition where life testing is halted, either because criteria specified in the test plan are reached, or because it is not possible to continue testing.

Energy Margin – for a given HPPC Test data set, the difference between either the CS or the CD Available Energy and the energy target for a given application and operating mode.

Fully Charged – The condition reached by a device when it is subjected to the manufacturer's recommended recharge algorithm. This state is defined as 100% state-of-charge, or 0% depth-of-discharge.

HPPC-Current rate – the constant current equivalent of a BSF-scaled 10-kW rate (see Section 3.1.3).

Hybrid Pulse Power Characterization (HPPC) Test – a test procedure whose results are used to calculate pulse power and energy capability under operating conditions.

Maximum Rated Current (Imax) – the maximum discharge current that a manufacturer will permit to be sustained by a device for 10 seconds. (This value need not be achievable at all DOD values).

PHEV Charge Target—the upper regen limit used during PHEV operation, also known as the charge limit during charging.

Power Fade—the change in CS Available Power from the beginning-of-life value to the value determined at some later time, expressed as a percentage of the BOL value. (Similar definitions apply to Capacity Fade and CS or CD Available Energy Fade, although these are not included in this glossary).

Power Margin – for a given HPPC Test data set, the difference between the maximum power at which the applicable energy target can be met and the power target for a given application.

Profile – a connected sequence of pulses used as the basic 'building block' of many test procedures. A test profile normally includes discharge, rest and charge steps in a specific order, and each step is normally defined as having a fixed time duration and a particular (fixed) value of current or power.

Recharge – any device charge interval corresponding to the sustained replenishment of energy by a continuous power source (such as an engine-generator or off-board charger).

Regen – any device charge interval corresponding to the return of vehicle kinetic energy to a device (typically from braking). Because of physical limitations, high rates of regen can only persist for a few seconds at a time.

Rest – the condition in which energy is neither supplied to the device nor removed from the device. Rest is indicated by zero current

State- of-Charge (SOC)—the available capacity in a battery expressed as a percentage of rated capacity (Handbook of Batteries, 3rd Edition).

Useable Energy – a value (calculated from HPPC Test results) that represents the discharge energy available over a DOD range corresponding to any pair of discharge and regen power values whose ratio is that of the corresponding power targets. Charge-Sustaining Available Energy is the value of useable energy at the actual power target values. (Useable energy has been frequently but inaccurately called "Available Energy").

Appendix 2: Raw Testing Data

Capacity Data (Ah) Char – RPT 6

Cell #	Condition Char		RPT 0	RPT 1	RPT 2	RPT 3	RPT 4	RPT 5	RPT 6
1	CD 30/15	1.2709	1.2436	1.2023	1.1719	1.1431	1.1195	1.0945	1.0665
2	CD 30/15	1.2717	1.2465	1.2074	1.1794	1.1520	1.1289	1.1036	1.0748
3	CD 30/15	1.2692	1.2437	1.2057	1.1777	1.1504	1.1282	1.1042	1.0770
4	CD 30/15	1.2740	1.2483	1.2118	1.1834	1.1563	1.1342	1.1112	1.0844
5	CD 30/15	1.2708	1.2452	1.2077	1.1798	1.1527	1.1303	1.1059	1.0782
6	CD 30/15	1.2695	1.2442	1.2065	1.1790	1.1522	1.1297	1.1053	1.0779
7	CD 30/15	1.2775	1.2517	1.2106	1.1819	1.1536	1.1296	1.1036	1.0748
8	CD 30/15	1.2772	1.2517	1.2115	1.1832	1.1550	1.1311	1.1052	1.0762
9	CD 30/15	1.2689	1.2420	1.2010	1.1708	1.1429	1.1195	1.0942	1.0656
10	CD 30/15	1.2739	1.2485	1.2089	1.1804	1.1537	1.1311	1.1061	1.0784
11	Cal 30/60	1.2756	1.2498	1.2608	1.2571	1.2542	1.2506	1.2462	1.2423
12	Cal 30/60	1.2807	1.2541	1.2659	1.2628	1.2579	1.2538	1.2482	1.2435
13	Cal 30/60	1.2801	1.2536	1.2649	1.2621	1.2571	1.2530	1.2477	1.2431
14	Cal 30/60	1.2744	1.2487	1.2597	1.2564	1.2532	1.2493	1.2448	1.2411
15	Cal 30/60	1.2801	1.2532	1.2650	1.2623	1.2572	1.2529	1.2475	1.2431
16	Cal 30/60	1.2796	1.2526	1.2643	1.2615	1.2565	1.2524	1.2473	1.2429
17	Cal 30/60	1.2798	1.2532	1.2641	1.2608	1.2563	1.2526	1.2473	1.2431
18	Cal 30/60	1.2790	1.2530	1.2637	1.2611	1.2559	1.2519	1.2468	1.2426
19	Cal 30/60	1.2755	1.2496	1.2610	1.2580	1.2543	1.2511	1.2468	1.2433
20	Cal 30/60	1.2753	1.2490	1.2594	1.2571	1.2508	1.2468	1.2415	1.2374
21	Cal 30/30	1.2800	1.2539	1.2722	1.2698	1.2657	1.2623	1.2584	1.2548
22	Cal 30/30	1.2744	1.2487	1.2673	1.2646	1.2617	1.2585	1.2554	1.2524
23	Cal 30/30	1.2697	1.2430	1.2608	1.2587	1.2538	1.2499	1.2457	1.2420
24	Cal 30/30	1.2784	1.2515	1.2699	1.2672	1.2634	1.2596	1.2560	1.2524
25	Cal 30/30	1.2708	1.2443	1.2624	1.2583	1.2553	1.2512	1.2468	1.2429
26	Cal 30/90	1.2775	1.2522	1.2576	1.2561	1.2386	1.2309	1.2204	1.2096
27	Cal 30/90	1.2784	1.2523	1.2573	1.2551	1.2358	1.2281	1.2176	1.2061
28	Cal 30/90	1.2747	1.2482	1.2530	1.2524	1.2329	1.2251	1.2145	1.2033
29	Cal 30/90	1.2736	1.2472	1.2526	1.2510	1.2312	1.2235	1.2130	1.2021
30	Cal 30/90	1.2789	1.2537	1.2592	1.2577	1.2401	1.2320	1.2220	1.2113
31	CD 40/15	1.2711	1.2448	1.1921	1.1450	1.0995	1.0607	1.0231	0.9857
32	CD 40/15	1.2730	1.2473	1.1927	1.1450	1.0990	1.0597	1.0203	0.9820
33	CD 40/15	1.2742	1.2489	1.1934	1.1460	1.0998	1.0614	1.0223	0.9835
34	CD 40/15	1.2752	1.2502	1.1965	1.1498	1.1052	1.0671	1.0299	0.9927
35	CD 40/15	1.2747	1.2501	1.1948	1.1484	1.1019	1.0624	1.0217	0.9790
36	Cal 40/60	1.2716	1.2469	1.2487	1.2414	1.2274	1.2161	1.2017	1.1884

37	Cal 40/60	1.2704	1.2450	1.2464	1.2388	1.2239	1.2118	1.1973	1.1837
38	Cal 40/60	1.2738	1.2483	1.2505	1.2431	1.2288	1.2171	1.2029	1.1895
39	Cal 40/60	1.2759	1.2511	1.2523	1.2445	1.2306	1.2189	1.2050	1.1916
40	Cal 40/60	1.2703	1.2454	1.2475	1.2408	1.2268	1.2156	1.2016	1.1885
41	CD 50/15	1.2765	1.2525	1.1375	1.0291	0.9375	0.8546	0.7637	0.6823
42	CD 50/15	1.2773	1.2540	1.1371	1.0274	0.9298	0.8466	0.7589	0.6797
43	CD 50/15	1.2750	1.2498	1.1345	1.0259	0.9342	0.8510	0.7610	0.6816
44	CD 50/15	1.2712	1.2460	1.1276	1.0174	0.9230	0.8366	0.7394	0.6586
45	CD 50/15	1.2740	1.2488	1.1299	1.0195	0.9252	0.8395	0.7507	0.6724
46	Cal 50/60	1.2759	1.2527	1.2250	1.1768	1.1190	1.0699	1.0224	0.9787
47	Cal 50/60	1.2732	1.2484	1.2192	1.1703	1.1118	1.0627	1.0146	0.9720
48	Cal 50/60	1.2723	1.2503	1.2182	1.1723	1.1152	1.0665	1.0187	0.9763
49	Cal 50/60	1.2725	1.2472	1.2185	1.1702	1.1115	1.0625	1.0142	0.9706
50	Cal 50/60	1.2721	1.2472	1.2180	1.1699	1.1104	1.0616	1.0132	0.9698
51	CD 60/15	1.2742	1.2480	1.0101	0.8226	0.6688	0.6107	0.5709	0.5724
52	CD 60/15	1.2781	1.2512	1.0171	0.8321	0.6776	0.6173	0.5797	0.5798
53	CD 60/15	1.2783	1.2517	1.0151	0.8300	0.6754	0.6170	0.5807	0.5812
54	CD 60/15	1.2791	1.2520	1.0140	0.8284	0.6749	0.6144	0.5759	0.5773
55	CD 60/15	1.2803	1.2545	1.0111	0.8227	0.6729	0.6138	0.5730	0.5765
56	Cal 60/60	1.2745	1.2475	1.1250	0.9917	0.8801	0.8036	0.7377	0.6839
57	Cal 60/60	1.2800	1.2540	1.1306	0.9956	0.8830	0.8089	0.7451	0.6916
58	Cal 60/60	1.2779	1.2514	1.1328	1.0057	0.8968	0.8194	0.7535	0.6991
59	Cal 60/60	1.2793	1.2535	1.1318	0.9975	0.8835	0.8083	0.7442	0.6898
60	Cal 60/60	1.2797	1.2551	1.1321	0.9979	0.8844	0.8101	0.7465	0.6928

Capacity Data (Ah) RPT 7-RPT 14

Cell #	Condition	RPT 7	RPT 8	RPT 9	RPT 10	RPT 11	RPT 12	RPT 13	RPT 14
1	CD 30/15	1.0412	1.0189	0.9962	0.9776	0.9617	0.9419	0.9272	
2	CD 30/15	1.0487	1.0239	1.0004	0.9810	0.9637	0.9435	0.9318	
3	CD 30/15	1.0533	1.0291	1.0059	0.9879	0.9754	0.9533	0.9382	
4	CD 30/15	1.0613	1.0398	1.0196	1.0036	0.9901	0.9714	0.9555	
5	CD 30/15	1.0538	1.0296	1.0058	0.9865	0.9694	0.9500	0.9358	
6	CD 30/15	1.0536	1.0295	1.0063	0.9874	0.9707	0.9515	0.9373	
7	CD 30/15	1.0489	1.0235	1.0002	0.9800	0.9618	0.9412	0.9305	
8	CD 30/15	1.0502	1.0243	1.0011	0.9808	0.9620	0.9417	0.9297	
9	CD 30/15	1.0402	1.0192	0.9968	0.9786	0.9629	0.9435	0.9279	
10	CD 30/15	1.0537	1.0300	1.0062	0.9871	0.9704	0.9507	0.9374	

11	Cal 30/60	1.2370	1.2260	1.2253	1.2140	1.2137	1.2076	1.1981	1.1955
12	Cal 30/60	1.2381	1.2273	1.2252	1.2137	1.2134	1.2073	1.1978	1.1950
13	Cal 30/60	1.2378	1.2273	1.2256	1.2142	1.2139	1.2079	1.1988	1.1954
14	Cal 30/60	1.2359	1.2245	1.2238	1.2125	1.2123	1.2067	1.1965	1.1936
15	Cal 30/60	1.2377	1.2265	1.2251	1.2138	1.2138	1.2079	1.1984	1.1957
16	Cal 30/60	1.2377	1.2267	1.2248	1.2135	1.2133	1.2073	1.1980	1.1955
17	Cal 30/60	1.2377	1.2257	1.2249	1.2133	1.2132	1.2070	1.1979	1.1955
18	Cal 30/60	1.2376	1.2249	1.2239	1.2128	1.2129	1.2069	1.1975	1.1951
19	Cal 30/60	1.2384	1.2255	1.2253	1.2141	1.2140	1.2082	1.1988	1.1963
20	Cal 30/60	1.2323	1.2184	1.2174	1.2060	1.2060	1.2001	1.1900	1.1875
21	Cal 30/30	1.2515	1.2483	1.2418	1.2333	1.2335	1.2287	1.2219	1.2195
22	Cal 30/30	1.2496	1.2462	1.2405	1.2324	1.2325	1.2279	1.2209	1.2188
23	Cal 30/30	1.2386	1.2347	1.2277	1.2193	1.2195	1.2146	1.2075	1.2053
24	Cal 30/30	1.2495	1.2455	1.2388	1.2308	1.2310	1.2259	1.2195	1.2174
25	Cal 30/30	1.2392	1.2373	1.2297	1.2208	1.2209	1.2158	1.2089	1.2061
26	Cal 30/90	1.2030	1.2019	1.1805	1.1552	1.1602	1.1499	1.1353	1.1353
27	Cal 30/90	1.1999	1.1996	1.1772	1.1529	1.1566	1.1462	1.1322	1.1332
28	Cal 30/90	1.1971	1.1958	1.1727	1.1477	1.1523	1.1416	1.1269	1.1269
29	Cal 30/90	1.1962	1.1951	1.1728	1.1482	1.1526	1.1419	1.1280	1.1289
30	Cal 30/90	1.2050	1.2026	1.1816	1.1562	1.1609	1.1506	1.1361	1.1369
31	CD 40/15	0.9506	0.9138	0.8806	0.8453	0.8051	0.7652	0.7205	
32	CD 40/15	0.9458	0.9085	0.8731	0.8376	0.7987	0.7946		
33	CD 40/15	0.9485	0.9145	0.8804	0.8454	0.8059	0.7621	0.7125	
34	CD 40/15	0.9552	0.9201	0.8850	0.8500	0.8098	0.7702	0.7264	
35	CD 40/15	0.9424	0.9062	0.8715	0.8375	0.7991	0.7603	0.7180	
36	Cal 40/60	1.1696	1.1603	1.1395	1.1179	1.1090	1.0948	1.0749	
37	Cal 40/60	1.1653	1.1549	1.1340	1.1119	1.1027	1.0885	1.0685	
38	Cal 40/60	1.1708	1.1607	1.1404	1.1186	1.1097	1.0954	1.0756	1.0666
39	Cal 40/60	1.1730	1.1630	1.1428	1.1210	1.1119	1.0979	1.0776	1.0686
40	Cal 40/60	1.1703	1.1611	1.1403	1.1190	1.1101	1.0962	1.0765	1.0679

Capacity Data(Ah) RPT 15 – RPT 22

Cell #	Condition RPT 15	RPT 16	RPT 17	RPT 18	RPT 19	RPT 20	RPT 21	RPT 22
11	Cal 30/60	1.1898	1.1843	1.1778	1.1727	1.1560	1.1598	1.1519	1.1506
12	Cal 30/60	1.1890	1.1836	1.1770	1.1716	1.1558	1.1588	1.1515	1.1495
13	Cal 30/60	1.1899	1.1844	1.1784	1.1729	1.1571	1.1607	1.1532	1.1518

14	Cal 30/60	1.1878	1.1816	1.1760	1.1703	1.1540	1.1582	1.1503	1.1490
15	Cal 30/60	1.1898	1.1840	1.1778	1.1726	1.1567	1.1602	1.1524	1.1507
16	Cal 30/60	1.1898	1.1840	1.1776	1.1654	1.1549	1.1584	1.1512	1.1493
17	Cal 30/60	1.1897	1.1841	1.1776	1.1714	1.1560	1.1592	1.1524	1.1504
18	Cal 30/60	1.1895	1.1838	1.1772	1.1712	1.1560	1.1594	1.1526	1.1491
19	Cal 30/60	1.1908	1.1853	1.1789	1.1727	1.1568	1.1610	1.1537	1.1518
20	Cal 30/60	1.1816	1.1758	1.1694	1.1630	1.1475	1.1511	1.1441	1.1420
21	Cal 30/30	1.2148	1.2105	1.2049	1.2000	1.1901	1.1901	1.1839	1.1839
22	Cal 30/30	1.2140	1.2096	1.2041	1.1992	1.1886	1.1892	1.1826	1.1813
23	Cal 30/30	1.2005	1.1960	1.1905	1.1856	1.1752	1.1753	1.1693	1.1680
24	Cal 30/30	1.2127	1.2083	1.2026	1.1975	1.1872	1.1875	1.1813	1.1800
25	Cal 30/30	1.2013	1.1969	1.1912	1.1868	1.1757	1.1759	1.1689	1.1670
26	Cal 30/90	1.1258	1.1190	1.1066	1.0974	1.0737	1.0793	1.0749	1.0688
27	Cal 30/90	1.1238	1.1179	1.1050	1.0963	1.0734	1.0786	1.0748	1.0659
28	Cal 30/90	1.1170	1.1103	1.0975	1.0884	1.0651	1.0702	1.0660	1.0573
29	Cal 30/90	1.1196	1.1135	1.1008	1.0922	1.0694	1.0745	1.0700	1.0639
30	Cal 30/90	1.1271	1.1205	1.1077	1.0984	1.0748	1.0803	1.0736	1.0663

Capacity Data (Ah) RPT 23 – RPT 30

Cell #	Condition RPT 23	RPT 24	RPT 25	RPT 26	RPT 27	RPT 28	RPT 29	RPT 30
11	Cal 30/60	1.1487	1.1435	1.1315	1.1275	1.1194	1.1091	1.1133	1.1030
12	Cal 30/60	1.1483	1.1429	1.1302	1.1264	1.1174	1.1073	1.1121	1.1008
13	Cal 30/60	1.1501	1.1447	1.1324	1.1290	1.1204	1.1101	1.1148	1.1039
14	Cal 30/60	1.1468	1.1409	1.1290	1.1250	1.1166	1.1065	1.1107	1.1003
15	Cal 30/60	1.1490	1.1437	1.1318	1.1277	1.1189	1.1088	1.1134	1.1024
16	Cal 30/60	1.1480	1.1430	1.1301	1.1268	1.1176	1.1073	1.1120	1.1007
17	Cal 30/60	1.1488	1.1439	1.1315	1.1278	1.1189	1.1085	1.1133	1.1025
18	Cal 30/60	1.1477	1.1422	1.1301	1.1269	1.1176	1.1075	1.1125	1.1013
19	Cal 30/60	1.1498	1.1447	1.1326	1.1295	1.1207	1.1107	1.1150	1.1047
20	Cal 30/60	1.1401	1.1344	1.1224	1.1188	1.1090	1.0989	1.1034	1.0922
21	Cal 30/30	1.1840	1.1801	1.1687	1.1649	1.1571	1.1488	1.1525	1.1432
22	Cal 30/30	1.1813	1.1773	1.1660	1.1626	1.1550	1.1466	1.1504	1.1413
23	Cal 30/30	1.1682	1.1637	1.1525	1.1492	1.1408	1.1326	1.1364	1.1267
24	Cal 30/30	1.1806	1.1762	1.1654	1.1623	1.1542	1.1459	1.1497	1.1402
25	Cal 30/30	1.2042	1.1625	1.1506	1.1477	1.1400	1.1319	1.1355	1.1262
26	Cal 30/90	1.1123	1.0709	1.0475	1.0462	1.0408	1.0136	1.0300	1.0085

27	Cal 30/90	1.1130	1.0693	1.0481	1.0473	1.0424	1.0172	1.0332	1.0133
28	Cal 30/90	1.1017	1.0594	1.0373	1.0369	1.0313	1.0053	1.0215	1.0011
29	Cal 30/90	1.1089	1.0662	1.0450	1.0440	1.0390	1.0138	1.0295	1.0101
30	Cal 30/90	1.1114	1.0683	1.0458	1.0452	1.0393	1.0126	1.0292	1.0072

Available Power Data (W) Char – RPT 6

Cell #	Condition Char		RPT 0	RPT 1	RPT 2	RPT 3	RPT 4	RPT 5	RPT 6
1	CD 30/15	57014	57365	59283	58599	55996	54088	51685	49609
2	CD 30/15	57485	57688	60045	59345	56583	54658	52190	49947
3	CD 30/15	57609	57860	60305	59624	57135	55267	52843	50567
4	CD 30/15	57306	57726	59498	58758	56359	54511	52199	50201
5	CD 30/15	57814	58120	60438	59739	57288	55323	52785	50407
6	CD 30/15	57781	58095	60395	59835	57194	55293	52821	50454
7	CD 30/15	56908	57177	59409	58707	55472	53636	51205	49046
8	CD 30/15	57691	57899	60273	59464	56904	54960	52436	50057
9	CD 30/15	57648	58053	59963	59111	56584	54624	52173	50062
10	CD 30/15	57487	57784	60200	59570	57187	55259	52785	50448
11	Cal 30/60	57604	57931	57275	57828	56941	57227	57076	57181
12	Cal 30/60	56674	57063	56455	57193	56184	56308	56032	55712
13	Cal 30/60	57508	57896	57278	57820	56209	56274	56091	56123
14	Cal 30/60	58508	58849	58174	58782	57889	58177	58073	58164
15	Cal 30/60	57409	57805	57226	57731	56717	56852	56643	56674
16	Cal 30/60	57878	58296	57678	58237	57285	57389	57151	57244
17	Cal 30/60	58248	58674	58050	58751	57520	57575	57267	57368
18	Cal 30/60	58243	58642	58034	58735	57500	57583	57358	57430
19	Cal 30/60	57507	57828	57156	57964	56872	57116	56968	57108
20	Cal 30/60	57749	58115	57530	58300	56574	56698	56522	56617
21	Cal 30/30	57758	58171	57959	58755	57811	57967	58054	58433
22	Cal 30/30	57798	58072	57948	58841	57763	57988	58117	58568
23	Cal 30/30	57684	58056	57904	58768	57713	57974	58043	58442
24	Cal 30/30	57688	58114	57911	58766	57679	57841	57890	58301
25	Cal 30/30	57594	57986	57887	58749	57652	57857	57899	58274
26	Cal 30/90	57751	57976	58092	58910	57715	57516	56949	56665
27	Cal 30/90	58133	58579	58747	59449	58213	57906	57297	56936
28	Cal 30/90	58081	58512	58768	59522	58314	58113	57576	57288
29	Cal 30/90	57963	58324	58504	59242	57118	56909	56314	55984
30	Cal 30/90	58085	58276	58428	59260	57929	57690	57097	56828

31	CD 40/15	57470	57874	59183	56498	52142	50089	47040	44583
32	CD 40/15	57407	57818	59474	56877	52524	50503	47386	44800
33	CD 40/15	56913	57226	58463	55667	51251	49241	46060	43643
34	CD 40/15	57230	57627	59035	56330	52165	50287	47178	44709
35	CD 40/15	57507	57695	59914	57355	53015	50967	47715	45144
36	Cal 40/60	56679	57100	56537	56200	54320	54730	53913	53211
37	Cal 40/60	57103	57468	56860	56583	53985	54397	53650	52972
38	Cal 40/60	57554	57918	57420	57085	55104	55547	54739	53992
39	Cal 40/60	56108	56311	55650	55482	53625	54155	53404	52699
40	Cal 40/60	57765	58136	57578	57252	55226	55763	54972	54203
41	CD 50/15	58511	59378	55898	50312	46597	42512	38699	35927
42	CD 50/15	58141	58757	56266	50565	46199	42272	38724	35961
43	CD 50/15	58914	59644	56444	50842	46806	43067	39149	36407
44	CD 50/15	57299	57901	54664	49012	45009	41340	37643	34353
45	CD 50/15	57626	58238	55277	49603	45542	41865	38397	35590
46	Cal 50/60	58315	58967	55322	52975	50518	48175	46162	43773
47	Cal 50/60	58755	59493	55998	53519	50873	48622	46349	44020
48	Cal 50/60	57723	58324	55013	52702	50264	48091	46099	43886
49	Cal 50/60	57487	58157	54805	52361	49765	47559	45455	43159
50	Cal 50/60	57073	57658	54362	51978	49395	47282	45187	42943
51	CD 60/15	58487	58871	48839	39735	32104	30672	31290	30068
52	CD 60/15	57389	57731	47770	39076	31642	29824	30657	29188
53	CD 60/15	58278	58669	48569	39758	32094	30016	30725	29319
54	CD 60/15	58307	58718	48790	40118	32322	30223	30925	29554
55	CD 60/15	59330	59635	48932	39287	32046	30628	31273	29953
56	Cal 60/60	58265	58629	50831	44181	39370	35057	30539	28317
57	Cal 60/60	58948	59191	51091	44440	39253	34872	30323	28084
58	Cal 60/60	59131	59642	51775	45490	40708	36492	31725	29820
59	Cal 60/60	58778	59015	50900	44286	39146	34725	30277	27969
60	Cal 60/60	58622	58849	50792	44240	39191	34771	30360	28095

Available Power Data (W) RPT 7 – RPT 14

Cell #	Condition	RPT 7	RPT 8	RPT 9	RPT 10	RPT 11	RPT 12	RPT 13	RPT 14
1	CD 30/15	47337	44262	42602	40886	34399	38327	31424	
2	CD 30/15	47462	44500	42725	41059	34733	38381	31725	
3	CD 30/15	48032	45142	43304	41559	35202	38604	32018	
4	CD 30/15	47797	45004	43233	41571	35141	38652	32074	

5	CD 30/15	47867	44841	42969	41182	34919	38343	31671	
6	CD 30/15	48074	44923	43090	41303	34867	38486	31706	
7	CD 30/15	46553	43597	41923	40272	34087	37766	31119	
8	CD 30/15	47576	44662	42899	41152	34887	38380	31779	
9	CD 30/15	47560	44746	43008	41282	35097	38501	31972	
10	CD 30/15	48002	44991	43165	41399	35204	38565	31939	
11	Cal 30/60	57196	55934	55556	55029	53859	54585	47753	47810
12	Cal 30/60	55714	54370	53984	53478	52271	52988	46312	46148
13	Cal 30/60	56510	55104	54744	54224	52380	53044	46095	46457
14	Cal 30/60	58186	56961	56563	56090	54651	55436	48219	48557
15	Cal 30/60	56718	55455	55051	54574	53138	53910	47058	47365
16	Cal 30/60	57175	55886	55443	54943	53672	54351	47410	47763
17	Cal 30/60	57471	55991	55584	55060	53702	54439	47353	47691
18	Cal 30/60	57590	56040	55647	55135	53704	54580	47376	47735
19	Cal 30/60	57310	55798	55457	54966	53518	54227	46926	47489
20	Cal 30/60	57298	55719	55369	54896	52468	53499	46347	46807
21	Cal 30/30	58882	57827	57649	57368	56137	57196	50651	51293
22	Cal 30/30	59208	58107	58010	57795	56502	57675	51043	51770
23	Cal 30/30	58808	57651	57447	57248	55762	57151	50536	51210
24	Cal 30/30	58783	57661	57444	57184	56084	57045	50429	51050
25	Cal 30/30	58732	57691	57462	57194	55907	56740	49892	50660
26	Cal 30/90	56437	54798	54357	53796	50286	52732	45327	45840
27	Cal 30/90	56693	54995	54509	53924	50680	52942	45511	46021
28	Cal 30/90	57054	55337	54848	54267	50877	53314	45865	46336
29	Cal 30/90	56287	54351	53857	53297	49558	51785	44621	45102
30	Cal 30/90	56646	54872	54439	53884	50420	52593	45176	45614
31	CD 40/15	41975	40377	38845	37353	35530	33972	31912	
32	CD 40/15	42129	40549	38932	37388	35554	34818		
33	CD 40/15	41008	39595	38165	36724	34986	33270	31222	
34	CD 40/15	41915	40459	38923	37419	35530	33976	32187	
35	CD 40/15	42476	40895	39354	37820	36017	34559	32601	
36	Cal 40/60	52195	51491	50527	49680	48949	48310	47742	
37	Cal 40/60	51977	51254	50294	49405	48596	47918	47318	
38	Cal 40/60	52958	52210	51260	50411	49638	48954	48381	47959
39	Cal 40/60	51660	50917	49943	49054	48284	47636	47012	46658
40	Cal 40/60	53177	52428	51462	50565	49788	49100	48549	48113

Available Power Data (W) RPT 15 – RPT 22

Cell #	Condition RPT 15	RPT 16	RPT 17	RPT 18	RPT 19	RPT 20	RPT 21	RPT 22
11	Cal 30/60 52972	52525	52118	46767	46767	51354	50838	50182
12	Cal 30/60 51024	50586	50276	45232	45232	49516	49034	48420
13	Cal 30/60 51599	51122	50764	45384	45384	49917	49341	48777
14	Cal 30/60 53944	53474	53081	47516	47516	52281	51701	51066
15	Cal 30/60 52303	51825	51431	46214	46214	50566	50058	49411
16	Cal 30/60 52723	52239	51863	46543	46543	50933	50385	49751
17	Cal 30/60 52664	52173	51775	46480	46480	50887	50376	49723
18	Cal 30/60 52910	52423	51984	46520	46520	51112	50510	49895
19	Cal 30/60 52919	52426	52050	46433	46433	51216	50604	50027
20	Cal 30/60 51739	51263	50895	45770	45770	50061	49495	48935
21	Cal 30/30 56121	55836	55562	50673	50673	54996	54554	54017
22	Cal 30/30 56603	56355	56099	51206	51206	55609	55135	54628
23	Cal 30/30 55976	55664	55373	50554	50554	54833	54338	53824
24	Cal 30/30 55943	55641	55355	50376	50376	54816	54302	53769
25	Cal 30/30 55864	55579	55271	50067	50067	54718	54293	53721
26	Cal 30/90 50527	49929	49375	44218	44218	48081	47331	46961
27	Cal 30/90 50662	50078	49549	44396	44396	48286	47563	47099
28	Cal 30/90 50913	50301	47603	44571	44571	48516	47689	47181
29	Cal 30/90 49459	48917	48438	43469	43469	47298	46528	46093
30	Cal 30/90 50230	49643	49117	43912	43912	47821	46971	46603

Available Power Data (W) RPT 23 – RPT 30

Cell #	Condition RPT 23	RPT 24	RPT 25	RPT 26	RPT 27	RPT 28	RPT 29	RPT 30
11	Cal 30/60 49946	49456	51106	48538	48243	47845	47597	47249
12	Cal 30/60 48232	47719	49243	46873	46577	46195	45898	45586
13	Cal 30/60 48550	48108	49619	47217	46916	46514	46292	45937
14	Cal 30/60 50834	50356	52129	49414	49093	48687	48454	48091
15	Cal 30/60 49188	48715	50421	47814	47499	47116	46877	46540
16	Cal 30/60 49486	49024	50707	48088	47799	47358	47122	46785
17	Cal 30/60 49520	48999	50635	48049	47734	47348	47114	46748
18	Cal 30/60 49716	49130	50827	48229	47937	47510	47266	46908
19	Cal 30/60 49799	49295	50930	48412	48055	47657	47424	47067

20	Cal 30/60	48760	48272	50444	47610	47040	46650	46411	46059
21	Cal 30/30	53887	53497	55151	52641	52355	52008	51825	51483
22	Cal 30/30	54494	54109	55813	53311	53036	52680	52471	52162
23	Cal 30/30	53705	53275	54903	52451	52180	51839	51615	51309
24	Cal 30/30	53753	53286	54867	52458	52184	51838	51648	51326
25	Cal 30/30	54346	53255	54576	52354	52062	51719	51512	51201
26	Cal 30/90	47281	45854	47465	44958	44622	44615	43750	43708
27	Cal 30/90	47513	45949	47635	45091	44795	44793	44006	43969
28	Cal 30/90	47602	46026	47639	45050	44727	44727	43892	43920
29	Cal 30/90	46480	44959	46571	44156	43862	43834	43093	43033
30	Cal 30/90	47026	45476	47035	44607	44308	44278	43439	43373

Resistance Data (ohms) Char – RPT 6

Cell #	Condition Char	RPT 0	RPT 1	RPT 2	RPT 3	RPT 4	RPT 5	RPT 6
1	CD 30/15	0.04929	0.04783	0.04842	0.05131	0.05240	0.05475	0.05732
2	CD 30/15	0.04898	0.04718	0.04783	0.05071	0.05184	0.05419	0.05676
3	CD 30/15	0.04863	0.04699	0.04760	0.05025	0.05126	0.05352	0.05601
4	CD 30/15	0.04895	0.04771	0.04836	0.05098	0.05205	0.05427	0.05670
5	CD 30/15	0.04853	0.04690	0.04757	0.05014	0.05126	0.05367	0.05631
6	CD 30/15	0.04852	0.04688	0.04746	0.05020	0.05129	0.05364	0.05621
7	CD 30/15	0.04945	0.04767	0.04835	0.05181	0.05288	0.05531	0.05786
8	CD 30/15	0.04884	0.04701	0.04773	0.05048	0.05158	0.05395	0.05664
9	CD 30/15	0.04866	0.04726	0.04797	0.05070	0.05186	0.05421	0.05679
10	CD 30/15	0.04877	0.04715	0.04770	0.05026	0.05132	0.05370	0.05624
11	Cal 30/60	0.04866	0.05001	0.04966	0.05105	0.05023	0.05036	0.05038
12	Cal 30/60	0.04957	0.05080	0.05028	0.05180	0.05110	0.05128	0.05168
13	Cal 30/60	0.04877	0.05006	0.04970	0.05175	0.05110	0.05126	0.05130
14	Cal 30/60	0.04789	0.04922	0.04887	0.05021	0.04937	0.04951	0.04949
15	Cal 30/60	0.04881	0.05007	0.04972	0.05128	0.05056	0.05076	0.05079
16	Cal 30/60	0.04847	0.04971	0.04933	0.05079	0.05006	0.05025	0.05034
17	Cal 30/60	0.04809	0.04943	0.04877	0.05065	0.04997	0.05015	0.05022
18	Cal 30/60	0.04816	0.04949	0.04893	0.05064	0.04995	0.05011	0.05015
19	Cal 30/60	0.04880	0.05009	0.04954	0.05111	0.05032	0.05049	0.05045
20	Cal 30/60	0.04852	0.04985	0.04927	0.05124	0.05072	0.05086	0.05087
21	Cal 30/30	0.04858	0.04839	0.04769	0.04887	0.04812	0.04792	0.04764
22	Cal 30/30	0.04853	0.04833	0.04760	0.04882	0.04804	0.04780	0.04750
23	Cal 30/30	0.04863	0.04842	0.04769	0.04890	0.04809	0.04787	0.04763

24	Cal 30/30	0.04862	0.04846	0.04779	0.04900	0.04820	0.04804	0.04775
25	Cal 30/30	0.04867	0.04845	0.04774	0.04899	0.04826	0.04798	0.04774
26	Cal 30/90	0.04872	0.04856	0.04776	0.04910	0.04853	0.04879	0.04893
27	Cal 30/90	0.04822	0.04806	0.04734	0.04880	0.04833	0.04859	0.04892
28	Cal 30/90	0.04823	0.04803	0.04721	0.04864	0.04810	0.04839	0.04859
29	Cal 30/90	0.04837	0.04822	0.04740	0.04968	0.04919	0.04945	0.04971
30	Cal 30/90	0.04844	0.04829	0.04749	0.04893	0.04839	0.04861	0.04883
31	CD 40/15	0.04844	0.04830	0.05065	0.05525	0.05707	0.06089	0.06459
32	CD 40/15	0.04870	0.04803	0.05034	0.05481	0.05662	0.06044	0.06421
33	CD 40/15	0.04909	0.04888	0.05140	0.05621	0.05822	0.06228	0.06613
34	CD 40/15	0.04890	0.04841	0.05081	0.05533	0.05700	0.06080	0.06447
35	CD 40/15	0.04878	0.04766	0.04990	0.05433	0.05606	0.05995	0.06375
36	Cal 40/60	0.04935	0.05097	0.05142	0.05380	0.05284	0.05357	0.05430
37	Cal 40/60	0.04896	0.05071	0.05103	0.05410	0.05315	0.05389	0.05461
38	Cal 40/60	0.04863	0.05019	0.05057	0.05308	0.05200	0.05276	0.05352
39	Cal 40/60	0.05012	0.05185	0.05211	0.05449	0.05340	0.05413	0.05486
40	Cal 40/60	0.04845	0.05005	0.05052	0.05293	0.05183	0.05252	0.05336
41	CD 50/15	0.04751	0.05122	0.05653	0.06171	0.06666	0.07175	0.07714
42	CD 50/15	0.04806	0.05081	0.05616	0.06155	0.06700	0.07179	0.07722
43	CD 50/15	0.04727	0.05064	0.05588	0.06071	0.06568	0.07081	0.07577
44	CD 50/15	0.04870	0.05223	0.05783	0.06312	0.06849	0.07399	0.07908
45	CD 50/15	0.04843	0.05172	0.05716	0.06237	0.06770	0.07248	0.07730
46	Cal 50/60	0.04787	0.05229	0.05457	0.05729	0.05915	0.06157	0.06451
47	Cal 50/60	0.04736	0.05166	0.05405	0.05683	0.05865	0.06123	0.06414
48	Cal 50/60	0.04825	0.05263	0.05490	0.05762	0.05930	0.06168	0.06444
49	Cal 50/60	0.04848	0.05279	0.05519	0.05814	0.05996	0.06249	0.06542
50	Cal 50/60	0.04882	0.05321	0.05561	0.05849	0.06034	0.06282	0.06574
51	CD 60/15	0.04797	0.05756	0.07024	0.08068	0.08427	0.08987	0.09363
52	CD 60/15	0.04899	0.05907	0.07133	0.08150	0.08530	0.09088	0.09495
53	CD 60/15	0.04819	0.05803	0.07003	0.08020	0.08477	0.09066	0.09452
54	CD 60/15	0.04816	0.05773	0.06944	0.07956	0.08434	0.09020	0.09398
55	CD 60/15	0.04746	0.05749	0.07082	0.08080	0.08419	0.08978	0.09364
56	Cal 60/60	0.04819	0.05653	0.06394	0.07230	0.08088	0.09035	0.10069
57	Cal 60/60	0.04774	0.05627	0.06359	0.07244	0.08123	0.09074	0.10136
58	Cal 60/60	0.04741	0.05550	0.06222	0.06986	0.07758	0.08595	0.09482
59	Cal 60/60	0.04790	0.05654	0.06385	0.07266	0.08159	0.09112	0.10178
60	Cal 60/60	0.04809	0.05659	0.06388	0.07254	0.08144	0.09079	0.10131

Resistance Data (ohms) RPT 7 – RPT 14

Cell #	Condition	RPT 7	RPT 8	RPT 9	RPT 10	RPT 11	RPT 12	RPT 13	RPT 14
1	CD 30/15	0.06005	0.06453	0.06768	0.07095	0.08523	0.07646	0.09470	
2	CD 30/15	0.05991	0.06426	0.06741	0.07061	0.08439	0.07628	0.09357	
3	CD 30/15	0.05914	0.06320	0.06640	0.06964	0.08333	0.07574	0.09256	
4	CD 30/15	0.05958	0.06356	0.06655	0.06971	0.08292	0.07558	0.09206	
5	CD 30/15	0.05942	0.06381	0.06713	0.07052	0.08423	0.07661	0.09393	
6	CD 30/15	0.05913	0.06363	0.06693	0.07021	0.08426	0.07615	0.09363	
7	CD 30/15	0.06116	0.06567	0.06886	0.07212	0.08616	0.07768	0.09568	
8	CD 30/15	0.05983	0.06403	0.06723	0.07052	0.08401	0.07643	0.09357	
9	CD 30/15	0.05975	0.06384	0.06693	0.07016	0.08337	0.07610	0.09285	
10	CD 30/15	0.05932	0.06362	0.06678	0.07010	0.08345	0.07603	0.09306	
11	Cal 30/60	0.05034	0.05143	0.05184	0.05239	0.05791	0.05263	0.05971	0.05951
12	Cal 30/60	0.05167	0.05296	0.05338	0.05391	0.05971	0.05406	0.06153	0.06167
13	Cal 30/60	0.05091	0.05223	0.05266	0.05315	0.05987	0.05387	0.06190	0.06134
14	Cal 30/60	0.04948	0.05052	0.05093	0.05141	0.05734	0.05170	0.05922	0.05872
15	Cal 30/60	0.05073	0.05185	0.05230	0.05281	0.05867	0.05321	0.06065	0.06018
16	Cal 30/60	0.05034	0.05151	0.05196	0.05248	0.05825	0.05279	0.06020	0.05967
17	Cal 30/60	0.05013	0.05145	0.05188	0.05236	0.05826	0.05267	0.06026	0.05972
18	Cal 30/60	0.04996	0.05141	0.05178	0.05234	0.05825	0.05247	0.06019	0.05965
19	Cal 30/60	0.05026	0.05160	0.05194	0.05245	0.05876	0.05256	0.06083	0.05999
20	Cal 30/60	0.05023	0.05166	0.05202	0.05253	0.05944	0.05341	0.06164	0.06096
21	Cal 30/30	0.04737	0.04806	0.04811	0.04819	0.05265	0.04799	0.05371	0.05301
22	Cal 30/30	0.04705	0.04776	0.04779	0.04785	0.05219	0.04756	0.05319	0.05244
23	Cal 30/30	0.04736	0.04820	0.04822	0.04833	0.05268	0.04808	0.05374	0.05301
24	Cal 30/30	0.04739	0.04822	0.04829	0.04834	0.05282	0.04810	0.05384	0.05316
25	Cal 30/30	0.04747	0.04816	0.04828	0.04840	0.05323	0.04815	0.05438	0.05356
26	Cal 30/90	0.04906	0.05036	0.05069	0.05112	0.05712	0.05150	0.05937	0.05856
27	Cal 30/90	0.04900	0.05037	0.05068	0.05112	0.05700	0.05159	0.05929	0.05855
28	Cal 30/90	0.04866	0.05002	0.05037	0.05079	0.05655	0.05123	0.05881	0.05805
29	Cal 30/90	0.04931	0.05097	0.05128	0.05174	0.05813	0.05282	0.06055	0.05978
30	Cal 30/90	0.04885	0.05028	0.05061	0.05100	0.05717	0.05174	0.05943	0.05871
31	CD 40/15	0.06895	0.07231	0.07549	0.07839	0.08213	0.08575	0.09072	
32	CD 40/15	0.06863	0.07208	0.07536	0.07838	0.08206	0.08361		
33	CD 40/15	0.07056	0.07382	0.07667	0.07975	0.08326	0.08753	0.09256	
34	CD 40/15	0.06881	0.07216	0.07515	0.07835	0.08213	0.08576	0.09032	
35	CD 40/15	0.06806	0.07150	0.07438	0.07752	0.08085	0.08426	0.08902	
36	Cal 40/60	0.05522	0.05579	0.05694	0.05785	0.05861	0.05936	0.05992	

37	Cal 40/60	0.05542	0.05602	0.05723	0.05812	0.05901	0.05974	0.06042	
38	Cal 40/60	0.05437	0.05501	0.05617	0.05699	0.05780	0.05862	0.05912	0.05955
39	Cal 40/60	0.05584	0.05653	0.05773	0.05864	0.05947	0.06026	0.06090	0.06128
40	Cal 40/60	0.05419	0.05481	0.05599	0.05686	0.05766	0.05842	0.05898	0.05943

Resistance Data (ohms) RPT 15 – RPT 22

Cell #	Condition RPT 15	RPT 16	RPT 17	RPT 18	RPT 19	RPT 20	RPT 21	RPT 22
11	Cal 30/60	0.05435	0.05479	0.05523	0.06127	0.05587	0.05621	0.05649	0.05733
12	Cal 30/60	0.05642	0.05693	0.05724	0.06338	0.05791	0.05820	0.05856	0.05935
13	Cal 30/60	0.05578	0.05631	0.05672	0.06309	0.05750	0.05780	0.05818	0.05898
14	Cal 30/60	0.05341	0.05387	0.05424	0.06032	0.05498	0.05524	0.05554	0.05632
15	Cal 30/60	0.05502	0.05550	0.05593	0.06198	0.05665	0.05700	0.05731	0.05814
16	Cal 30/60	0.05462	0.05512	0.05554	0.06168	0.05631	0.05666	0.05698	0.05784
17	Cal 30/60	0.05469	0.05518	0.05560	0.06171	0.05640	0.05670	0.05702	0.05780
18	Cal 30/60	0.05443	0.05493	0.05536	0.06163	0.05620	0.05649	0.05691	0.05765
19	Cal 30/60	0.05442	0.05491	0.05534	0.06171	0.05611	0.05641	0.05681	0.05756
20	Cal 30/60	0.05566	0.05616	0.05653	0.06263	0.05732	0.05760	0.05801	0.05872
21	Cal 30/30	0.04908	0.04929	0.04945	0.05358	0.04980	0.04992	0.05024	0.05064
22	Cal 30/30	0.04863	0.04880	0.04897	0.05303	0.04923	0.04939	0.04973	0.05005
23	Cal 30/30	0.04917	0.04939	0.04961	0.05369	0.04987	0.05008	0.05042	0.05076
24	Cal 30/30	0.04921	0.04942	0.04962	0.05394	0.04993	0.05015	0.05051	0.05086
25	Cal 30/30	0.04929	0.04948	0.04966	0.05409	0.04999	0.05016	0.05048	0.05083
26	Cal 30/90	0.05379	0.05427	0.05481	0.06065	0.05564	0.05628	0.05689	0.05743
27	Cal 30/90	0.05380	0.05432	0.05482	0.06061	0.05557	0.05618	0.05683	0.05735
28	Cal 30/90	0.05346	0.05399	0.05452	0.06029	0.05535	0.05599	0.05664	0.05716
29	Cal 30/90	0.05518	0.05568	0.05620	0.06200	0.05695	0.05752	0.05819	0.05867
30	Cal 30/90	0.05402	0.05457	0.05511	0.06106	0.05589	0.05653	0.05728	0.05784

Resistance Data (ohms) RPT 23 – RPT 30

Cell #	Condition RPT 23	RPT 24	RPT 25	RPT 26	RPT 27	RPT 28	RPT 29	RPT 30
11	Cal 30/60	0.05742	0.05789	0.05660	0.05902	0.05945	0.06004	0.06019	0.06074
12	Cal 30/60	0.05942	0.05994	0.05872	0.06112	0.06157	0.06220	0.06238	0.06300
13	Cal 30/60	0.05904	0.05951	0.05824	0.06069	0.06114	0.06175	0.06187	0.06246
14	Cal 30/60	0.05638	0.05685	0.05554	0.05799	0.05839	0.05906	0.05911	0.05969

15	Cal 30/60	0.05824	0.05874	0.05736	0.05989	0.06035	0.06092	0.06107	0.06166
16	Cal 30/60	0.05791	0.05846	0.05705	0.05965	0.06006	0.06068	0.06079	0.06142
17	Cal 30/60	0.05790	0.05846	0.05713	0.05965	0.06008	0.06075	0.06084	0.06144
18	Cal 30/60	0.05768	0.05828	0.05692	0.05944	0.05991	0.06052	0.06064	0.06128
19	Cal 30/60	0.05756	0.05808	0.05677	0.05924	0.05967	0.06029	0.06044	0.06102
20	Cal 30/60	0.05870	0.05924	0.05730	0.06013	0.06091	0.06147	0.06163	0.06220
21	Cal 30/30	0.05069	0.05097	0.04991	0.05164	0.05184	0.05205	0.05229	0.05254
22	Cal 30/30	0.05014	0.05039	0.04933	0.05098	0.05121	0.05141	0.05162	0.05186
23	Cal 30/30	0.05078	0.05116	0.05008	0.05183	0.05194	0.05223	0.05244	0.05262
24	Cal 30/30	0.05088	0.05122	0.05019	0.05184	0.05203	0.05231	0.05249	0.05273
25	Cal 30/30	0.05029	0.05120	0.05028	0.05188	0.05211	0.05232	0.05249	0.05276
26	Cal 30/90	0.05709	0.05850	0.05717	0.05961	0.05996	0.06004	0.06102	0.06113
27	Cal 30/90	0.05694	0.05844	0.05707	0.05948	0.05981	0.05990	0.06068	0.06093
28	Cal 30/90	0.05683	0.05829	0.05693	0.05939	0.05979	0.05984	0.06075	0.06090
29	Cal 30/90	0.05830	0.05981	0.05842	0.06081	0.06110	0.06124	0.06204	0.06223
30	Cal 30/90	0.05743	0.05896	0.05762	0.06003	0.06038	0.06046	0.06146	0.06159